Contents

Contents

Chapter 1 **Introduction**

In order to understand the concept of ultrasound, one must begin to realize what sound is. Generally sound is propagation of pressure waves through some physical elastic medium. The most known medium is air, where sound can travel and reach us. However air is not the only medium. The reality is that where molecules are found, sound can propagate. Due to the linear mass density of molecules, sound can travel faster in liquid than in air. There is no sound in vacuum.

Ultrasound can be defined as a beam of acoustic waves that travel at frequencies greater than *20,000* vibration per second or *20 kHz*. Human hearing is limited. Human can only hear sounds in the range of about *20* to *30 kHz*. Generally, high frequencies are used for medical imaging, such as investigating a fetus in the mother's womb. It's difficult to generate and measure high frequencies. Medical ultrasound has an upper limit of about 10 MHz, but higher frequencies are possible. Ultrasound images are generated by sending sound pulses from a probe (transducer). The sound reflects from structures in the body and is received by the probe again. These pulses are processed and interpreted by considering depth and direction, and are shown as an image on a screen.

Beamforming techniques play one of the most important roles in ultrasound imaging. Our objective is to look into theoretical background (solutions) of the acoustic wave equation for *limited diffraction beams*. The advantages and disadvantages of these solutions for ultrasound imaging will be discussed. Simulation models are developed in order to visualize the beam characterizations (like *lateral resolutions, depth of*

field etc.). We will be comparing our results from the *limited diffraction beam* simulations with the results achieved by applying conventional focused beamforming.

The simulation software is developed in the Matlab environment and is meant to be integrated into Ultrasim simulator. We have also presented a paper based on this work at IEEE international ultrasonics symposium 1996 conference [34].

Chapter 2 The wave equation

A second order partial differential equation which occurs frequently in applied mathematics is the wave equation. Some form of this equation, or a generalization of it, almost inevitably arises in any mathematical analysis of phenomena involving the propagation of waves in a continuous medium. For example, the studies of acoustic waves, water waves, and electromagnetic waves are all based on this equation. There are two basic types of waves that are important in acoustic wave propagation [1]. The first is *longitudinal wave*, in which the motion of a particle in the acoustic medium is along the direction of wave propagation. The second type of wave is *shear wave (transverse wave)*, in which the motion of a particle in the medium is transverse to the direction of propagation. In this chapter, the derivation of the wave equation in cartesian (one and three-dimensional) and spherical coordinates will be described.

2.1 The one-dimensional wave equation

Starting from the basic linear equation of motion in one dimension, one can derive the one-dimensional wave equation, which is an equation for wave propagation that operates in one dimension only. First, we shall establish the equation expressing Newton's second law of motion, the gas law [2]:

$$\textit{Equation of motion} \qquad \frac{\partial p}{\partial x} + \rho_o \frac{\partial v}{\partial t} = 0 \tag{1}$$

$$Gas\ \ law \qquad \frac{1}{P_o}\frac{\partial p}{\partial t} + \frac{\gamma}{V_o}\frac{\partial \tau}{\partial t} = 0 \tag{2}$$

where p is the pressure, and ρ_o is the density of the medium, and τ is the incremental volume, and V_o and P_o are the undisturbed volume and gas pressure respectively and v is velocity.

The second important equation is that of mass conservation [2]:

$$V_o \frac{\partial u}{\partial x} - \frac{\partial \tau}{\partial t} = 0 \tag{3}$$

Combination of Eq. 2 and Eq. 3 gives:

$$\frac{\partial p}{\partial t} + \gamma P_o \frac{\partial v}{\partial x} = 0 \tag{4}$$

Differentiating Eq. 4 with respect to time t, and Eq. 1 with respect to the spatial coordinate x:

$$\frac{\partial^2 p}{\partial t^2} + \gamma P_o \frac{\partial^2 v}{\partial x \partial t} = 0 \tag{5}$$

$$\rho_o \frac{\partial^2 v}{\partial x \partial t} + \frac{\partial^2 p}{\partial x^2} = 0 \tag{6}$$

The one-dimensional wave equation is obtained by combining Eq. 5 and Eq. 6 :

$$\frac{\partial^2 p}{\partial x^2} + \frac{\rho_o}{\gamma P_o}\frac{\partial^2 p}{\partial t^2} = 0 \tag{7}$$

Where $\sqrt{(P_o\ \gamma)/\rho_o} = c$ is the speed of propagation of sound wave in the medium. Then Eq. 7 becomes:

$$\frac{\partial^2 p}{\partial x^2} - \frac{1}{c^2}\frac{\partial^2 p}{\partial t^2} = 0 \tag{8}$$

This second-order differential equation is called the one-dimensional wave equation. It can be proved that any solution of the wave equation has the form:

$$p(x,t) = f(x \pm ct) \tag{9}$$

where the negative sign indicates a wave travelling in the *x-direction,* whereas the positive sign indicates a wave travelling in the *-x-direction*. Since the displacement is in the same direction as the wave propagation, this type of wave is called longitudinal wave. The sinusoidal solution for this equation is:

$$p = p_o e^{j(\omega t \pm kx)} \tag{10}$$

where $\omega=2\pi f$ is the angular frequency and $k=\omega/c$ is the wave number.

2.2 The three-dimensional wave equation for sound

The general case of sound propagation involves three dimensions. Let us suppose the sound pressure p changes in space at the rate of [2]:

$$\nabla p = i\frac{\partial p}{\partial x} + j\frac{\partial p}{\partial y} + k\frac{\partial p}{\partial z} \tag{11}$$

where i, j and k are unit vectors in the x, y and z directions, respectively, and p is the acoustic pressure at an arbitrary point in space $\vec{x}$. The basis of the derivation is three relations.

Euler's equation of ***motion*** for a fluid which is a relation between pressure and particle velocity:

$$\rho_o \frac{\partial \vec{v}}{\partial t} = -\nabla p \tag{12}$$

where velocity $\vec{v}$ is now a vector.

The second relation is the ***mass conservation***. This gives a relation between density and particle velocity.

$$\frac{\partial \rho}{\partial t} = -\rho_o \nabla \cdot \vec{v} \tag{13}$$

Finally the relation between pressure and density is given by [5]:

$$p = c^2 \rho \tag{14}$$

where ρ is the density at a point and c is the speed of sound in the medium.

By combining Eq. 13 and Eq. 14 one can obtain:

$$\frac{1}{c^2}\frac{\partial p}{\partial t} + \rho_o \nabla \cdot \vec{v} = 0 \tag{15}$$

Differentiating Eq. 15 with respect to time *t* gives:

$$\frac{1}{c^2}\frac{\partial^2 p}{\partial t^2} + \rho_o \nabla \cdot \frac{\partial \vec{v}}{\partial t} = 0 \tag{16}$$

and using Eq. 12 to eliminate $\vec{v}$ results in:

$$\nabla^2 p - \frac{1}{c^2}\frac{\partial^2 p}{\partial t^2} = 0 \tag{17}$$

which is three-dimensional form of the wave equation. The symbol ∇^2 is the Laplacian operator in three-dimensions [6].

2.3 Wave equation in spherical coordinates

Many acoustical problems are concerned with spherical diverging waves. If we look at the sound from a simple “point source”, we expect that the sound field should be symmetric about the source position [3]. In spherical coordinates (r,ϕ,θ):

$x = r\sin\phi\cos\theta$

$y = r\sin\phi\sin\theta$

$z = r\cos\phi$

where *r* is the distance from the centre, ϕ is the angle between *r* and the *z*-axis, and θ is the angle between the projection of *r* on the *yx* plane.

In spherical coordinates, the wave equation is [6]:

$$\frac{1}{r^2}\frac{\partial}{\partial r}\left(r^2\frac{\partial p}{\partial r}\right) + \frac{1}{r^2\sin\phi}\frac{\partial}{\partial\phi}\left(\sin\phi\frac{\partial p}{\partial\phi}\right) + \frac{1}{r^2\sin^2\phi}\frac{\partial^2 p}{\partial\phi^2} = \frac{1}{c^2}\frac{\partial^2 p}{\partial t^2} \tag{18}$$

For spherical symmetry about origin, the general spherical wave equation becomes:

$$\frac{\partial^2(rp)}{\partial r^2} - \frac{1}{c^2}\frac{\partial^2(rp)}{\partial t^2} = 0 \tag{19}$$

Which is just the same as Eq. 1 except that now we are working in terms of rp rather than p.

The solution of the wave equation takes the same form as before and is finite everywhere except at r=0. Thus a general solution of this equation is [6]:

$$rp = \frac{1}{r} f\left(t - \frac{r}{c}\right) + g\left(t + \frac{r}{c}\right) \tag{20}$$

where f and g are arbitrary functions.

The free space scalar wave equation in ***cylindrical coordinate*** is given by [6],[9];

$$\left(\frac{1}{r^2}\frac{\partial}{\partial r}\left(r^2\frac{\partial}{\partial r}\right) + \frac{1}{r^2}\frac{\partial^2}{\partial \phi^2} + \frac{\partial^2}{\partial z^2} - \frac{1}{c^2}\frac{\partial^2}{\partial t^2}\right) p(r,t) = 0 \tag{21}$$

where $r = \sqrt{x^2 + y^2}$ represents a radial coordinate, ϕ is an azimuthal angle, z represents an axial axis that is perpendicular to the plane defined by r and ϕ, t is time and p represents sound pressure.

From Eq. 21 one can obtain following exact solution for scalar field propagating into the source-free region[10]:

$$p(r,t) = e^{(\beta z - \omega t)} \int_0^{2\pi} A(\phi) \frac{e^{-\alpha j(x\cos\phi + y\sin\phi)}}{2\pi} d\phi \tag{22}$$

where $\beta^2 + \alpha^2 = (\omega/c)^2$, ω is the angular frequency, α is constant, β is real, and $A(\phi)$ is an arbitrary complex function of ϕ.

These solutions are nonsingular and, like plane waves, have finite energy density rather than finite energy. They can have sharply defined intensity distributions as small as several wavelengths in every transverse plane, independent of propagation distance.

Chapter 3 Transducers and Image quality In medical Ultrasonic

In practice an array consists of individual sensors located at distinct spatial locations and thus sampling the wavefield spatially (an example acoustic field). There are three types of array transducers: *annular* array transducers and *one*- and *two-dimensional* array transducers. A one-dimensional array has its elements(sensors) arranged in a line, while a two-dimensional array consists of elements that are arranged in a plane and thus can scan and focus beams electronically in any plane. In this chapter we will take a look at different arrays such as linear phased array, linear switched array and the annular array. These arrays are commonly used in ultrasonic imaging. The factors that determine the image quality of a system and the effect of sidelobes on image quality will also be discussed.

3.1 A linear switched array

The linear switched array (***one-dimensional array***) is schematically shown in figure 3.1. This array is composed of a large number of elements in a line. The beam is stepped along by selecting a subset of the elements of each beam position. The ultrasonic beam generated by a switched linear array can be both steered and focused by adding a parabolic delay to each of the element channel. The linear arrays are usually *0.5* to *1 cm* wide and *2* to *10 cm* long with *64* to *256* elements and has a flat front producing a rectangular image format which is used for peripheral vascular imaging and some abdominal imaging [4].

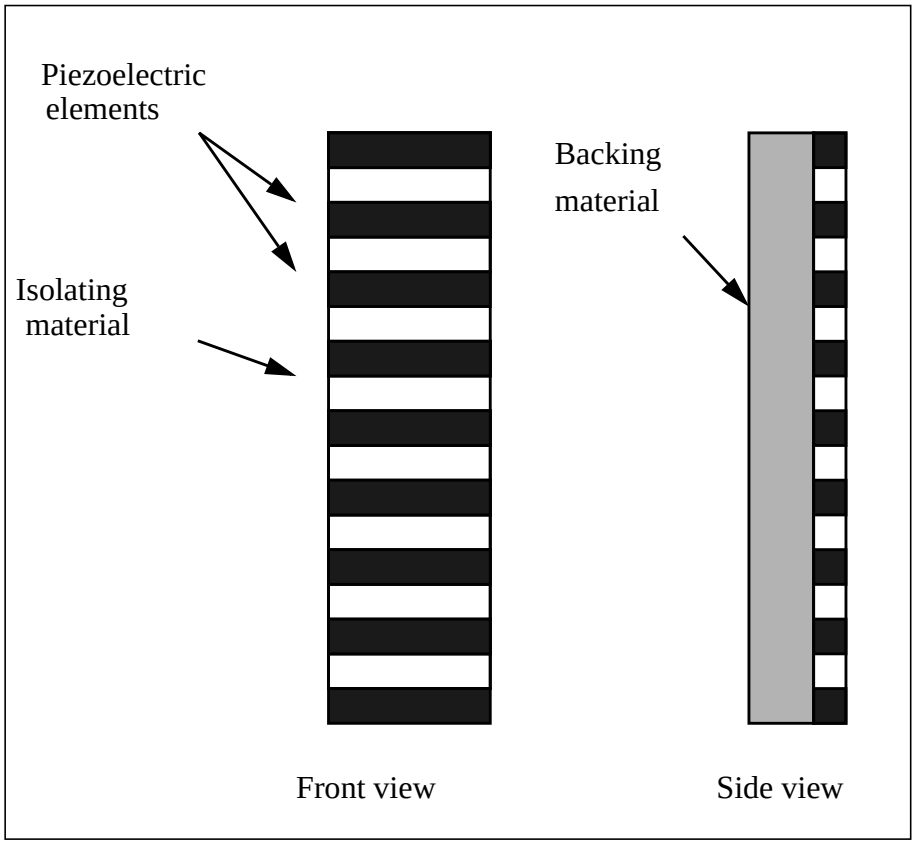

Figur 3.1: *Construction of linear array: a) front view; b) side view [14].*

The disadvantage of this array is its large aperture, which makes it unsuitable for applications where there is only a limited acoustic window such as cardiac examinations. Therefore, in these situations linear phased array systems, because of their small aperture, are preferred.

3.2 The linear phased array

The linear phased array is similar to switched linear array in construction, but is different in operation. A linear phased array is smaller than the switched one and usually contains fewer elements (*1 cm* wide and *1* to *3 cm* long, and *32* to *128* elements). The ultrasonic beam generated by phased array can be both focused and steered by properly delaying the signals going to the elements for transmission or arriving at the elements for receiving. Figure 3.2 *(a)* and *(b)* show how focusing and steering can be achieved with a five-element array.

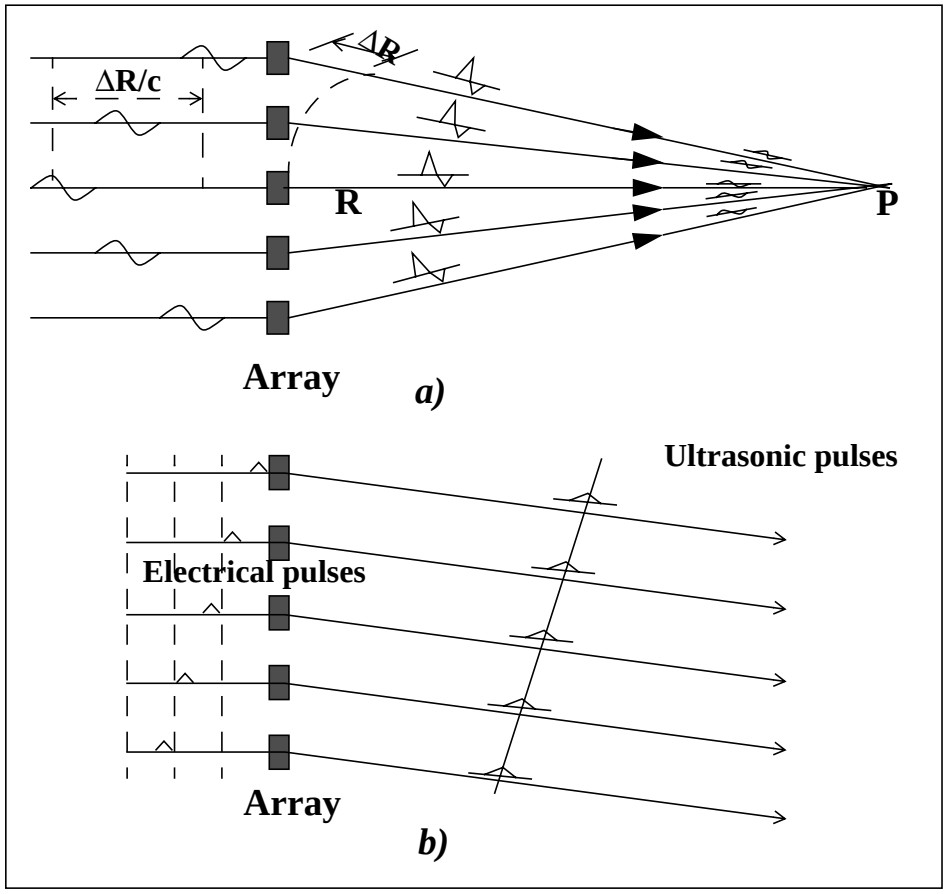

Figur 3.2: *a) Linear phased array focuses beam in transmission by appropriately delaying excitation pulses to different elements. b) Steering of beam produced by linear phased array [14].*

The pulse exiting the centre element is delayed by a time $\Delta R/c$ relative to the pulses exiting the elements on the perimeter, so that all ultrasonic pulses arrive at point *P* simultaneously.

The disadvantages of the phased arrays are their complexity and presence of gratin lobes in comparison to mechanical sector scanners.

3.3 Two-dimensional arrays

The major issue with *two-dimensional* arrays is the important improvement of the image quality of ultrasonic systems. Recall that linear arrays can be focused and steered only in one dimension i.e. beamwidth improvements are restricted in the so-called azimuth direction. Since they only have a signal element in the elevation

direction, they cannot be steered and focused in this direction. However, it is rather difficult for one-dimensional arrays to scan or focus beams electronically in an elevation plane of the arrays (a plane which is perpendicular to the scan plane that is defined by the line of elements and the size of the arrays).

This problem may be alleviated by using two-dimensional arrays. Two-dimensional arrays arrange elements in a plane (planar arrays figure 3.3) and thus can be both mechanically and electronically steered and focused.

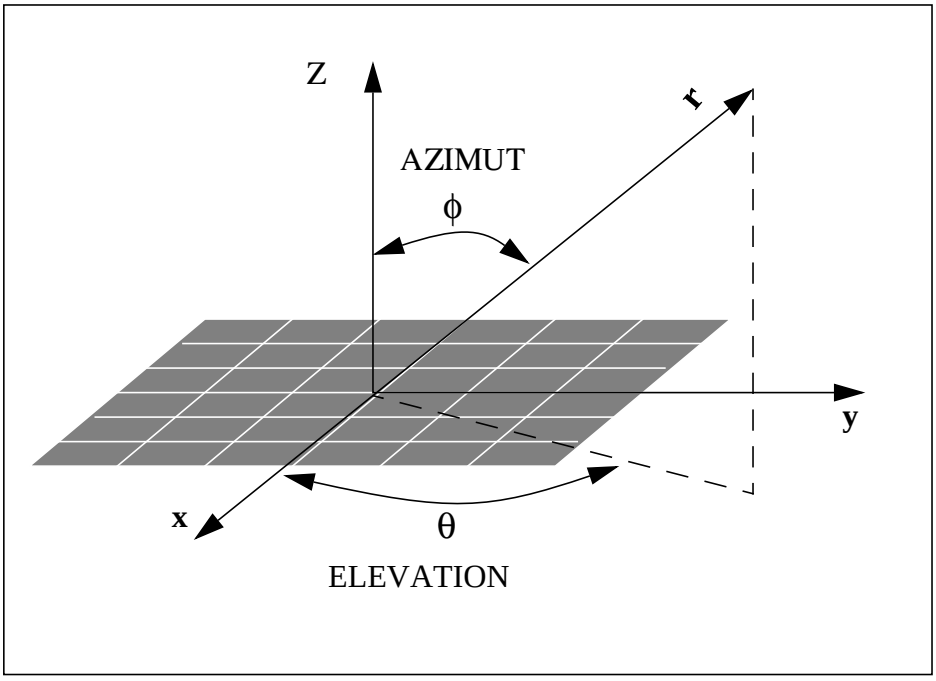

Figur 3.3: *A two-dimensional planar array both with cartesian and spherical coordinates given. The array could also be curved in both azimuth an elevation dimension e.g. in order to allow focusing [5].*

One of the disadvantages of the one- and two-dimensional scanning systems is that the area of the effective aperture of the arrays is reduced in the scan direction. As an example, use of two-dimensional array transducer for limited diffraction beams reduces the effective aperture size results in lower quality images in large steering angles [8]. But the major disadvantages of two-dimensional arrays are its great complexity, the large number of transducer elements, and the large amount of electronics which must be integrated on the transducer array. In fact an electronically scanned system can provide good range resolution as well as good transverse resolution.

Several examples of improvements due to the use of such arrays are suggested in [4], [7], [8].

3.4 Annular arrays transducers

There are several methods for increasing depth of focus of circular transducer without reducing the lateral beamwidth, such as:

- Axicon transducer [20]
- Dynamically focused transmission [17], [19]
- Dynamically focused reception [17], [19] for annular transducer or ring transducer [17]

The focus of this section is based on the latter method. The annular array (transducer) is an interesting method of electronically focusing. Annular transducer are composed of a set of concentric circular elements (rings) as illustrated in figure 3.4, where one obtains a steerable focus by individually delaying the signal to and from different elements.

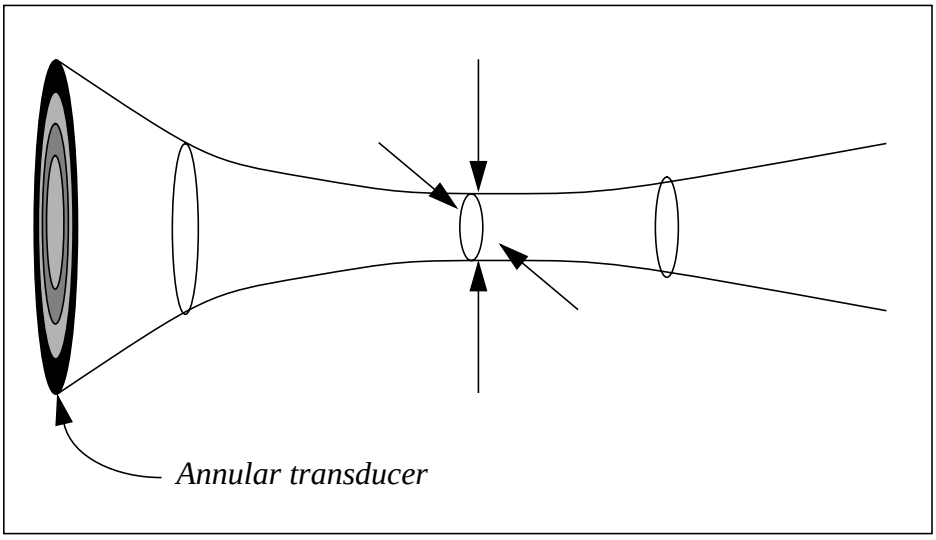

Figur 3.4: *Symmetric electronic focus in the plane and transverse to the plane of the beam with annular phased array.*

The beam steering is obtained by mechanical rotation of the transducer to make a sector image format.

The advantage of an annular transducer is that the electronic focusing is the same in all directions normal to the beam, i.e., focus is symmetric. This symmetric focus is only obtained with a phased annular array in contrast to the other arrays where electronic can only be obtained in the scan plane.

3.5 Image quality

The most important goal in biomedical ultrasound beamforming is to achieve “optimum image quality” such that the “best” clinical diagnosis can be obtained. In this section we will review some factors which control the quality of an image. These parameters are: lateral resolution, axial resolution, contrast resolution, and frame rate.

3.5.1 Lateral Resolution

The resolution is an important factor that determines the imaging quality of a ultrasound beamforming. The resolution transverse to the beam is called the *lateral resolution*, and is determined by width (main lobe width) of the beam (-6 dB beam width), as shown in figure 3.5 [27].

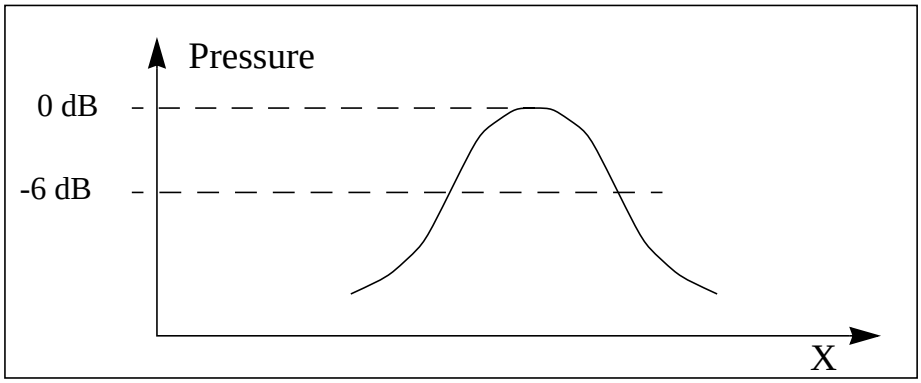

Figur 3.5: *The -6 dB lateral resolution or -6 dB beam width.*

3.5.2 Axial resolution or Range resolution

The ***axial resolution*** of a transducer is determined by the spatial extent of the transmitted ultrasonic pulse given by [27]:

$$r = \tau\frac{c}{2} \tag{23}$$

where is the time lag between transmission of a short pulse until we receive the reflected pulse from a target at range *r*, and *c* is the speed of sound in the tissue. The image range resolution determined by the length of the transmitted pulse is given by:

$$\Delta r = c\frac{\Delta T}{2} \tag{24}$$

where ΔT is the pulse length measured at -6 dB relative to the peak of the pulse envelope.

3.5.3 Contrast resolution

Another important factor affecting the quality of an image is contrast resolution. The level of sidelobes and multiple reflections (reverberation) of the ultrasound pulse create noise on the image and therefore limit the contrast resolution in the image. Clearly to obtain a good image with high quality, the level of sidelobes must therefore be kept the lowest possible.

3.5.4 Frame rate

The frame rate is the number of images per unit time [14]. The maximum frame rate, depth of image, and number of scan lines (or number of beams) per image are related by equation [14], [19]

$$R_f = \frac{1}{T} = \frac{1}{T_b N} = \frac{c}{2ND} \tag{25}$$

where R_f is the frame rate ($\sec^{-1}$) T is the time it takes to generate an image and is equal to the time per beam, T_b, multiplied by the number of beams, *N, D* is the depth of image (*m*), and c is speed of sound.

One can see from Eq. 25 that to achieve an improvement in one factor, one must sacrifice another factor. For example, to obtain larger image depth, either the frame rate or the number of beams must increase. Typically in a real-time ultrasonic image there are *128* lines [14]. For *19.5* cm depth we are able to obtain *30* frames per second, which is acceptable for cardiac imaging.

3.6 Effect of sidelobes on image quality

The sidelobe level is important in ultrasound beamforming because it dictates how well the transducer can respond to a wanted signal rather than to an interfering one.

The sidelobes of a beam have the shape of skirt around the mainlobe and pick up signals from many directions, including directions that are outside the image plane. The sidelobes may lower contrast in medical imaging affecting the detection of low scattering objects such as small cysts. The sidelobes also increase the effective sampling volume in tissue characterization. In addition, the sidelobes are a source of multiple scattering in nondestractive evaluation of materials.

There are several methods for reducing sidelobes level of a beam. As an example, the conventional technique for reducing sidelobe levels of a linear array is aperture apodization. This involves the use of aperture weighting functions, such as a Gaussian or Hanning functions, on the array elements. Using these sidelobe level reduction methods can be achieved at the expense of some loss in the lateral spatial resolution. Essentially, by reducing the energy under sidelobes, more energy is introduced under the mainlobe. Other methods are sidelobe reduction by using different size apertures on transmit and receive [20], and summation-subtraction method for reducing the sidelobes of limited diffraction beams [23].

3.7 Pulse echo systems

The ultrasonic diagnostic imaging systems are mostly operated in the pulse-echo mode. The transducer is used both for transmitting an ultrasonic pulse into the objects and receiving the return echoes from the objects. The pulse echo systems can be classified as *A*, *B*, or *M* modes.

3.7.1 A-Mode or Amplitude Mode

The oldest and simplest type of pulse-echo ultrasound instruments uses *A-mode* (amplitude mode). This is performed by transmitting an ultrasonic pulse into the object and the ultrasonic echoes received by the transducer are electronically interpreted and graphically displayed. The graphics displayed are either as a histogram or a spike pattern on the screen. A-mode has been used to accurately measure the axial length of the eye in order to calculate an intraocular lens power. All A-mode ultrasonography devices produce one-dimensional ultrasound waves when in axial alignment. These waves travel along the eye’s visual axis

until they meet a tissue surface. A portion of the wave is reflected at each tissue interface, i.e., cornea, anterior lens capsule, posterior lens capsule, retina and sclera. A portion of the sound wave continues to travel through the tissue until it meets the next tissue interface.

3.7.2 B-mode or Brightness mode

The B-mode (Brightness mode) ultrasonography is a two-dimensional approach. The primary use of B-scan ultrasonography is the diagnostic imaging of tissue structures.

The image displayed on the monitor is actually made up of over a hundred separate lines of information. At the beginning of the sweep of the transducer, a pulse is fired, the echo data is received along that line. The system plots the echo data along that line based on depth, which is calculated by the time it takes for the echo to return. The brightness of the echo is determined by the strength of the reflection. The transducer then moves over a fraction of a degree, and fires the next pulse. This process is continued until the image is built up line by line.

3.7.3 M-mode or Motion mode

In the M-mode the depth in tissue is displayed along the one axis while the other axis represent time. Imaging in M-mode will give a two-dimensional image with time as one of the axis. A beam is fired in a particular direction. The amplitude of the reflected or back-scattered waves are measured at a given number of depths. Then new beams are fired at the same direction and new echoes are received. By doing this repeatedly we get a real-time image of the moving structure in the beam direction [5].

Chapter 4 Field from circular transducer

For sound waves that have wavelengths comparable with the structures they meet, diffraction cause the wave to deviate from the straight-line propagation. Diffraction effects increase as the physical dimension of the aperture approaches the wavelength of the radiation. Diffraction of radiation results in interference that produces dark and bright rings, lines, or spots, depending on the geometry of the object causing the diffraction [13]. In this chapter we will discuss the field pattern of a unfocused and focused circular transducer and trade-off between some beam parameters, such as *lateral beamwidth, depth of focus* and *sidelobes*.

4.1 Huygens principle

The Huygens principle describes sound as spherical waves emanating from a source. Each point on the wavefront is considered to be a source of *secondary* spherical wavelets with appropriate *amplitude* and *phase*. The amplitude of the pressure field in front of the wavefront is the superposition of these wavelets, taking into account their relative amplitudes and phases. The amplitude of each wavelet is largest in the direction of the original wavefront's propagation and zero in the opposite direction. The position of the wavefront at some later time would correspond to the envelope of the radiation from the secondary sources [14].

To calculate the beam profile of an ultrasound transducer, one can consider the transducer surface to be made of an infinite number of point sources while a spherical wave is emitted by each point source.

4.2 The radiated field from a plane circular transducer

In this section we will discuss the field pattern of a circular transducer. Because of diffraction, the acoustic beam emitted from the transducer will increase its diameter with distance and the field components in the beam will exhibit fine structure vibration, both along its length and across its diameter. In the same manner as in optics, there are two distinct regions of interest, the *near-field* region, or *Fresnel* region, and the *far-field* region, or the *Fraunhofer* region. Within the Fresnel region, the outside diameter of the beam remains essentially uniform, the beam spreads beyond this region [16].

Basic principle of beamforming are given by *Rayleigh-Sommerfeld* diffraction formula. The formula can be interpreted in term of the Huygens principle of *secondary* sources, and can accurately predict the field at any spatial point produced by a finite aperture. Assum that the aperture is a circular transducer with the diameter *D=2a* [17].

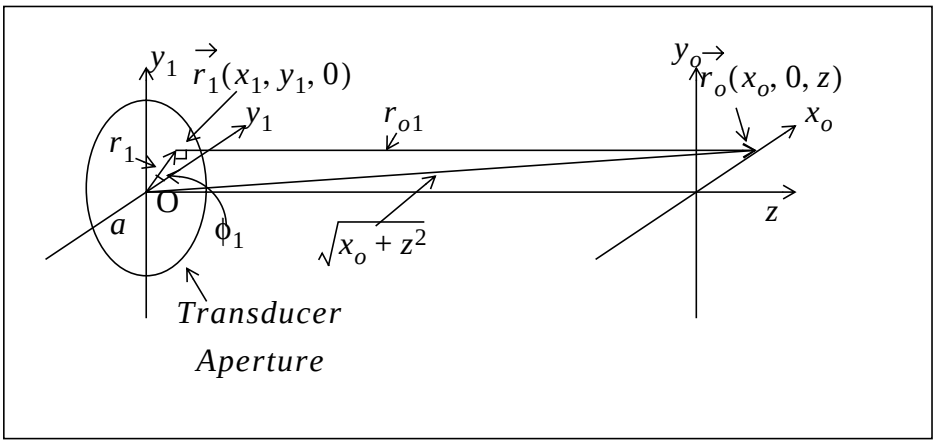

Figure 4.1: *Coordinate system used for Eq. 26 to calculate field in space. Wave sources are located on the surface of the transducer at plane z=0. Fields are calculated at spatial point* $\vec{r}_o$.

Let source point $\vec{r}_1$ on the surface of transducer be represented by the coordinates $\vec{r}_1 = (x_1, y_1, 0)$ and any spatial point $\vec{r}_o$ on the observation plane by $\vec{r}_o = (x_o, y_o, z)$ (see figure 4.1) then we have [17];

$$\tilde{\Phi}(r_o, \omega) = \frac{1}{i\lambda}\int_{0}^{a}\int_{-\pi}^{\pi} \tilde{\Phi}(\vec{r}_1, \omega)\frac{e^{ikr_{o1}}}{r_{o1}^2} z\, r_1 dr_1 d\phi_1 + \frac{1}{2\pi}\int_{0}^{a}\int_{-\pi}^{\pi} \tilde{\Phi}(\vec{r}_1, \omega)\frac{e^{ikr_{o1}}}{r_{o1}^3} z\, r_1 dr_1 d\phi_1 \quad (26)$$

The first and second term in Eq. 26 represent high and low frequency contributions, respectively. The parameters involved are:

r_{o1} : Distance between the aperture plane(z=0) and parallel observation plane containing the point $\vec{r}_o$, which is given by:

$$r_{o1} = \sqrt{(x_o - x_1)^2 + (y_o - y_1)^2 + z^2} \quad (27)$$

$\tilde{\Phi}(\vec{r}_o, \omega)$: The Fourier transform of the wave field $\Phi(\vec{r}_o, t)$, at the spatial point $\vec{r}_o$.

$\tilde{\Phi}(\vec{r}_1, \omega)$: The Fourier transform of a complex aperture weighting function, $\tilde{\Phi}(\vec{r}_1, t)$ applying at a source point $\vec{r}_1$ on the surface of the transducer

λ : wavelength

ω : angular frequency

f_o : frequency

k : wave number, $k = 2\pi/\lambda$

a : radius of aperture

From practical point of view, the *Rayleigh-Sommerfeld* diffraction formula is difficult to evaluate. The Eq. 26 is constituted two double integrals, and therefore its computation is usually time consuming.

The second term will approach zero as the value of r_{o1} increases well over $\lambda/2\pi$. This means that the second term can be negligible [17]. Then Eq. 26 becomes:

$$\tilde{\Phi}(r_o, \omega) = \frac{1}{i\lambda}\int_{0}^{a}\int_{-\pi}^{\pi} \tilde{\Phi}(\vec{r}_1, \omega)\frac{e^{ikr_{o1}}}{r_{o1}^2} z\, r_1 dr_1 d\phi_1 \quad (28)$$

4.2.1 Far-field or Fraunhofer region

The far-field applies when the observation plane is far away from the aperture, i.e. when [19], [17]:

$$r_{o1} \gg \frac{a^2}{\lambda} \tag{29}$$

4.2.2 Near-field or Fresnel region

The near-field region is the region between the far-field and the transducer. Thus for a plane circular transducer it is when [19], [17]:

$$r_{o1} \ll \frac{a^2}{\lambda} \tag{30}$$

4.3 The radiated field from a circular transducer on the plane $y_o = 0$

In this section we will use Eq. 27 and figure 4.1 to calculate the field at the spatial point $\vec{r}_o$. If we study the field on the plane $y_o = 0$, the distance between the source and field points will be simplified. As we illustrated in figure 4.1 one can find:

$$x_1 = r_1 \cos(\phi_1) \tag{31}$$

$$y_1 = r_1 \sin(\phi_1) \tag{32}$$

Substituting Eq. 31 and Eq. 32 into Eq. 28 gives:

$$r_{o1} = z\sqrt{1 + \frac{r_1^2}{z^2} + \frac{x_o^2}{z^2} - \frac{2x_o r_1 \cos(\phi_1)}{z^2}} \tag{33}$$

with the Fresnel approximation [3], [18] r_{o1} in denominators and in the phase of Eq. 28 can be approximated by:

$$r_{o1} \approx z \tag{34}$$

and

$$r_{o1} \approx \left(z + \frac{r_1^2}{2z} + \frac{x_o^2}{2z} - \frac{x_o r_1 \cos(\phi_1)}{z}\right) \tag{35}$$

respectively. Substituting Eq. 34 and Eq. 35 into Eq. 27, the field from a circular transducer at plane $y_o = 0$ under Fresnel approximation becomes:

$$\tilde{\Phi}(\vec{r}_o, \omega) = \frac{1}{i\lambda}\frac{e^{ik\left(z+\frac{x_o^2}{2z}\right)a}}{z}\int_0 \tilde{\Phi}_1(r_1, \omega)e^{ikr_1^2/(2z)} \cdot \left(\int_{-\pi}^{\pi} e^{-i\frac{kx_o r_1 \cos\phi_1}{z}} d\phi_1\right) r_1 dr_1 \tag{36}$$

As it can be seen, the above equation have two integral. To simplify this equation the Bessel function is employed [21]:

$$J_o(z) = \frac{1}{2\pi}\int_{-\pi}^{\pi} e^{iz\cos\phi} d\phi \tag{37}$$

where $J_o(z)$ is a Bessel function of the first kind of zeroth-order. Then Eq. 36 becomes:

$$\tilde{\Phi}(\vec{r}_o, \omega) = \frac{2\pi}{i\lambda}\frac{e^{ik\left(z+\frac{x_o^2}{2z}\right)a}}{z}\int_0 \tilde{\Phi}_1(r_1, \omega)e^{ikr_1^2/(2z)} \cdot \left(J_o\left(\frac{kx_o r_1}{z}\right)\right) r_1 dr_1 \tag{38}$$

4.4 Field of unfocused circular transducer

In this section we will use the result of section 4.3, to calculate the field of unfocused circular transducer. For an unfocused circular transducer, the surface of the transducer is uniformly weighted:

$$\tilde{\Phi}_1(r_1, \omega) \equiv 1 \tag{39}$$

Substituting Eq. 39 into Eq. 38 we have:

$$\tilde{\Phi}(\vec{r}_o, \omega) = \frac{2\pi}{i\lambda}\frac{e^{ik\left(z+\frac{x_o^2}{2z}\right)a}}{z}\int_0 e^{ikr_1^2/(2z)} \cdot \left(J_o\left(\frac{kx_o r_1}{z}\right)\right) r_1 dr_1 \tag{40}$$

In the far-field of the transducer, where $r_{o1} \approx z$ and $z \gg kr_1^2/2$ then the quadratic phase factor in Eq. 40 is approximately one over the entire aperture [18]:

$$e^{ikr_1^2/(2z)} \approx 1 \tag{41}$$

then Eq. 40 becomes:

$$\tilde{\Phi}(\vec{r}_o, \omega) = \frac{2\pi e^{ik\left(z + \frac{x_o^2}{2z}\right)a}}{i\lambda z} \int_0 \left(J_o\left(\frac{kx_o r_1}{z}\right)\right) r_1 dr_1 \tag{42}$$

using the relation $\int zJ_0(z)dz = zJ_1(z)$, where $J_1(z)$ is a first-order Bessel function of the first kind [19], we obtain the result [17]:

$$\tilde{\Phi}(\vec{r}_o, \omega) = \frac{ka^2}{iz} e^{ik\left(z + \frac{x_o^2}{2z}\right)} \left(\frac{2J_1((kx_o a)/z)}{kx_o a/z} \right) \tag{43}$$

Defining the jinc(X) function as:

$$jinc(X) = \frac{2(J_1(\pi X))}{\pi X} \tag{44}$$

we can write Eq. 43 as:

$$\tilde{\Phi}(\vec{r}_o, \omega) = \frac{ka^2}{iz} e^{ik\left(z + \frac{x_o^2}{2z}\right)} \left(jinc\left(\frac{2ax_o}{\lambda z}\right)\right) \tag{45}$$

Thus the beam intensity becomes:

$$\left|\tilde{\Phi}(\vec{r}_o, \omega)\right| = \left(\frac{ka^2}{z}\right)^2 \left(jinc^2\left(\frac{2ax_o}{\lambda z}\right)\right) \tag{46}$$

The *jinc* function is plotted in figure 4.2. The first zero of $\left|\tilde{\Phi}(\vec{r}_o, \omega)\right|$ along the radius is at [17]:

$$x_o = 1.22\frac{\lambda z}{2a} \tag{47}$$

where x_o represents half of the main beamwidth of the unfocused circular transducer.

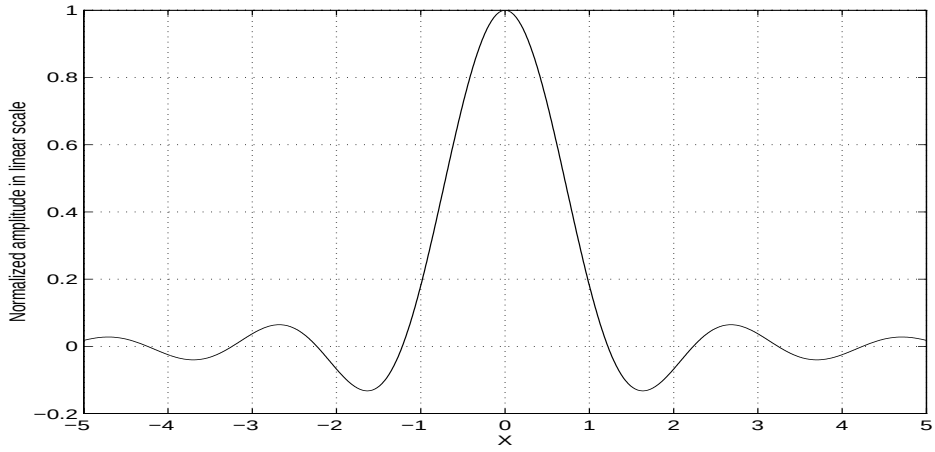

Figure 4.2: *$jinc(x)$ for the circular transducer where $X = 2ax_o/(\lambda z)$*

4.4.1 Field of unfocused circular transducer on centre axis

For the field on centre axis ($x_o = 0$) Eq. 40 becomes:

$$\tilde{\Phi}(\vec{r}_o, \omega) = \frac{1}{i\lambda}\frac{e^{ikz}}{z} \cdot \int_0^a e^{ikr_1^2/(2z)} r_1 dr_1 \tag{48}$$

Substitute $u = ikr_1^2/(2z)$, so that $du = (ikr_1/z)dr_1$ then we have $r_1 dr_1 = (z/(ik))du$ and hence we obtain:

$$\tilde{\Phi}(\vec{r}_o, \omega) = e^{ikz}\left(1 - e^{ik\frac{a^2}{2z}}\right) \tag{49}$$

and the absolute value of Eq. 49 becomes:

$$\left|\tilde{\Phi}(\vec{r}_o, \omega)\right| = U(z) = \sqrt{2 - 2\cos\left(\frac{ka^2}{2z}\right)} \tag{50}$$

The approximate intensity from Eq. 50 as a function of $S = (z\lambda/a^2)$ on the centre axis, is shown in Figure 4.3 where *S* is a Fresnel parameter. Beyond the region *S<1* or $z < a^2/\lambda$ (the near-field region) the beam is confined within its original diameter. For *S>1* or $z > a^2/\lambda$ (far-field region) the beam drops steadily until zero at $S \to \infty$.

The point where *S=1*, is the crossover point between the *near-field* and the *far-field.* The maximum field on centre axis (Rayleig distance) of an unfocused transducer becomes [16]:

$$Z_{o_{max}} = \frac{2a^2}{\lambda} \tag{51}$$

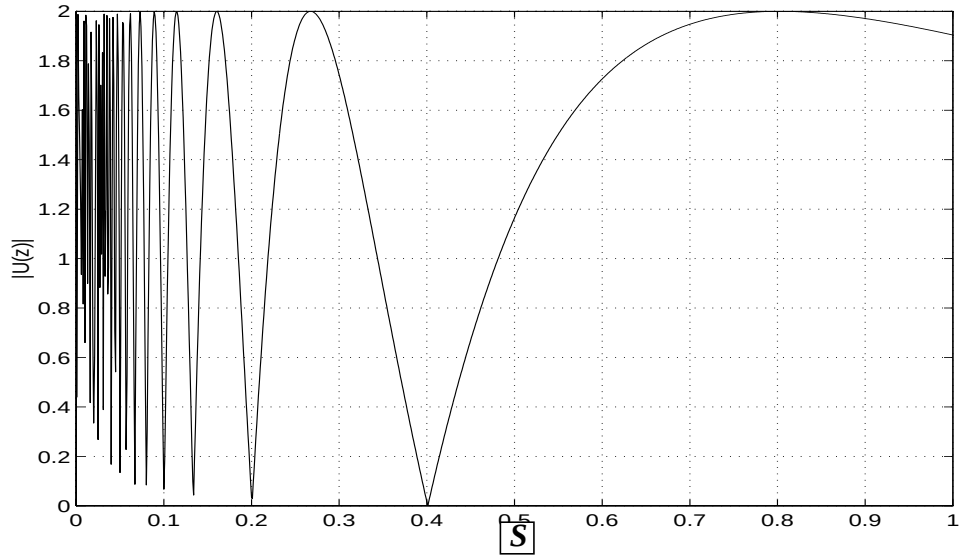

Figure 4.3: *Field of unfocused transducer on centre axis* $x_o = 0$ *Eq. 50 as a function of S where* $S = (z\lambda/a^2)$.

Figure 4.4 shows the schematic pressure profile from an unfocused circular transducer. Usually in the far-field region, the distance between two points where the pressure drops to *-3dB (see section 4.5.2,)* of the maximal value is defined as beamwidth or main lobe width. The 3dB definition beamwidth for an unfocused circular transducer is approximately the same as the diameter of the transducer.

$$D_{unfocused}(3dB) = 2a \tag{52}$$

As z becomes greater than z_o (after the Rayleigh distance), the beam starts to diverge. The angle of divergence can be calculated approximately using the following formula [14], [19]:

$$\sin(\theta) = 1.22\frac{\lambda}{2a} \tag{53}$$

The first zero or the angle at which the main lobe becomes zero occurs at:

$$\theta = \sin^{-1}(1.22\lambda/2a) \tag{54}$$

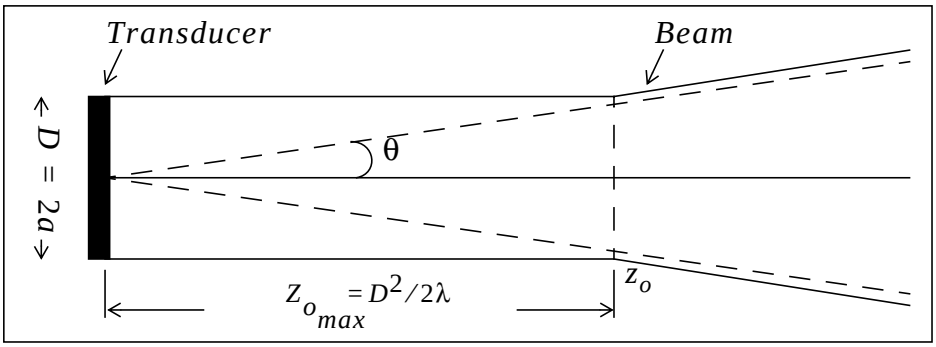

Figure 4.4: *Pressure profile of an unfocused circular transducer. The beam has spreading within the near-field region and has a beamwidth about as wide as the diameter of transducer. In the far_field region the beam spreads out at an angle* $\theta = \sin^{-1}(1.22\lambda/2a)$.

Figure 4.5 shows the contour plot of the acoustic field of the unfocused circular transducer along the propagation axis (central axis). The aperture has a diameter of *D=15 mm* with a centre frequency of *3.5 MHz (*λ*=.44 mm).* The distance $z_{max} = D^2/(2\lambda)$ along the transducer axis to the start of the far-field region is about 255.6 mm.

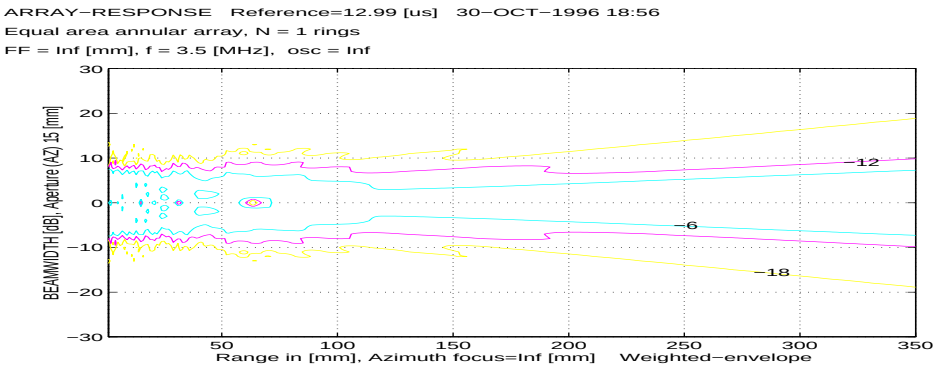

Figure 4.5: *Normalized contour plot showing -6, -12, -18dB contours for an unfocused circular transducer.*

4.5 Focused circular transducers

As we discussed in section 4.3, the beam emitted from an unfocused transducer spreads radially due to diffraction, and has a very large beamwidth. Therefore, we often employ a focused acoustic beam, as in optics, to obtain good transverse definition and high acoustic beam intensity at a point of interest.

As in optics, we can use lenses to focus the acoustic beam. But often the simplest way to obtain a focused acoustic beam is to use a spherically shaped transducer. Such a transducer will produce a focused beam near its centre of curvature. We normally focus the beam to a spot smaller then the transducer diameter, thus obtaining a beam intensity much higher then that at the transducer itself. In this section we will use the Rayleigh-Sommerfeld integral to calculate the field of a focused circular transducer.

4.5.1 Spherical focused transducer

We consider a spherical transducer with a diameter of $D=2a$ and a radius of curvature F,(focal length) as illustrated in figure 4.5. We shall use Fresnel approximation to treat the properties of the beam emitted from the transducer.

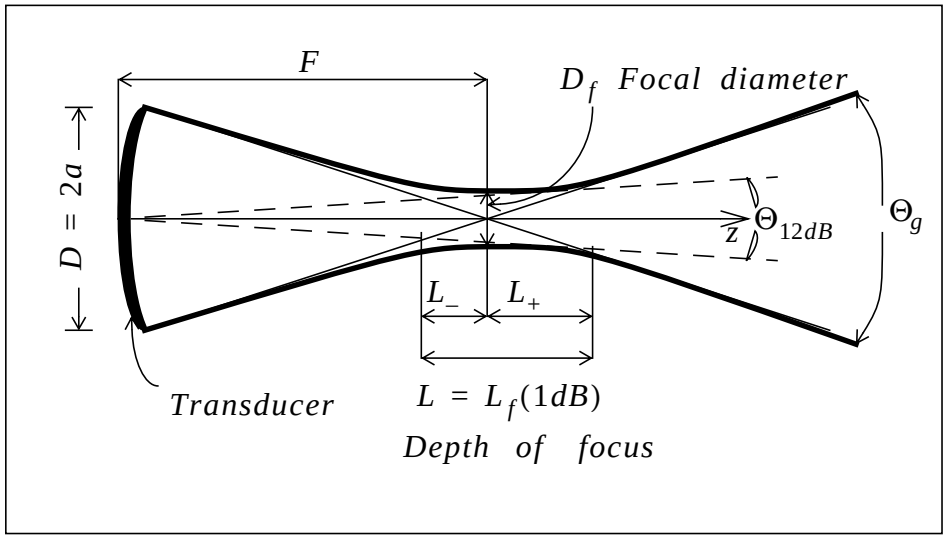

Figure 4.6: *Pressure profile of a spherical focused circular transducer. For $F < D^2/(2\lambda)$ (Fresnel zone) or $S < 1$ we get $\Theta_f < \Theta_g$ (efficient focusing).*

The field of focused circular transducer can be calculated by Eq. 38 For a focused circular transducer, the surface of transducer is weighted by following weighting function [17] that is a spherical shifter along the radial distance, r_1 :

$$\tilde{\Phi}_1(r_1, \omega) = e^{-ik(\sqrt{F^2 + r_1^2} - F)} \tag{55}$$

Substituting Eq. 55 into Eq. 38 and when *z=F, i.e. field in focal plane,* we have:

$$\tilde{\Phi}(\vec{r}_o, \omega) = \frac{2\pi e}{i\lambda} \frac{e^{ik\left(F + \frac{x_o^2}{2F}\right)a}}{F} \int_0 e^{-ik(\sqrt{F^2 + r_1^2} - F)} e^{ikr_1^2/(2F)} \cdot \left(J_o\left(\frac{kx_o r_1}{F}\right)\right) r_1 dr_1 \tag{56}$$

with the Fresnel approximation, in which:

$$F^2 \gg a^2 \tag{57}$$

one has:

$$(\sqrt{F^2 + r_1^2} - F) \approx \frac{r_1^2}{2F} \tag{58}$$

Then Eq. 56 can be written as:

$$\tilde{\Phi}(\vec{r}_o, \omega) = \frac{ka^2}{iF} e^{ik\left(F + \frac{x_o^2}{2F}\right)} \left(\frac{2J_1((kx_o a)/F)}{kx_o a/F}\right) \tag{59}$$

Thus the beam intensity at the plane $z=F$ varies as:

$$\left|\tilde{\Phi}(\vec{r}_o, \omega)\right| = \left(\frac{ka^2}{F}\right)\left(jinc^2\left(\frac{x_o a}{\lambda F}\right)\right) \tag{60}$$

The variation of the beam intensity at the focal plane is exactly the same in form as that in the Fraunhofer region for a plane circular transducer at $z=F$. However, the beam intensity can now be chosen at will and can also be much larger than at the transducer itself, which changes the scales of the axial and radial variations of the field.

4.5.2 The lateral beamwidth in the focal plane of a focused circular transducer (focal diameter)

The lateral beamwidth in the focal plane of a focused circular transducer is determined by the width of the mainlobe of the beam. If the beam has zeroes located symmetrically about the mainlobe, the peak-to-zero distance can serve as one measure of the width.

The absolute value of Eq. 59 (field of focused circular transducer) is shown in figure 4.7 in dB scale. The peak-to-zero distance in this figure along the radius is at:

$$x_o = 1.22\frac{\lambda F}{2a} = 1.22\lambda FN \tag{61}$$

where x_o represents half of the main beamwidth of the focused circular transducer and where we call *FN=F/2a* the *F-number* of a transducer.

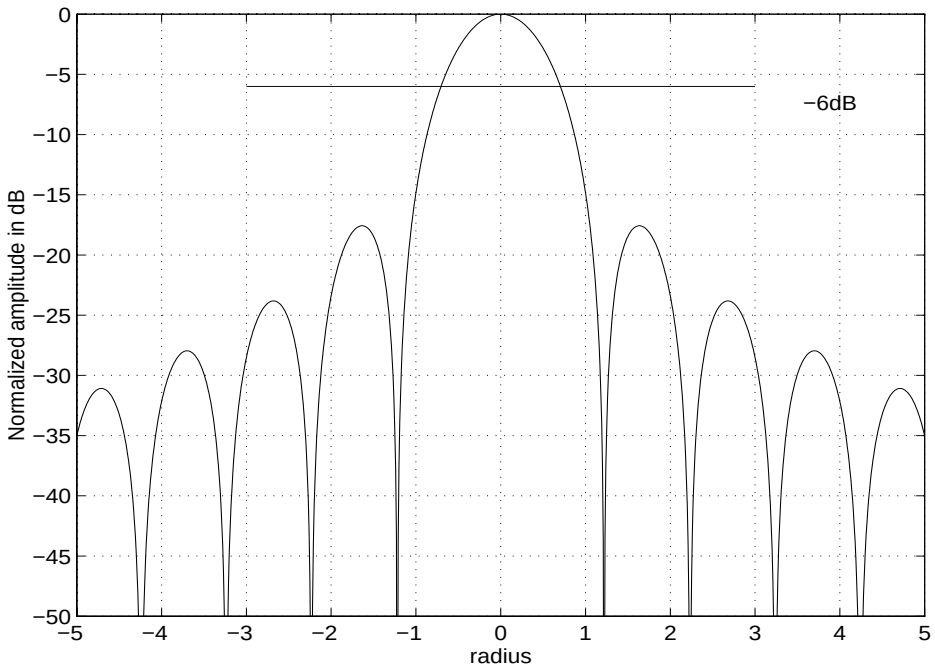

Figure 4.7: *jinc(X) for the circular focused transducer in dB scale where* $X = kax_o/F$. *The -6dB value of* k_x *obtained from this figure is about 1.5 mm and peak-to-zero distance is about 1.219 mm.*

The focal diameter (lateral beamwidth) D_f for *XdB* definitions of the beamwidth becomes:

$$D_f\,(XdB) = k_x\frac{\lambda F}{2a} \tag{62}$$

As shown in figure 4.7 the beam diameter at *-6dB* point is:

$$D_f\,(6dB) = 1.44\frac{\lambda F}{2a} \tag{63}$$

The values of k_x for different values of *X* (obtained from figure 4.7) are given in table 4.1.

XdB	1	3	4	6	10	12
kx	0.63	1.0	1.18	1.44	1.8	2

Table 4.1: *Corresponding values of* k_x *for different values of XdB.*

4.5.3 Depth-of-focus for a focused circular transducer

In this section we will find a simple approximation for the depth-of-focus of the circular transducer. Depth of focus is defined as the region around the focal point where the beam diameter is limited by diffraction. (see figure 4.6).

Within the limit $F \ll a^2/\lambda$ or $S \ll 1$ (i.e., deep in the Fresnel zone), we can use this limit to define a depth-of-focus (L_f) as the distance between the points where the field on axis is *kdB* less then that at focal point. We return to equations 38 and 58 , by substituting Eq. 58 into Eq. 38. Where $z \neq F$ and $x_o = 0$ we have:

$$\tilde{\Phi}(0, \omega) = \frac{ke^{ikz}}{iz} \int_0^a e^{ik\frac{r_1^2}{2F}\left(\frac{F}{z}-1\right)} (r_1\, dr_1) \tag{64}$$

Equation 64 can then be integrated directly to yield:

$$\tilde{\Phi}(0, \omega) = \frac{ke^{ikz}}{iF} e^{ik\frac{a^2}{4F}\left(\frac{F}{z}-1\right)} \frac{F}{z} \sin c\left(\frac{1}{2S}\left(\frac{F}{z}-1\right)\right) \tag{65}$$

where *sinc(X)=sin*$\pi X/\pi X$ and $S = \lambda F/a^2$.

We shall assume that the beams intensity is proportional to $\left|\Phi(\omega)^2\right|$. Then we have:

$$I(z) = \left(\sin c\left(\frac{1}{2S}\left(\frac{F}{z}-1\right)\right)\right)^2 \tag{66}$$

We can now define the depth-of-focus around the fixed focus *F* by the points along *z* where the intensity has dropped *kdB* from the maximum possible value at that location. Let a_k define the point where $\sin c(a_k/2)$ has dropped *kdB* from its maximum value for $a_k = 0$. Thus the *kdB* points occur where:

$$z - F = \pm a_k \frac{F^2\lambda}{a^2} \tag{67}$$

Thus a simple approximation for the depth-of-focus is:

$$L_f(kdB) = 2a_k \frac{F^2\lambda}{a^2} = 2a_k FS \tag{68}$$

One can rewrite Eq. 68 as:

$$L_f(kdB) = 8a_k\lambda\left(\frac{F}{2a}\right)^2 \tag{69}$$

where we can employ *F-number* $F_N = F/2a$ to give:

$$L_f(kdB) = 8a_k\lambda(F_N)^2 \tag{70}$$

In figure 4.8 we have plotted *sinc* function as a function of a_k to find the different values of a_k where the $\sin c(a_k/2)$ has dropped *kdB* from its maximum value for $a_k = 0$.

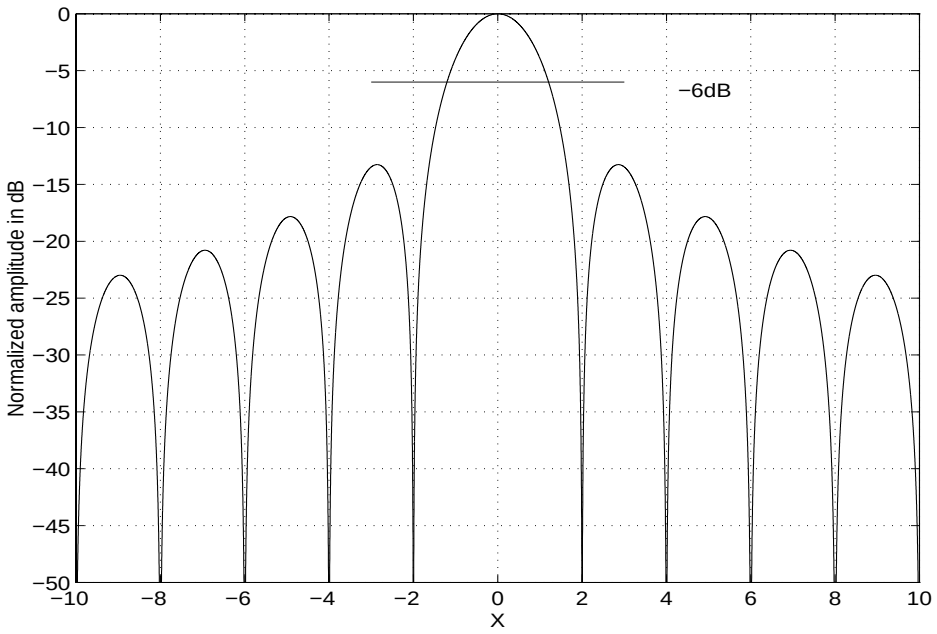

Figure 4.8: *The sinc function as function of* a_k.

The depth of focus at 6dB points (i.e., $a_{6dB} = 1.21$) obtained from this figure is:

$$L_f(6dB) = 9.68\lambda(F_N)^2 \tag{71}$$

The values of a_k for different values of *k* are given in table 4.2.

XdB	1	3	4	6	10	12
a_k	0.51	0.89	1.0	1.21	1.47	1.6

Table 4.2: *The values of* a_k *for different values of k that are obtained from figure 4.8.*

4.5.4 Geometrical interpretation of the depth of focus

The relation for depth-of-focus can be illustrated geometrically. As shown in figure 4.6, the beam profile converges along its geometrical optic path (a cone) but diverges from this path near the focus. In order to define the opening angle of the cone, we must specify the intensity drop from the axis that defines the beam. For a circular transducer we get the following dual sided opening angle:

$$\Theta_f = 2\theta_f = k_x \frac{\lambda}{D} \tag{72}$$

where θ_f is the single sided opening angle of the beam. In the following we use the *12dB* (From table 4.1 $k_x = 2$) opening angle of the beam which is:

$$\Theta_f = 2\frac{\lambda}{D} \tag{73}$$

Referring to figure 4.6 we see that the geometrical opening angle of the focused beam is:

$$\Theta_g = \frac{D}{F} \tag{74}$$

The Fresnel parameter for a focused circular transducer is defined as:

$$S = \frac{\lambda F}{a^2} \tag{75}$$

This parameter can be expressed by the diffraction and geometrical angles Eq. 73 and Eq. 74 respectively, then we have:

$$S = 2\frac{\Theta_f}{\Theta_g} \tag{76}$$

For efficient focusing of the beam, the geometrical opening angle Θ_g must be larger than the diffraction angle Θ_f. When $S<<1$, it therefore follows from Eq. 76 that:

$$\Theta_f \ll \Theta_g \tag{77}$$

For $S=2$ we get $\Theta_f = \Theta_g$, which gives $F = D^2/(2\lambda)$ which is the boundary between Fresnel and Fraunhofer regions for the plane circular transducer.

Defining L_- and L_+ as the distance from the focus (focal point) to the intersection between the geometrical boundary of the focused beam and the *12 dB* diffraction cone as illustrated in figure 4.6 then we have:

$$L_- = \frac{\Theta_f}{\Theta_g + \Theta_f} F \qquad L_+ = \frac{\Theta_f}{\Theta_g - \Theta_f} F \tag{78}$$

and

$$L = L_- + L_+ = \frac{2\Theta_f \Theta_g}{\Theta_g^2 - \Theta_f^2} F \tag{79}$$

Substituting Eq. 76 into Eq. 79 then we have:

$$L = \frac{S}{1 - (S/2)^2} F \tag{80}$$

As we have discussed above we should have $S<<1$, then Eq. 80 becomes:

$$L = L_f(1dB) = SF \tag{81}$$

Thus the intersection between the geometric beam definition and the *12dB* diffraction opening cone defines the *1dB* depth-of-focus.

The contour plot of the acoustic field for spherically focused circular transducer with a central frequency of *3.5 MHz* is shown in figure 4.8 The transducer has a diameter of *15 mm* and *4* annular elements, see section 3.4, when each element has the same area i.e., equal-area transducers. The transducer is focused at 75 mm away from the transducer centre (fixed focus *F=75 mm*), and the Fresnel parameter obtained from Eq. 75 is *S=0.59*. The *3-dB* depth-of-focus and *6-dB* beamwidth obtained from this figure are *79.2 mm* and *3.102 mm* respectively.

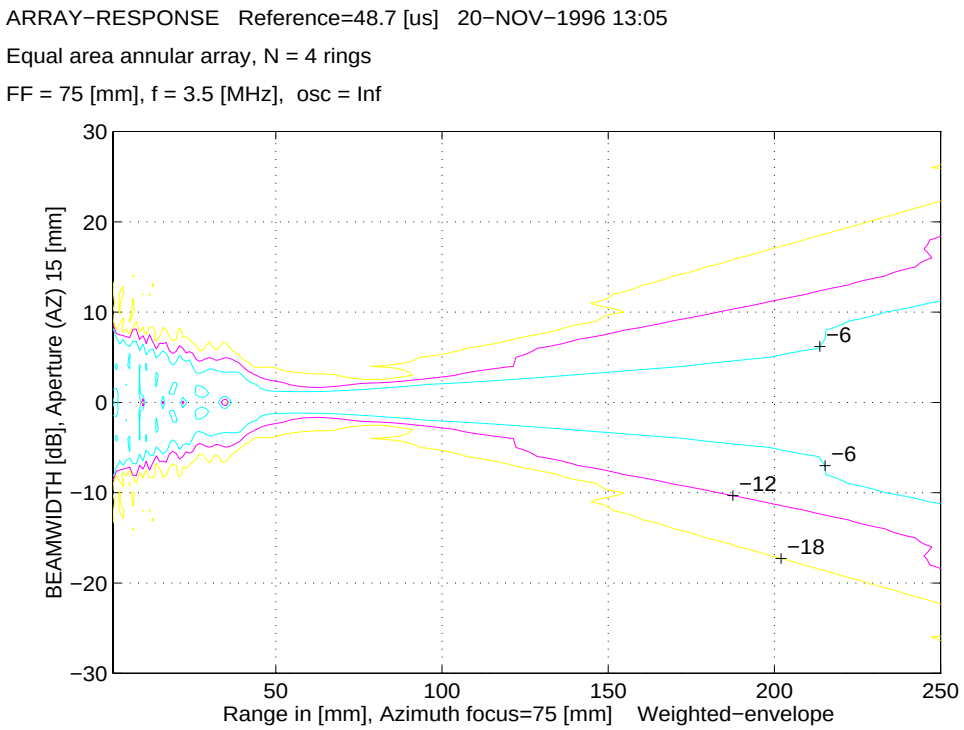

Figure 4.9: *Normalized contour plot showing -6, -12, -18dB contours for spherically focused circular transducer.*

The lateral beamwidth and the depth of focus of circular transducer are related to each other. This relation is demonstrated by Eq. 62 and Eq. 70 One can see from these equations, that for a given central wavelength,λ, to increase the depth of focus in the focal plane, the effective F-number,*FN*, must be increased. However, this increases the lateral beamwidth. Furthermore, for a given effective F-number, the diffraction of focused circular transducer is stronger as the central wavelength increases. This increases the lateral beamwidth and the depth of focus. Therefore, to obtain higher resolution in diagnostic ultrasound imaging, high frequency (small central wavelength) is desirable. However, the highest frequency used must be limited by the penetration depth of ultrasound in biological soft tissues in which higher frequencies have larger attenuation [17].

4.5.5 Sidelobes of a focused circular transducer

In this section we will describe the sidelobe of a focused circular transducer. The sidelobes of the beam have the shape of skirts around the main lobe, and will pick up signals from any direction, including directions that are outside the image plane. The sidelobes level is important because it dictates how well the transducer can respond to a wanted signal rather than to an interfering one.

Figure 4.10 (the same values as in figure 4.9) shows the one-way beam profile at *75 mm* depth of circular transducer which is discussed in above section. The first sidelobe is at $r = 0.82F\lambda/a$, and is 1*7.67dB* lower in amplitude than the mainlobe.

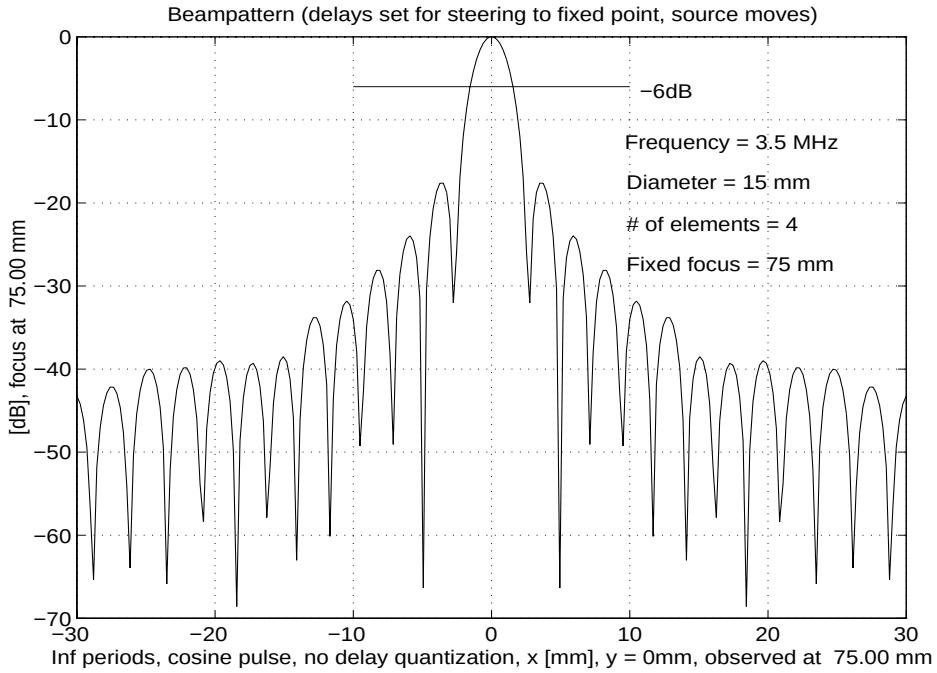

Figure 4.10: *One-way response for focused circular transducer with fixed focus at 75 mm.The 6-dB beamwidth obtained from figure is about 3.10 mm and the amplitude of the first sidelobe is about 17.67dB lower than the mainlobe.*

To reduce the sidelobe of focused circular transducer, various forms of the aperture weighting functions $\tilde{\Phi}(\vec{r}_1, \omega)$, of Eq. 26 can be applied. An example is the Hanning-weighting function [15]. By weighting (appodization) of the excitation amplitude over the transducer surface the width of the mainlobe increases, but the amplitude of the sidelobes decreases. The effective aperture size of the Hanning weighted transducer is smaller than that of the circular focused transducer with the

same radius. The reduced effective aperture size of the Hanning weighted transducer increases the mainlobe width in the focal plane [17]. Therefore, the lower sidelobes gained by the Hanning beam are at the expense of the lateral beamwidth.

In figure 4.11 we have plotted the beam profile of the same transducer as in figure 4.10 but the aperture weighting function is a Hanning window. For comparison, nonappodizeid beam (as shown in figure 4.10) is also shown. The lateral beamwidth obtained from Hanning beam is about *4.6 mm* and the first sidelobe is *25dB* lower in amplitude than the mainlobe. Therefore, the lower sidelobes are achieved at the expense of larger lateral beamwidth.

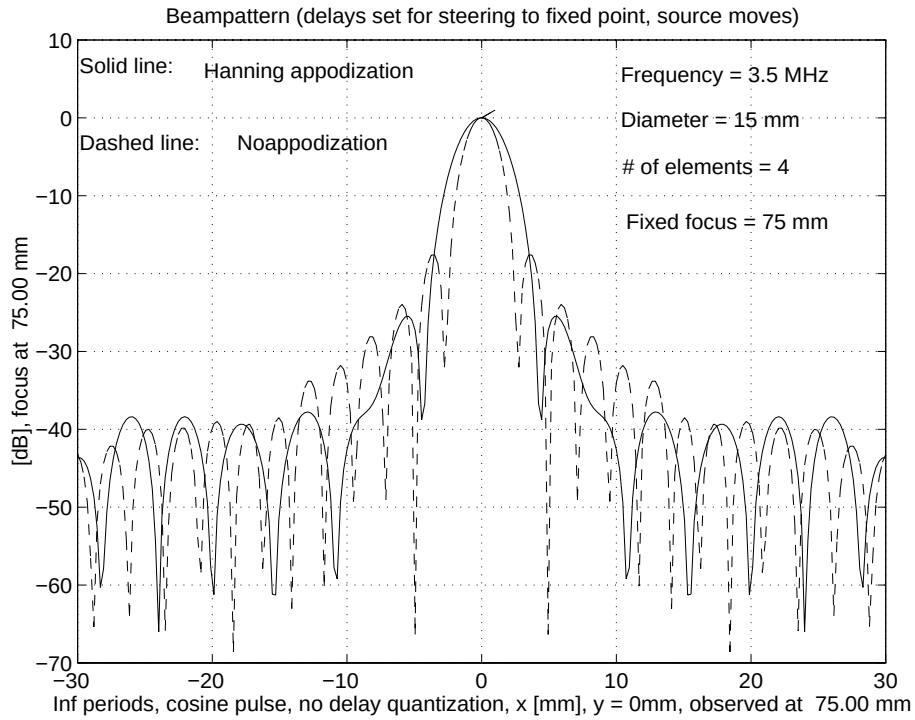

Figure 4.11: *One-way response for focused circular transducer with fixed focus at 75 mm. Solid line Hanning weighted, the -6dB beamwidth obtained from figure is about 4.6 mm and the amplitude of the first sidelobe is about 25dB lower than the mainlobe. Dashed line nonappodizeid transducer, the -6dB beamwidth obtained from figure is about 3.10 mm and the amplitude of the first sidelobe is about 17.6dB lower than the mainlobe.*

Chapter 5 Limited diffraction beams

We begin this chapter by reviewing Limited diffraction beams and describing the trade-off between some beam parameters, such as *resolutions, sidelobes, aperture* and *depth of field*.

Diffraction is one of the phenomena of physics. For sound waves that have wavelengths comparable with the structures they meet, diffraction can cause the wave to deviate from straight-line propagation.

The *Limited diffraction* beams are represented by a class of solutions to the isotropic/homogeneous scalar wave equations [10], [11], [12]. Theoretically, these beams can be produced by using infinite aperture and energy, and they can propagate without spreading [9]. This implies that limited diffraction beams would propagate to an infinite distance without spreading. In practice, however, limited diffraction beams can only be approximated over large depth of field by employing finite size transducer and finite energy. Because of these features, limited diffraction beams may have applications in medical imaging [17].

5.1 Theoretical Limited diffraction Beams

Limited diffraction beams also termed Bessel beams can be obtained from Eq. 22. If $A(\phi)$ is independent of ϕ, one can obtain the *nth-order* Bessel beam [10]:

$$p_n(\vec{r}, t) = J_n(\alpha r)e^{i(\beta z - \omega t + n\phi)} \qquad n = 0, 1, 2, 3\ldots \tag{82}$$

Where n is an integer. If $n = 0$, J_o is the *zeroth-order* Bessel function of the first kind [21], [22], and $r = \sqrt{x^2 + y^2}$ is the distance away from the centre axis of the transducer, β the propagation constant and is real, α is the scaling factor that controls the lateral resolution of Bessel beams. Substituting Eq. 82 in Eq. 21, we have:

$$\begin{aligned}
&\left(\frac{1}{r^2}\frac{\partial}{\partial r}\left(r^2\frac{\partial}{\partial r}\right) + \frac{1}{r^2}\frac{\partial^2}{\partial \phi^2} + \frac{\partial^2}{\partial z^2} - \frac{1}{c^2}\frac{\partial^2}{\partial t^2}\right)p_n(\vec{r}, t) \\
&\quad = e^{i(\beta z - \omega t + n\phi)}\frac{1}{r}\frac{\partial}{\partial r}\left(r^2\frac{\partial}{\partial r}J_n(\alpha r)\right) \\
&\quad + J_n(\alpha r)e^{i(\beta z - \omega t)}\frac{1}{r^2}\frac{\partial^2}{\partial \phi}e^{in\phi} \\
&\quad + J_n(\alpha r)e^{in}\left(\frac{\partial^2}{\partial z^2} - \frac{1}{c^2}\frac{\partial^2}{\partial t^2}\right)e^{i(\beta z - \omega t)} \\
&\quad = \left(\left(\frac{n^2}{r^2} - \alpha^2\right) + \left(-\frac{n^2}{r^2}\right) + \left(\frac{\omega^2}{c^2} - \beta^2\right)\right)p_n(\vec{r}, t)
\end{aligned} \tag{83}$$

since

$$\beta^2 = \frac{\omega^2}{c^2} - \alpha^2 \tag{84}$$

the right side of Eq. 83 is zero, i.e., Eq. 82 is an exact solution of Eq. 21.

One can express Eq. 82 in the form of a *non-rotating* Bessel beam [23], by replacing $e^{in\phi}$ with $\cos n(\phi - \phi_o)$, then the *non-rotating* Bessel beam of order n becomes:

$$p_n(\vec{r}, t) = J_n(\alpha r)e^{i(\beta z - \omega t)}\cos n(\phi - \phi_o) \qquad n = 0, 1, 2, 3\ldots \tag{85}$$

where ϕ_o is an initial azimuthal angle of the beam at the plane $z = 0$.

We have shown that Eq. 82 is an exact solution to Eq. 21. In the same way one can show that Eq. 85 is also a solution to Eq. 21.

When $\alpha = 0$ and $n = 0$ the solutions to Eq. 82 or Eq. 85 are simply plane waves, but for $0 < \alpha \le \omega / c$ the solution to Eq. 82 or Eq. 85 represents a nondiffracting beam because it has the same intensity distribution $J^2{}_o(\alpha r)$ in every plan normal to z-axis proportional to αr [10].

5.2 Lateral beamwidth (resolution) of the Bessel beam

Bessel beams have zeros located symmetrically about the mainlobe. The peak-to-zero distance can serve as one measure of the width. For Bessel beams this zero occur at $\alpha r = 2.4$, giving the diameter of the central maximum of the Bessel beam approximately:

$$D_{max} = \frac{2.4}{\alpha} \cdot 2 \approx \frac{3\pi}{2\alpha} \tag{86}$$

The effective width of the Bessel beam is determined by α, and when α is maximum i.e. $\alpha_{max} = k = 2\pi/\lambda$ (k is the wavenumber), the minimum beam width becomes:

$$D_{min} = \frac{3\pi}{2\alpha_{max}} = \frac{3}{4}\lambda \tag{87}$$

The full width of the mainlobe at one-half of the peak value (FWHM) is a useful measure for the mainlobe width. The lateral resolution of Bessel beam is defined as the FWHM of centre lobe of the beam. The -6 dB lateral beam width(FWHM) of the Bessel beam can be calculated from Eq. 82 with *n=0,* and $\alpha r = 1.52$:

$$J_o(\alpha r) = 0.5 \Rightarrow \alpha r = 1.52 \tag{88}$$

which is:

$$FWHM|_{-6dB} = 2r = \frac{3.04}{\alpha} \tag{89}$$

The envelope function is defined to be [10]:

$$envlope = \begin{cases} 1 & r = 0 \\ \dfrac{2}{\pi\alpha r} & r \neq 0 \end{cases} \tag{90}$$

The peak in the envelope occurs at $r = 0$, and when $r = 2.4/\alpha \approx 3\pi/(4\alpha)$ the envelope is 0.27. Figure 2.1 shows the intensity distribution for $J^2{}_o(\alpha r)$ and its envelope function.

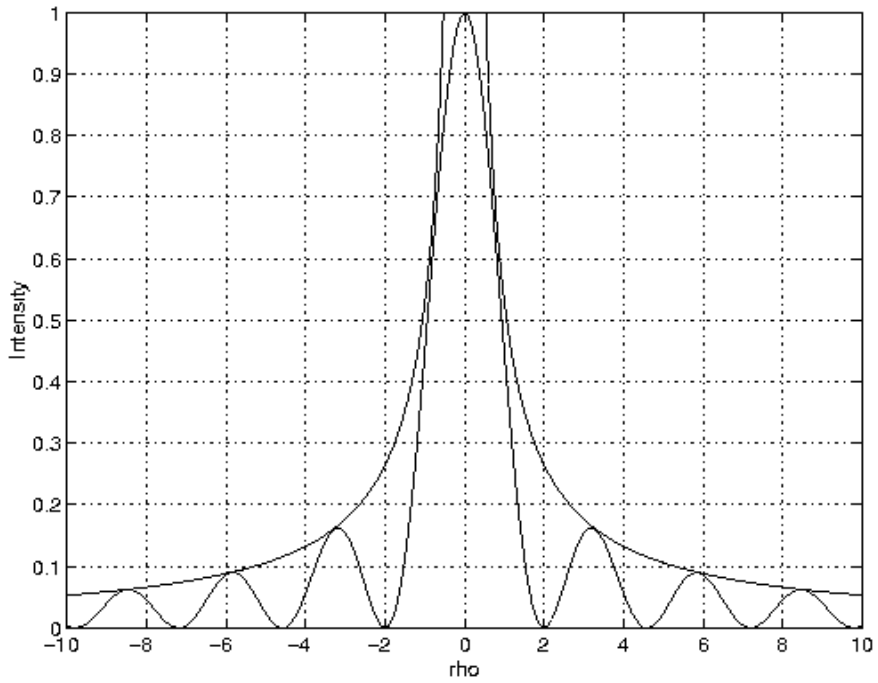

Figure 5.1: *Intensity distribution* $J^2{}_o(\alpha r)$ *and its envelop function* $2/(\pi\alpha r)$.

Figure 5.3 shows the zero order Bessel beam produced with a finite aperture, with a central frequency of 2.5 MHz($\lambda = 0.61mm$). The aperture has a diameter of 50 mm and 10 annular elements. The width of each annular element is designed to be equal to a lobe of zeroth-order Bessel function J_o with $\alpha = 1202\ m^{-1}$. The amplitude of each element at the surface of the transducer is proportional to the average amplitude (positive or negative) of the corresponding lobe of the zeroth-order Bessel function J_o (see figure 5.2).

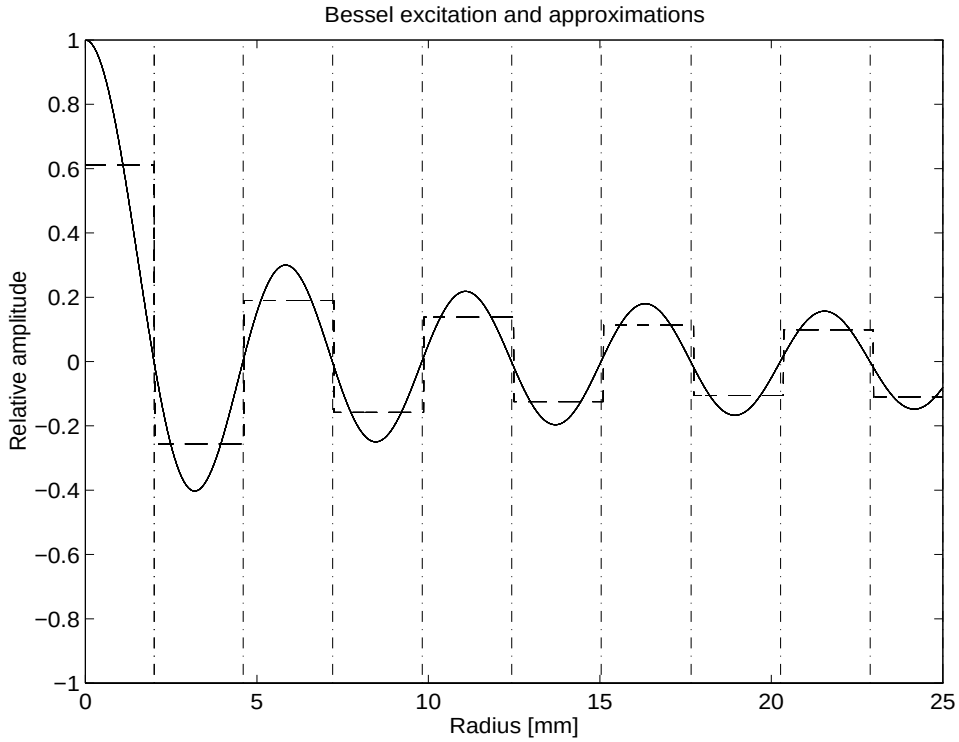

Figure 5.2: *Solid line shows the zeroth order Bessel function of first kind with scaling factor* $\alpha = 1202\ m^{-1}$ *.Dashdot lines show the 10 rings of the annular transducer. These rings are placed on the zeros of the Bessel function. Dashed lines show the average amplitude of the corresponding lobe of the zeroth-order Bessel function.*

The width and amplitude the of each ring are given in table 5.1. The -6 dB lateral beam width obtained from figure 5.3 is about 2.53 mm.

Element number	**1**	**2**	**3**	**4**	**5**	**6**	**7**	**8**	**9**	**10**
Separation position	2.01	4.60	7.21	9.82	12.43	15.04	17.66	20.27	22.88	25
Ring Amplitude	0.61	0.25	0.19	0.15	0.14	0.12	0.11	0.10	0.09	0.11

Table 5.1: *Width and amplitude of annular elements of the Bessel transducer obtained from the zeroth-order Bessel function.*

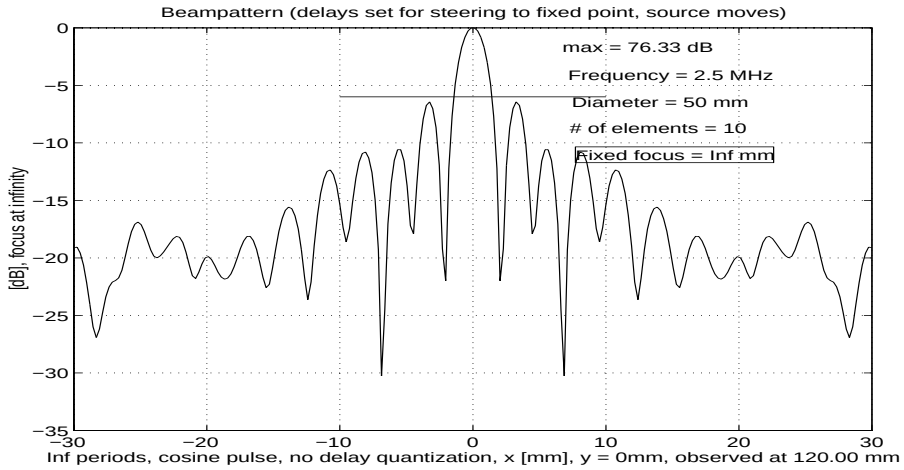

Figure 5.3: *Lateral line plot of the Bessel beam (Eq. 82 when n=0) produced with a finite aperture. The -6 dB beam width obtained from this figure is about 2.53 mm.*

5.3 Depth of field of the Bessel beam

In practice, the nondiffracting beam can only be produced with a finite aperture [9]. One sees from Eq. 82 with *n=0* that the J_o beam is a superposition of plane waves, all having the same amplitude an travelling at the same angle $\theta = \sin^{-1}(\alpha\lambda/2\pi)$ relative to the *z* axis but having different azimuthal angles ranging from *0* to 2π. According to geometrical optic [10], [11], as shown i figure 5.4 a *shadow zone* begins along *z* axis at a distance:

$$z_{max} = R/(\tan\theta) \tag{91}$$

from the aperture.

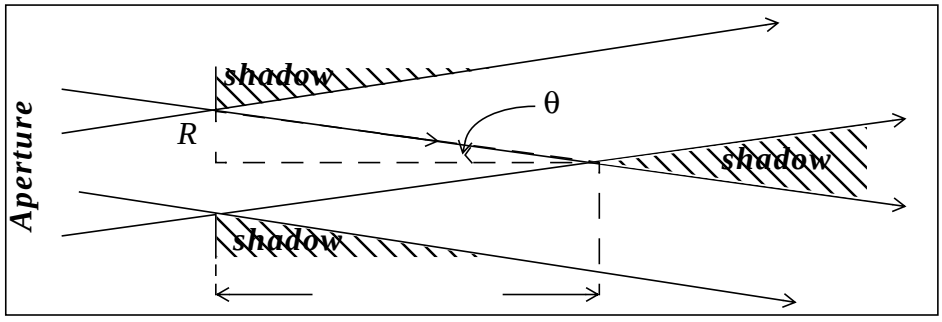

Figure 5.4: *Geometrical shadow zone for zeroth-order Bessel beam of a finite aperture* [11]

Since the beam radius is approximately α^{-1}, we can use $tan(\theta) \approx sin(\theta) = \alpha / k$, to express the maximum propagation distance as:

$$\begin{aligned} Zmax &= \frac{R}{\tan(\theta)} \\ &= \frac{R}{\frac{\sin(\theta)}{\sqrt{1-\sin^2(\theta)}}} \\ &= R\sqrt{(\sin^2\theta)^{-1} - 1} \\ &= R\sqrt{\left(\frac{2\pi}{\alpha\lambda}\right)^2 - 1} \end{aligned} \tag{92}$$

In fact, Eq. 92 has been found to predict accurately the effective range of the zeroth-order Bessel beams for a finite aperture for all values of α in the range:

$$\frac{2\pi}{R} \le \alpha \le \frac{\omega}{c} \tag{93}$$

When $\alpha > \omega / c$, the wave is evanescent, and $z_{max} = 0$. When $\alpha < 2\pi / R$, the source field is essentially just a disk of radius *R*, and z_{max} equals the Rayleigh range [10].

As one example, figure 5.3 shows the beam profile (one-way profile) of the Bessel transducer. Using the numerical values given above, one can find that the geometrical estimate *Zmax* for the maximum range of the Bessel beam is *216 mm*. Figure 5.5 shows the image of the computer simulated pressure field of a nondiffracting Bessel beam produced with the same transducer as in figure 5.3. Figure 5.6 shows the line plot of figure 5.5 long the propagation axis (*z-axis*). One can see from these two figures the maximum field of the Bessel beam to be at about *216 mm.*

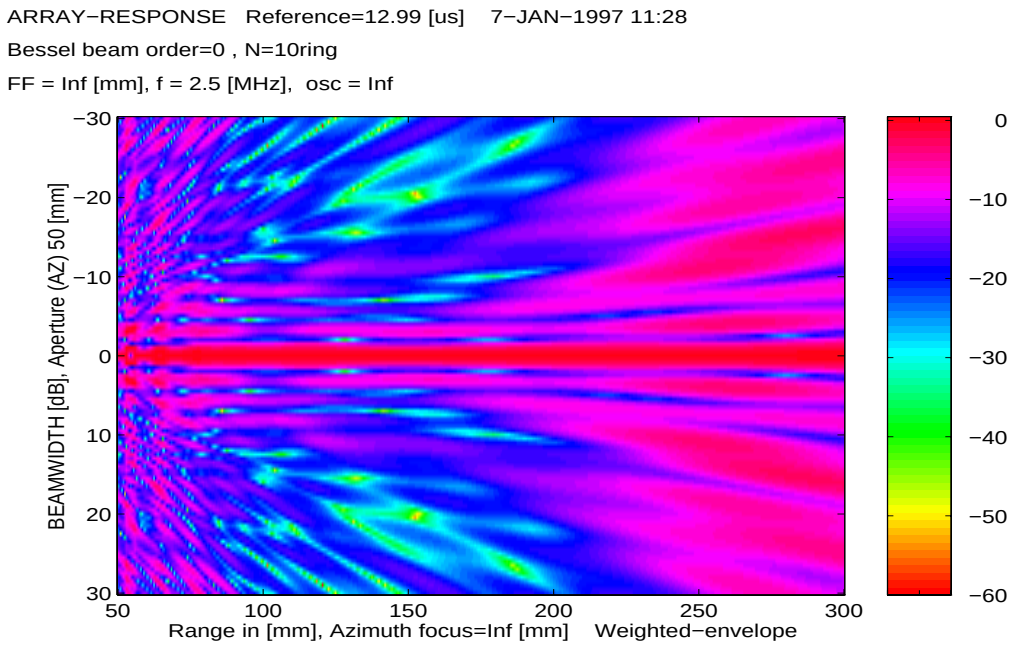

Figure 5.5: *Computer simulation for a nondiffracting Bessel beam transducer with the scaling factor* $\alpha = 1202\ m^{-1}$. *From this figure one can see that the maximum depth of field is about 216 mm.*

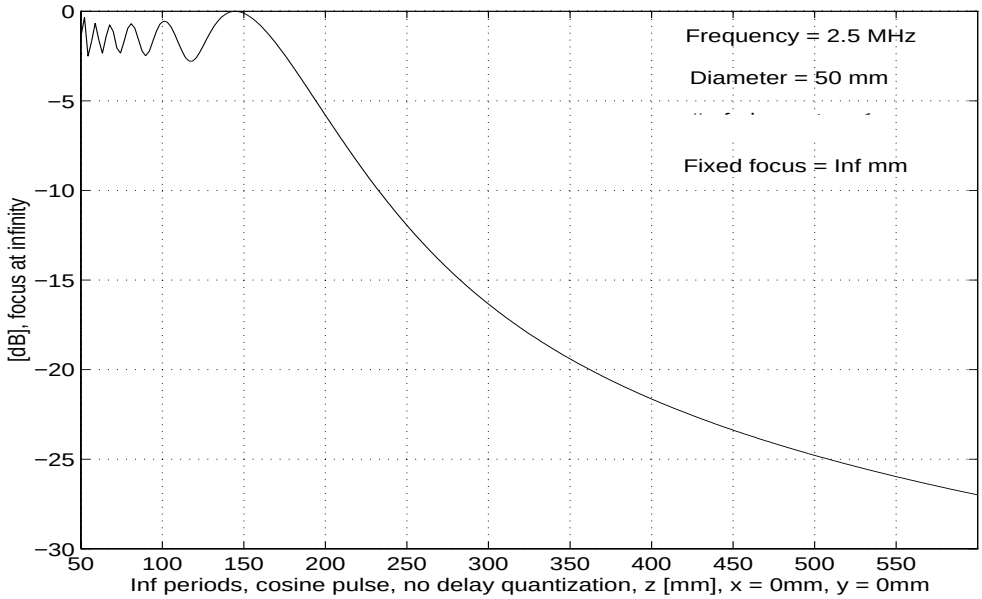

Figure 5.6: *The zeroth-order Bessel beam along the beam axis from 50 mm to 600 mm. The -6 dB depth of field of this beam is at about 212 mm.*

The lateral resolution (FWHM) and the maximum depth of field and the size of transducer, *R*, of Bessel beams are related to each other. One can see from Eq. 92 the relationship between the maximum depth of field and the scaling factor α. If the transducer size *R* is fixed to increase the depth of field, the scaling factor α must be decreased, i.e. with decreasing the scaling factor ,α, the lateral resolution is increased. If the maximum depth of field is fixed, to reduce the size of the centre lobe of the Bessel beam (by increasing α), the size of the transducer *R*, should be increased.

As obtained in the previous example, the maximum depth of field was about *216 mm* and the lateral resolution was about 2.53 mm. When the aperture size is reduced from *50 mm* to *25 mm*, the depth of field will decrease from *216 mm* to *100 mm*, but the lateral resolution will be unchanged. Figure 5.7 shows the simulation result of an aperture with *25 mm* diameter and figure 5.8 shows the line plot of figure 5.7 about the *z-axis*. In comparison with figure 5.5 and figure 5.6 the difference is evident.

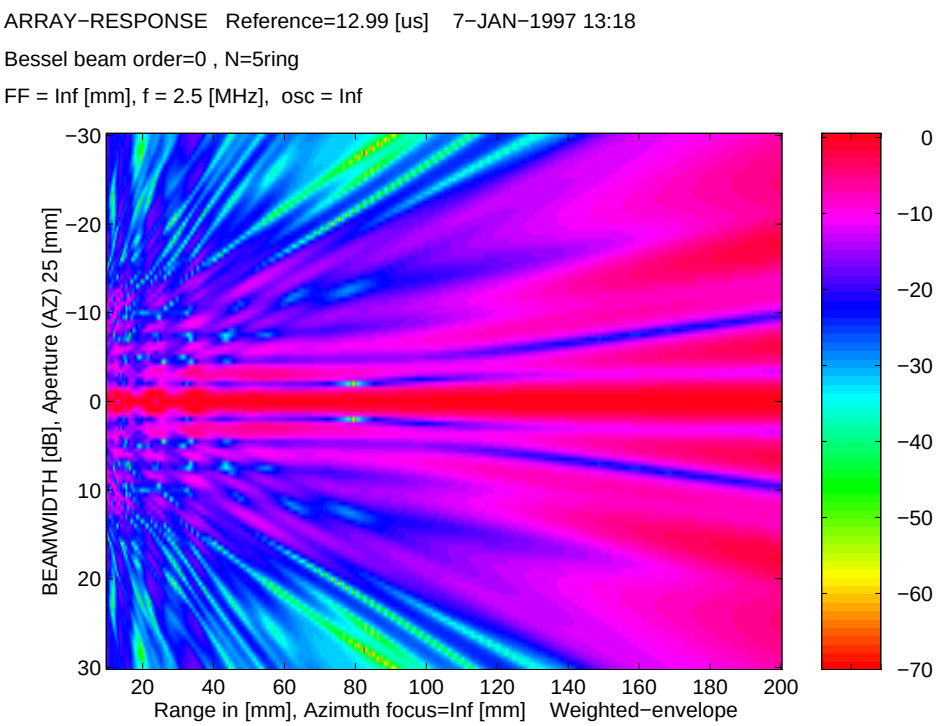

Figure 5.7: *Computer simulation for 25 mm Bessel nondiffracting transducer. From this figure one can see that the maximum depth of field is reduced to 100 mm in compare with* figure 5.5.

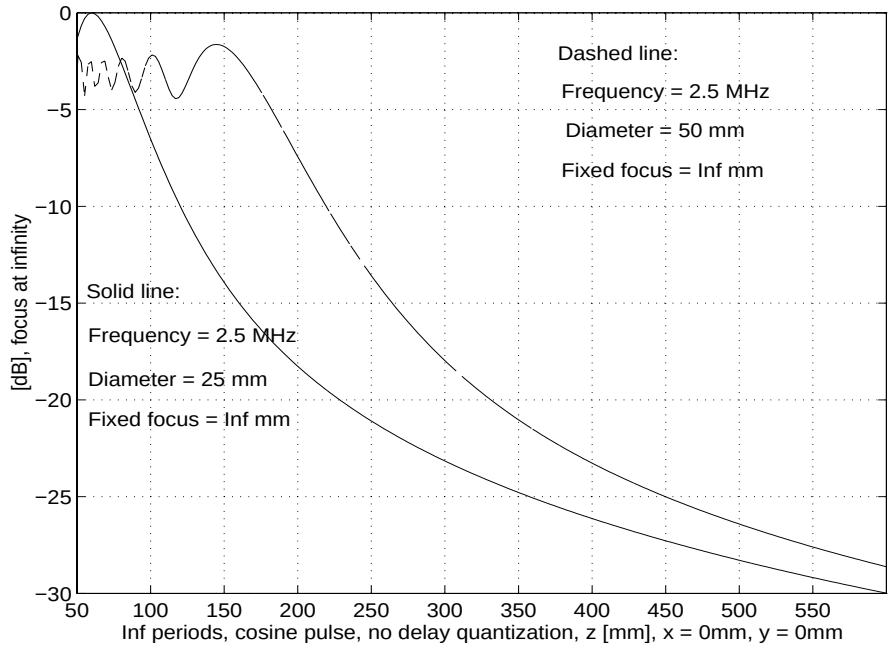

Figure 5.8: *The zeroth-order Bessel beam along the beam axis from 50 mm to 600 mm. Dashed line represents the beam plot when the diameter is 50 mm. The -6 dB depth of field of this beam is about 216 mm. Solid line represents the beam plot when the diameter is 25 mm. The -6 dB depth of field is about 100 mm.*

In order to obtain the same depth of field, α should increase which causes the lateral resolution to decrease, i.e. scaling factor α must be increased from $\alpha = 1202\ m^{-1}$ to $\alpha = 1666\ m{-}1$. This reduces the beam width from *2.53 mm* to *1.82 mm*. Figure 5.9 show the lateral line plot of the same transducer as in figure 5.7 but scaling factor is about $\alpha = 1666\ m^{-1}$. In comparison we plotted lateral plot when $\alpha = 1202\ m^{-1}$.

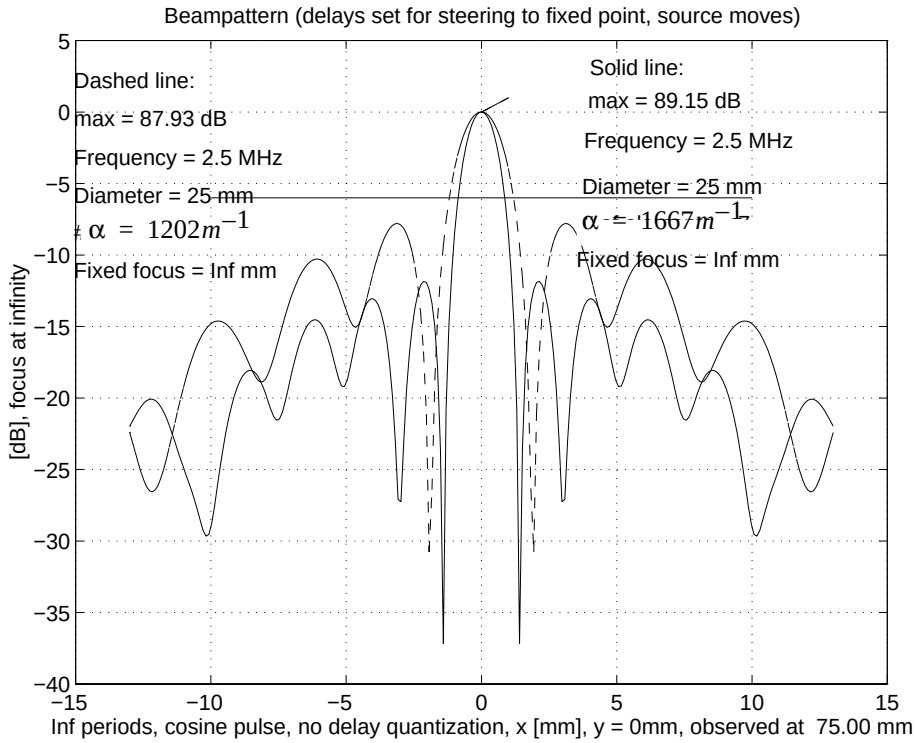

Figure 5.9: *Lateral line plot of the Bessel beam produced with a finite aperture. The -6 dB beam width obtained from this figure is about 1.82 mm when scaling factor* $\alpha = 1667\ m{-}1$ (solid line). *When* $\alpha = 1202\ m^{-1}$ *the beam width is 2.53 mm (dashed line).*

The depth of field and the lateral resolution are related directly or indirectly to the central frequency of the beam. A higher central frequency does not increase directly the lateral resolution of the Bessel beam, but it increases the depth of field. We showed in Fig. 5.5 the zero order Bessel beam produced with a finite aperture, with a central frequency of 2.5 MHz. When the central frequency increases from *2.5 MHz* ($\lambda = 0.61\ mm$) to *5 MHz* ($\lambda = 0.3\ mm$) while the transducer diameter *D=2R* and α are constant, the depth of field will increase from *213 mm* to *423 mm*, but the lateral resolution will not be changed.

Figures 5.10 and 5.5 shows the field from two transducers with the same diameter and operating respectively at *2.5 MHz* and *5 MHz* frequency. We see that when the frequency is doubled, the aperture of the transducer in number of wave lengths is doubled and the maximum depth of field is doubled. The line plot of figure 5.10 along the beam axis (*z-axis*) is plotted in figure 5.11.

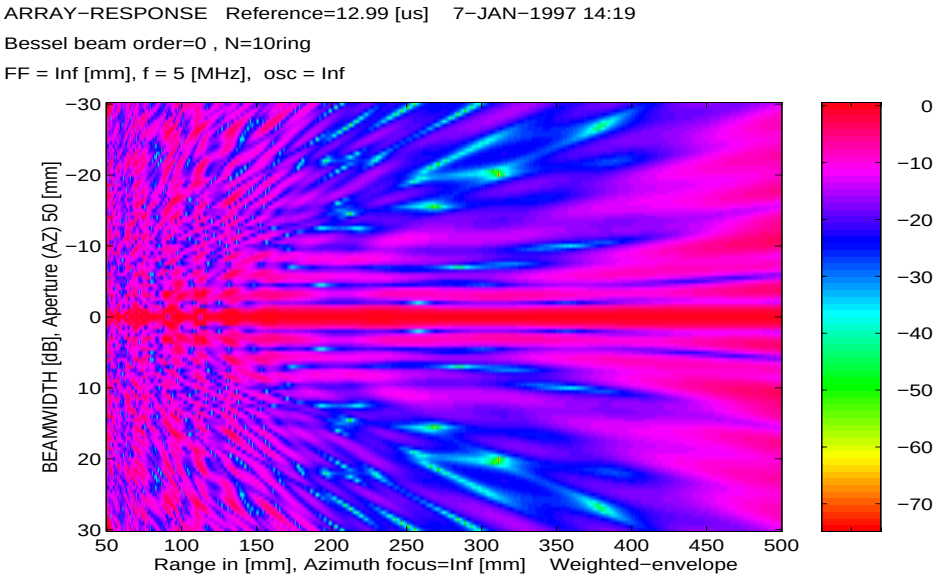

Figure 5.10: *Computer simulation for a nondiffracting Bessel beam transducer with a central frequency of 5 MHz*($\lambda = 0.308\ mm$). *From this figure one can see that the maximum depth of field is about 430 mm.*

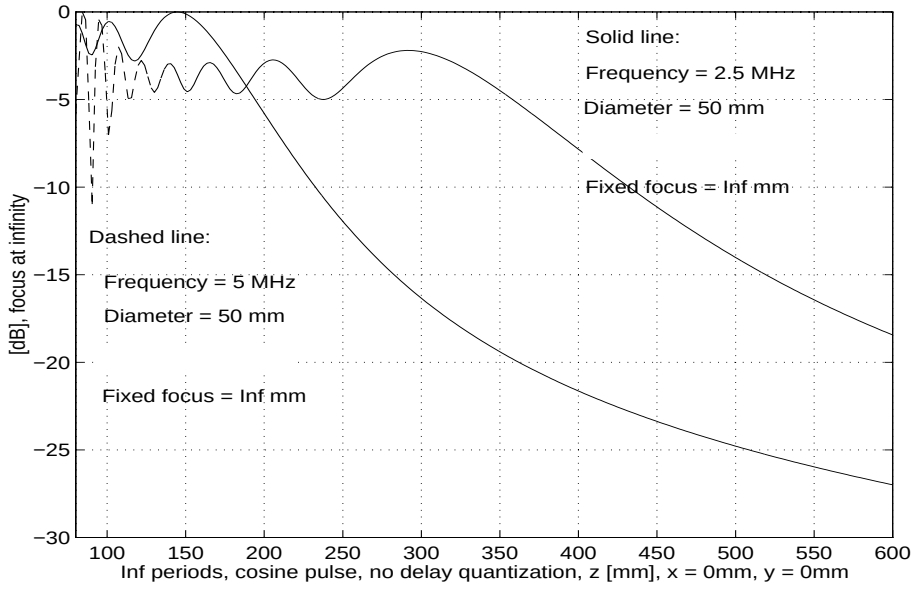

Figure 5.11: *The zeroth-order Bessel beam along the beam axis form 50 mm to 600 mm. Dashed line represents the beam plot with a central frequency of 5 MHz. The -6 dB depth of field of beam is about 423.6 mm. Full line represent the beam plot with a central frequency of 2.5 MHz. The -6 dB depth of field is about 216 mm.*

5.4 Sidelobes of Limited diffraction beams

The sidelobes of the Bessel beam are at about the same level as those of the Bessel function, and have the shape of skirts around the main lobe, The sidelobes pick up signals from many directions. In contrast to spherically focused beams, Bessel beams have high sidelobes. It is the sidelobes that construct the Bessel beams as they propagate. High sidelobes reduce contrast in imaging and cause artifact in nondestrative evaluation of materials, [28], [30], [31]. In addition, sidelobes increase the effective sampling volume and thus average out spatially distinguished information in tissue characterization [23], [33].

In figure 5.3 we have shown the beam profile of the zeroth-order Bessel beam produced with an annular transducer. The first sidelobe is *8 dB* lower in amplitude than the mainlobe. As we discussed in section 4.5.5 the first sidelobe of the focused beam is about *17.67 dB* lower in amplitude than the mainlobe.

There are several methods for reducing the sidelobes of limited diffraction beams, such as;

- deconvolution [28],
- dynamically focused reception [17],
- summation-subtraction [23], [24],
- Bowtie limited diffraction beams [29]

In this section we will take a look at the effect of sidelobes and the reason why their levels are reduce when we use s*ummation-subtraction* method, and how this method reduces the *frame rate*.

5.4.1 Summation-subtraction method

Although limited diffraction beams have a large depth of field, they have higher sidelobes as compared to the conventional focused beams in their focal plane.

Summation-subtraction method has been developed to reduce the sidelobes of the limited diffraction beams [24]. Limited diffraction beams are used in both transmission and reception. Sidelobes of the Bessel beam in Eq. 85 can be reduced by summing simulation result produced from the *second-order non-rotating* Bessel beams that are rotated around the beam axis by an initial angle $\phi_o = \pi/4$ with each other, and then subtracting the result from the simulation result obtained with the *zero-order* Bessel beam.

5.4.2 Simulation of summation-subtraction method

One can use a non-rotating limited diffraction solution Eq. 85 to simulate this method. In Eq. 85 by putting $n = 0$, the solution becomes:

$$p_o(\vec{r}, t) = J_0(\alpha r)e^{i(\beta z - \omega t)} \tag{94}$$

which is the zero-order Bessel beam. When $n = 2$, the solution is the second-order non-rotating Bessel beam:

$$p_2(\vec{r}, t) = J_2(\alpha r)e^{i(\beta z - \omega t)}\cos 2(\phi - \phi_o) \tag{95}$$

The zero-order Bessel beam has both a mainlobe and high sidelobes. The second order Bessel beam does not have mainlobe, but has sidelobes similar to the zero-order Bessel beam. In figure 5.12 we have calculated the squares of the zero-order and second-order Bessel function of first kind, and subtracted second-order from zero-order. This figure clearly shows the difference between the squares of the zeroth- and second-order Bessel functions and their difference. For comparison, the squares of zeroth-order Bessel function is also shown. As shows in figure 5.12 the summation-subtraction method reduces the sidelobes levels of the Bessel function from *-7.5 dB* to *-14.3 dB*.

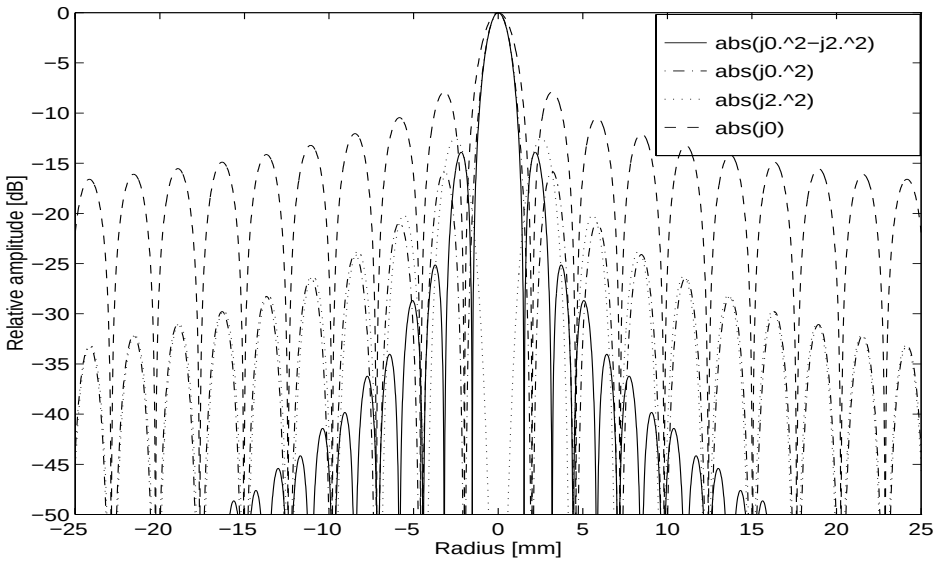

Figure 5.12: *Squares of the zeroth-order (dashdot line) and second-order (dotted line) Bessel function of first kind and the absolute values of their subtraction (solid line) and zeroth-order Bessel function (dashed line). The first sidelobe of summation-subtraction method (solid line) is about 6 dB lower in amplitude than the zeroth-order Bessel function (dashed line).*

The asymptotic expansion is one of the properties of the Bessel function. The nth-order Bessel integral is given by [21], [22]:

$$J_n(\alpha r) = \frac{1}{\pi}\int_0^{\pi} \cos(n\phi - \alpha r \sin\phi)\, d\phi \tag{96}$$

when $n = 0$ and $\alpha r = 0$, the square of the zeroth-order Bessel function becomes:

$$J_o^2(\alpha r) = \left(\frac{1}{\pi}\int_0^{\pi} \cos(0)\, d\phi\right)^2 = 1 \tag{97}$$

and when $\alpha r = 0$ and $n = 2$, the square of the second-order Bessel integral becomes zero:

$$J_2^2(\alpha r) = \left(\frac{1}{\pi}\int_0^{\pi} \cos(2\phi)\, d\phi\right)^2 = 0 \tag{98}$$

If the αr values are larger than one ($\alpha r \gg 1$) the squares of the *nth-order* Bessel function becomes [21], [22]:

$$J_n^2 \rightarrow \left(\sqrt{\frac{\pi}{\alpha r}}\cos\left(\alpha r - \frac{\pi}{2}(n+1)\right)\right)^2 \qquad \alpha r \rightarrow \infty \tag{99}$$

with *n=0* and *2*, $j_o^{\,2}(\alpha r)$ and $j_2^{\,2}(\alpha r)$ become:

$$\begin{cases} j_o^2(\alpha r) \\ j_2^2(\alpha r) \end{cases} \rightarrow \frac{2}{\pi\alpha r}\cos\left(\alpha r - \frac{\pi}{4}\right) \qquad when \quad \alpha \gg 1 \tag{100}$$

which is the general form of Eq. 90.

As shown in Fig. 5.12 $j_o^2(\alpha r)$ and $j_2^2(\alpha r)$ are also very close to each other for other values of αr except from the first few sidelobes. Therefore subtracting the squares of the zeroth-order from the second-order Bessel function gives a significant sidelobes reduction.

We will now report the results from the simulation of zeroth- and second-order Bessel beams. The intention with these simulations is to find how the sidelobes will be reduced by using the summation-subtraction method. In figure 5.13 we have calculated the zeroth- and second-order Bessel beam produced with a finite aperture, with a central frequency of 2.5 *MHz*. The aperture has a diameter of *50 mm* and one ring.

The simulation results of the zeroth-order and the second-order before rotation ($\phi_o = 0$) are shown in panel a) and b) respectively. The simulation result of the second-order after rotation ($\phi_o = \pi/4$) is shown in panel c). The summation result of panels b) and c), and the subtraction this result from panel a) is shown in figure 5.13 d).

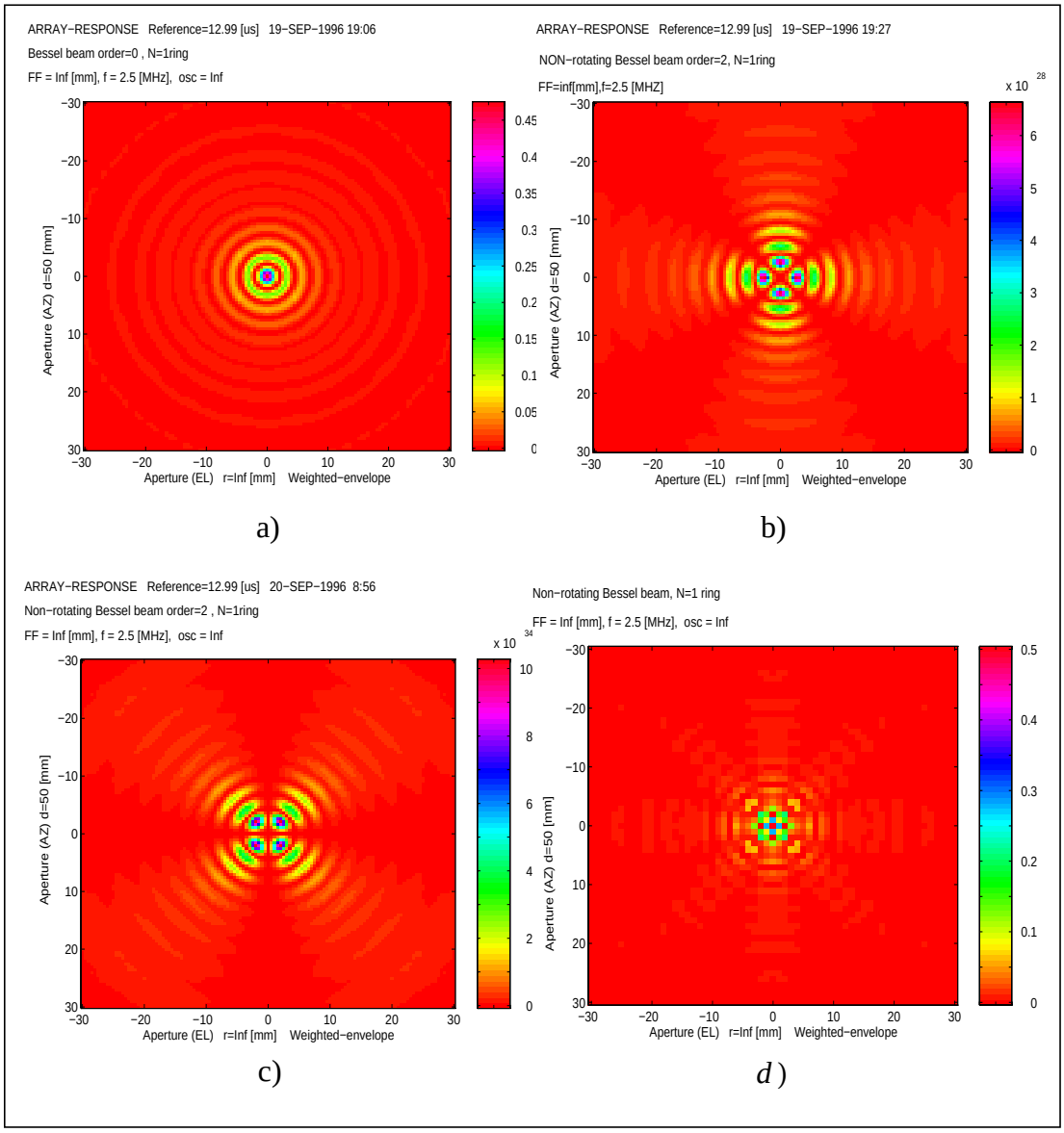

Figure 5.13: *Bessel beam produced with 50 mm aperture at the axial distance, z=120 mm and scaling factor* $\alpha = 1202\ m^{-1}$. *a) zeroth-order Bessel beam. b) second-order Bessel beam when initial angle* $\phi_o = 0$. *c) second-order Bessel beam after* $\pi/4$ *rotation about beam axis. d) The result of summation-subtraction method.*

The summation-subtraction method requires three scan_lines that need three transmissions at one transducer position, i.e., the first two scan_lines are added following that the result is subtracted from the third one.

This is to say:

$$E_{ss} = E_{J_o} - \left(E_{J_2}\Big|_{\phi_o = 0} - E_{J_2}\Big|_{\phi_o = \pi/4} \right) \tag{101}$$

where $E_{J_2}\Big|_{\phi_o = 0}$ and $E_{J_2}\Big|_{\phi_o = \pi/4}$ are scan-lines obtained with the second-order Bessel beams that are rotated one quarter relative to each other. E_{J_o} is a scan_line obtained with zeroth-order Bessel beam.

From definition of the frame rate in Eq. 25, one can show that three scan_lines (N=3) reducing the frame rate to 1/3 in imaging, i.e Eq. 25 will be changed to:

$$R_f = \frac{1}{T} = \frac{1}{T_b 3} = \frac{c}{2D_f}\frac{1}{3} \tag{102}$$

Because scan-lines are subtracted in this method, large contributions from sidelobes may be subtracted. This reduces the dynamic range of the signals after the subtraction and thus lower the *signal-to-noise ratio* [24].

The summation-subtraction method also will be sensitive to the moving objects since it involves scan-lines summation and subtraction. However, if the time between adjacent scan-lines for the summation and subtraction is short, the influence of motion will be small, else steering Bessel beams with a *two-dimensional phased array* may eliminate the motion of the transducer [25]. The two-dimensional array system has good definition in one transverse dimension, the x direction, and good range resolution in the z direction but definition in the other transverse dimension, the y direction, is relatively poor [16].

As we have shown earlier, the method described can reduce sidelobes of the limited diffraction beams dramatically (the first two sidelobes is reduced about 7 dB in amplitude), but it lowers the imaging frame rate to one third because of three scan-lines. In the next section derivation of the new equation of Bessel beam will be shown. These beams are called Bowtie Bessel beams (Bowtie limited diffraction beams).

Unlike the summation_subtraction method, this method does not change frame rate and is not motion sensitive but reduces sidelobes of limited diffraction beams.

5.5 Bowtie limited diffraction beams

In this section derivation of the new type of Bessel beams will be presented [29]. These beams are called ***bowtie limited diffraction beams*** (Bowtie Bessel beams) due to their particular shape in a plane perpendicular to their propagation axis. They are obtained from spatial derivatives of the Bessel beam in one transverse direction. Theoretically these beams have an infinite depth of field, but if produced with a finite aperture, they have the same large depth of field as the Bessel beams. This beam has a very low sidelobe in the direction perpendicular to that of derivatives, and the sidelobes are even lower as the order of the derivative increases. In this section we have chosen *4th*- and *10th*-derivative of Bessel beam to demonstrate the trend of the bowtie beams of increasing orders. The difference between the Bessel beams and bowtie Bessel beams is that the sidelobes of bowtie beams have strong angle dependency, see figure 5.15.

In the section 5.1 on page 41 we verified that the equation:

$$p(\vec{r}, t) = J_n(\alpha r)e^{i(\beta z - \omega t + n\phi)} \qquad n = 0, 1, 2, 3\ldots \tag{103}$$

is the solution to the three-dimensional isotropic/homogeneous wave equation in cylindrical coordinates Eq. 21.

Now we begin our development of bowtie Bessel beams by taking derivatives of the Bessel beams in Eq. 103 in one transverse direction, for instance in the *y* direction;

$$\frac{\partial^m}{\partial y^m}(q_n(r, t)) \tag{104}$$

where *m* is a nonnegative integer and is the order of the derivatives. These beams are also exact solution to the wave equation (Eq. 21) and they are still limited diffraction beams because they travel with a wave in propagation direction without any change in the wave pattern, i.e., propagation term, *z-ct*, is retained after derivation. Substitute Eq. 103 into Eq. 104 when *m=4* and *n=0*, the 4th-order bowtie Bessel beam becomes [29]:

$$\begin{aligned}\frac{\partial^4}{\partial y^4}(J_o(\alpha r)) = &\left(-\frac{24\alpha^2 y^4}{r^6} + \frac{\alpha^2 y^2(24 + \alpha^2 y^2)}{r^4} - \frac{3\alpha^2}{r^2}\right)J_o(\alpha r) \\ &+ \left(\frac{48\alpha y^4}{r^7} - \frac{8\alpha y^2(6 + \alpha^2 y^2)}{r^5} + \frac{6\alpha(1 + \alpha^2 y^2)}{r^3}\right)J_1(\alpha r)\end{aligned} \tag{105}$$

The simulated *4th*- and *10th*-derivative bowtie Bessl beams are shown in figure 5.14. They are one-way fields (transmission) and are produced with an annular transducer (acoustic field profile is an exact bowtie Bessel beam shading function at the transducer surface). The transducer has a diameter of *50 mm* with central frequency of 2.5 MHz and scaling factor $\alpha = 1202\ m^{-1}$. The field was calculated at the distance *z=120 mm* away from the surface of the transducer. For comparison, the zeroth-order Bessel beam is also shown (with exact aperture weightings).

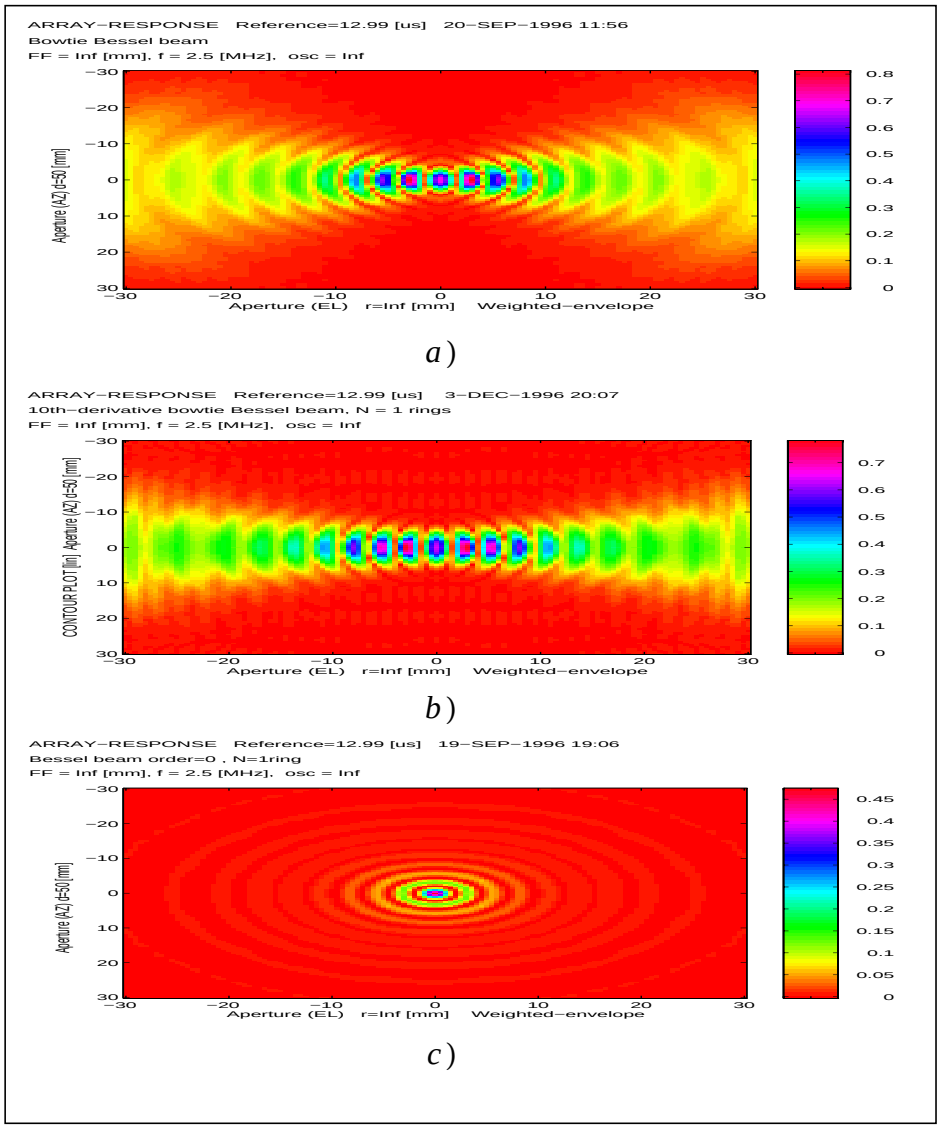

Figure 5.14: *One-way (transmission) bowtie Bessel beam produced with 50 mm transducer at the axial distance z=120 mm and at angle $\phi = 0°$ and the scaling factor $\alpha = 1202\ m^{-1}$. a) 4th-derivative bowtie beam. b) 10th-derivative bowtie beam c) zeroth-order Bessel beam.*

5.6 Sidelobes of the bowtie Bessel beams

In section 5.4 on page 53 we discussed the sidelobes of the Bessel beam. As we have shown in figure 5.12, the sidelobes of the Bessel beam are at the same level as those of the Bessel function. In contrast to the conventional beams, Bessel beams have large depth of field, good focus, but high sidelobes. These sidelobes can be reduced with summation-subtraction method studied previously (section 5.4.1 on page 53). But this method reduces the frame rate about one third (1/3).

To obtain low sidelobes without changing the frame rate, one can use a bowtie Bessel beam in the transmission and it's 90 degree rotated response in the reception [29].

The sidelobes of bowtie Bessel beam are strongly angle dependent. In Eq. 103 we have taken derivatives of a Bessel beams in the *y* direction, i.e., transverse direction. From the relationship between polar and rectangular coordinates, we have;

$$y = r\sin(\phi) \tag{106}$$

where ϕ is the angle in a plane perpendicular to the *z*-axis.

The highest sidelobes of the bowtie Bessel beam appear at an angle $\phi = 45°$ and the lowest at the angle $\phi = 0°$, see figures 5.15 (*a)* and (*b)*. When angle $\phi = 30°$, the first sidelobes are smallest and these beams have best lateral resolution.

Figure 5.15 show the line plots of the theoretical 4th- and 10th-derivative bowtie Bessel beams with the corresponding scaling factors. For comparison with the focused beams and the zeroth-order Bessel beams, the above derivatives are plotted in the same figure as the focused beam and the zeroth-order Bessel beam. The beam pattern of the focused circular transducer is determined by a *jinc* function (see chapter 4):

$$Jinc(\alpha_j r) = \frac{2J_1(\alpha_j r)}{\alpha_j r} \tag{107}$$

where *r* is the radial distance and α_j is a scaling factor that controls the mainlobe width of the function and is related to the *F-number (FN)* and the central wavelength of the beam. In figure 5.15, $\alpha_j = 1772.06\ m^{-1}$, so the *-6 dB* beamwidth of the *jinc* function is about the same as that of the zeroth-order Bessel function.

As one example, the first sidelobes of the *4th*- and *10th*-derivative bowtie Bessel beams at angle $\phi = 45°$ are about 6 *dB* and *3.4 dB* lower than the amplitude of the mainlobe respectively, see figure 5.15 (c) on page 62.

This implies that higher first sidelobes increase the effective main beamwidth and thus reduce the effective lateral resolution. However, at angle $\phi = 30°$ these sidelobes are about *-13 dB* for 4th-derivative and $-8dB$ for 10th-derivative bowtie Bessel beams, see figure 5.15 (*b)*. This implies that the best lateral resolution is around $\phi = 30°$. These sidelobes are lowest at angle $\phi = 0°$ but the lateral resolution is largest, see figure 5.15 (*a)*.

Because the bowtie Bessel beams have very low sidelobes in direction perpendicular to that of derivatives, therefore these sidelobes decrease as the order of derivatives increases. As shown in figure 5.15 these sidelobes are lowest when the order of derivation is *m=10*.

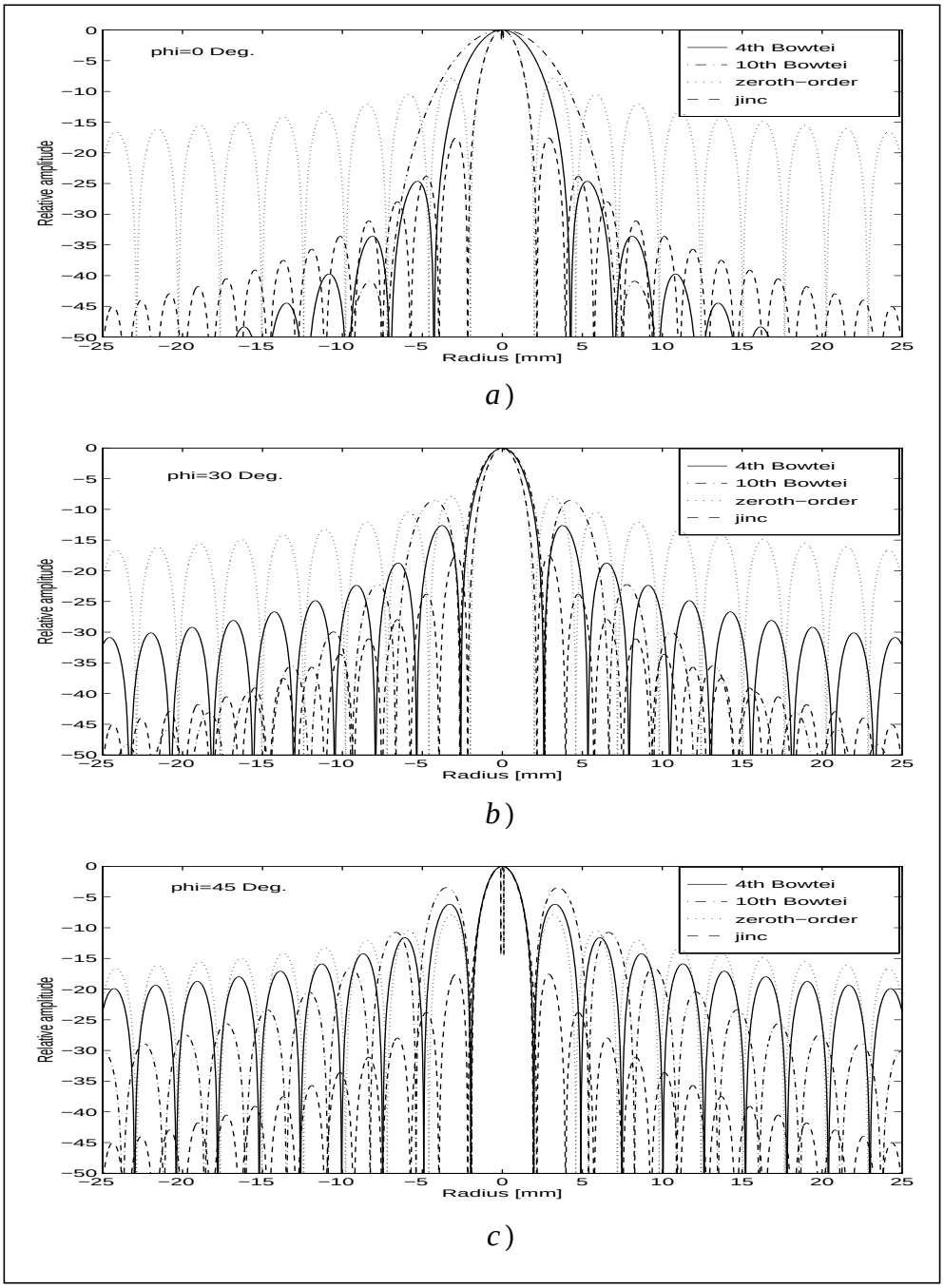

Figure 5.15: *Line plot of the theoretical 4th- and 10th derivative bowtie Bessel beam at three angles. a)* $\phi = 0°$. *b)* $\phi = 30°$. *c)* $\phi = 45°$. *The scaling factor for Bessel function is* $\alpha = 1202\ m^{-1}$. *For comparison the Jinc function (focused circular transducer) and zeroth-order Bessel beam are also shown. The scaling factor for the Jinc function is* $\alpha_j = 1772.06\ m^{-1}$.

The line plots of the one-way response of the 4th- and 10th-derivative bowtie Bessel beams (simulated) at three angles $\phi = 0°, 30°, 45°$ are shown in figure 5.16 (a), (b) and (c). The parameters used in simulation are the same as those used in figure 5.15. From figures 5.15 and 5.16, we see that the simulated bowtie Bessel beam is very close to those of the theoretical beams.

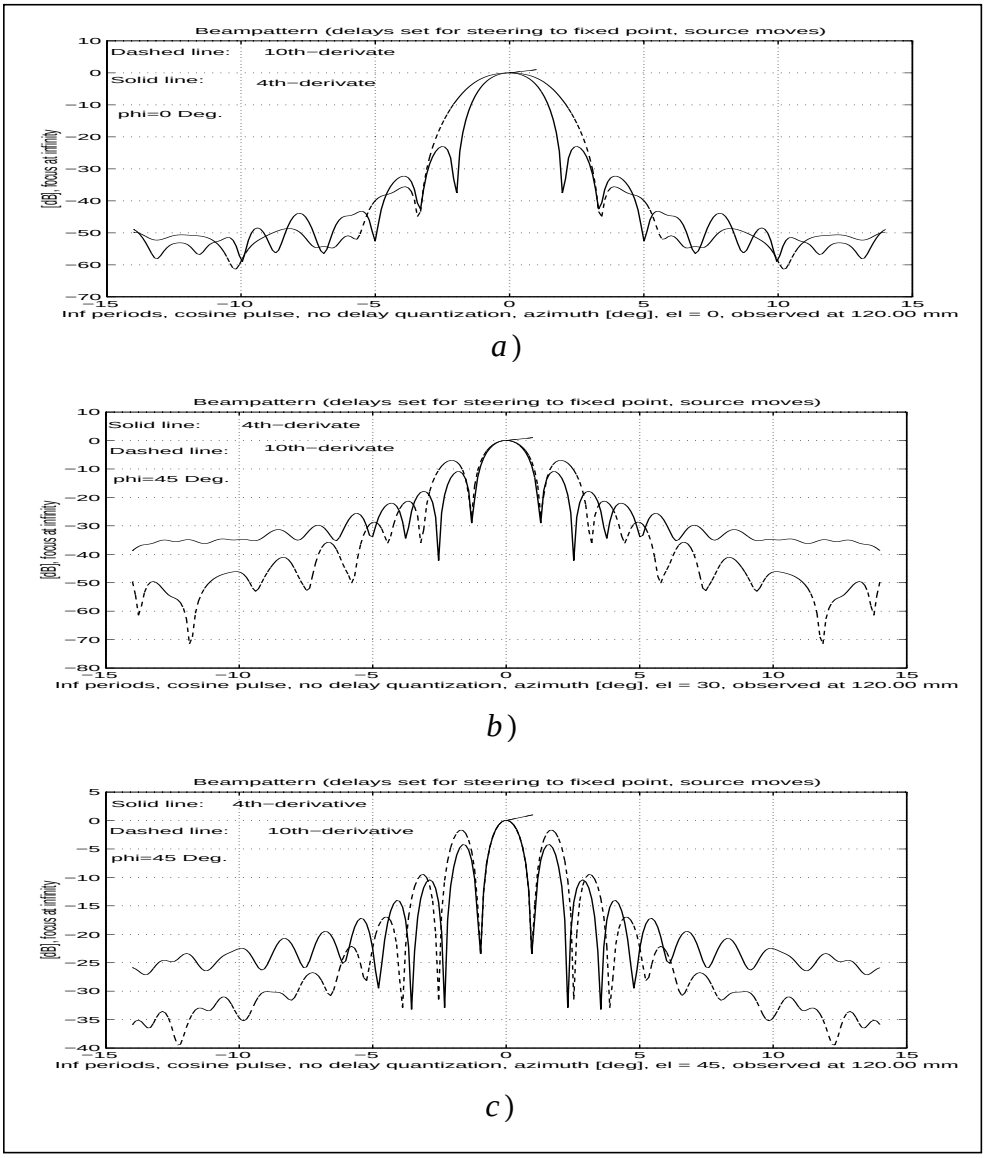

Figure 5.16: *Lateral line plots (simulated one-way) of 4th- and 10th-derivative bowtie Bessel beams at three angles: a)* $\phi = 0°$. *b)*$\phi = 30°$. *c)* $\phi = 45°$. *The diameter of the transducer for simulated beams is 50 mm with central frequency of 2.5 MHz and scaling factor* $\alpha = 1202 \ m^{-1}$.

5.7 The lateral resolution of bowtie Bessel baems

As we discussed previously (section 5.2 on page 43) the lateral resolution is determined by the width of the mainlobe (-6 dB beam width). The lateral resolution of bowtie Bessel beam increases as the central wavelength of the beam decreases. But for a given central wavelength, the lateral resolution of bowtie Bessel beams are comparable to those of the zeroth_order Bessel beams.

The difference between the lateral resolution of the bowtie Bessel beams and the Bessel beams is that the lateral resolution of bowtie Bessel beams will increase with the order of derivation.

As we have shown in figure 5.15, the lateral resolution of bowtie Bessel beams at angle $\phi = 30°$ is almost the same as the zeroth-order Bessel beam. At angle $\phi = 45°$ the lateral resolution of bowtie Bessel beam is larger than the zeoth-order Bessel beam, and the first sidelobes are higher. This implies that higher first sidelobes increase the effective main beamwidth and thus reduce the effective lateral resolution.

5.8 Depth of field of bowtie Bessel beams

In section 5.4.2 on page 54 we have verified the maximum depth of field of the Bessel beams. The depth of field for the bowtie beams of various derivative orders is the same as the Bessel beams, and can be calculated with the same formulas as of Bessel beams Eq. 92.

Line plots of the peak-to-peak values of the one-way *4th*- and *10th*_derivative bowtie Bessel beams and the zeroth-order Bessel beam are shown in figure 5.17. The parameters used in simulation are the same as those used in figure 5.15. As illustrated in figure 5.17 the bowtie Bessel beams are produced with the same aperture (*D=50 mm*) and scaling factor($\alpha = 1202 \ m^{-1}$) and have the same depth of field as the zeroth-order Bessel baem (*216 mm* in our examples).

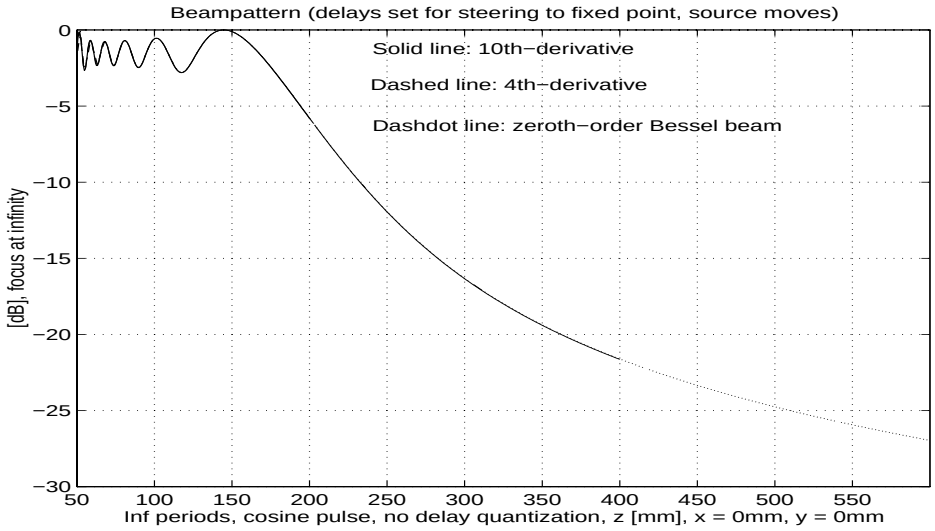

Figure 5.17: *The one-way 4th- and 10th-derivative bowtie Bessel beams and zeroth-order Bessel beams along the beam axis from 50 mm to 600 mm. As illustrated in this figure all these beams have the same depth of field (216 mm). The aperture size for these beams is 50 mm with a scaling factor.*

The amplitude (in dB scale) of the first sidelobes, depth of field, lateral resolution, of the bowtie Bessel beams, zeroth-order Bessel beams, and focused beams are given in table 5.2. In this table we have also shown the frame rate, changing in comparison with the conventionally focused beams. The diameter of the aperture is *50 mm* with a central frequency of *2.5 MHz* and scaling factor $\alpha = 1202 \ m^{-1}$. For circular transducer the scaling factor for the Jinc function is $\alpha_j = 1772.06 \ m^{-1}$.

Beams type	Aperture diameter	Amplitude of first sidelobes in dB	Depth of field in mm	-6 dB Lateral resolution in mm	Reduce frame rate to
Conv. focused beams	**50**	**-17.7**	**28**	**2.54**	**-**
zeroth-order Bessel beam	**50**	**-8**	**216**	**2.53**	**-**
Summation-subtraction method	**50**	**-14**	**216**	**2.53**	**1/3**
Bowtie 4th-derivatives $\phi=0$	**50**	**-24.5**	**216**	**4.73**	**-**
Bowtie 4th-derivatives $\phi=\pi/6$	**50**	**-12.3**	**216**	**3.34**	**-**
Bowie 4thth-derivatives $\phi=\pi/4$	**50**	**-6.0**	**216**	**6.8**	**-**
Bowtie 10th-derivatives $\phi=0$	**50**	**-41**	**216**	**7.0**	**-**
Bowtie 10th-derivatives $\phi=\pi/6$	**50**	**-8.4**	**216**	**3.35**	**-**
Bowtie 10th-derivatives $\phi=\pi/4$	**50**	**-3.7**	**216**	**9**	**-**

Table 5.2: *The amplitude of the first sidelobes, depth of field, lateral resolution, of the 4th- and 10th-derivative bowtie Bessel beam, zeroth-order Bessel beams, and circular focused transducer.*

Advantages of the bowtie Bessel beams

- They have large depth of field as the zeroth-order Bessel beams.
- They have very low sidelobes in the direction perpendicular to that of derivatives compared to the zeroth-order Bessel beams, and the sidelobes are even lower as the order of derivative increases
- They do not change the frame rate in comparison to the summation-subtraction method.
- They are not sensitive to the object motion because no subtraction of RF signals are involved.

Disadvantages of the bowtie Bessel beams

- The sidelobes of bowtie Bessel beams are higher than that of the conventional beams.

- They use a two-dimensional transducer in both transmission and reception and transducer is not symmetric. The large number of elements of a two-dimensional transducer in a small aperture may cause problem such as difficulty in wiring, electronic, mechanical crosstalk among the elements, high impedance of each element, and complex multiplexing among the elements [26].

Chapter 6 Comparison of Bessel beams with spherically focused beams

In this chapter we will compare the conventional focused beam with the limited diffraction beam. As in chapter 5 we discussed limited diffraction beams are a special class of solution to the isotropic-homogenous wave equation. They would propagate to infinite distance without spreading, provided that they were produced with an infinite aperture and energy. Even if produced with a finite aperture, these beams have a large depth of field, good focus, but high sidelobes compared to conventional focused beam in their focal plane.

6.1 Limited diffraction and conventional focused beams produced with a circular transducer

In this section we will take a look at the simulation results of a limited diffraction beam produced with a finite annular transducer and compare this result with the simulation result of focused beams produced with the same aperture.

In practical applications of limited diffraction beams, the apertures of transducers used to produce the beams are finite. In this case, limited diffraction beams such as the Bessel beam have a finite depth of field and can be approximately produced by truncating the finite aperture beams given by Eq. 82 at the transducer surface.

Example of zeroth-order Bessel beam is shown in figure 6.1lateral plot, 6.2 contour plot and 6.4 image of simulation. For the zeroth-order Bessel beam scaling factor α is 1.202 mm^{-1}. The diameter of the transducer, *D*, is *50 mm* having central frequency of *2.5 MHz* and the speed of sound, *c*, is *1540 m/s*.

The lateral plot, contour plot and image of the acoustic field for spherically focused beams with the same aperture size and frequency are shown in figures 6.1, 6.4 and 6.5 respectively. The beams of focused circular transducer are focused *140 mm* away from the transducer centre.

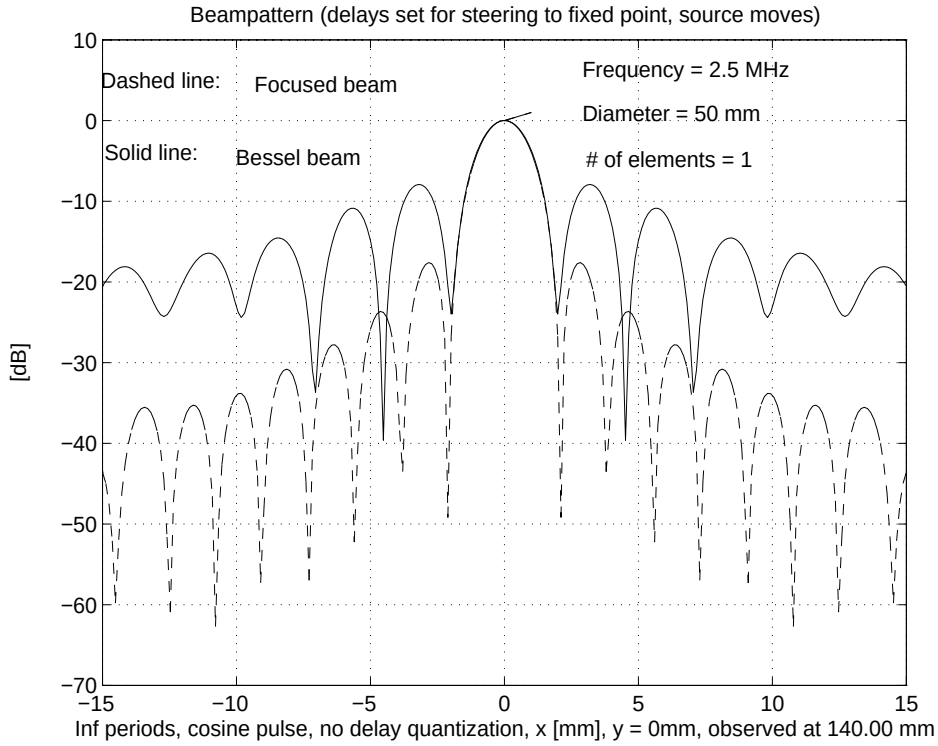

Figur 6.1: The lateral line plot of computer simulation of the zeroth-order Bessel beam (solid line) and the focused spherically beam (dashed line).The diameter of transducer is 50 mm, having a central frequency of 2.5 MHz. The scaling factor for the zeroth order Bessel beam is α = 1.202 mm^{-1}. *The -6 dB beamwidth of the mainlobe of the Bessel beam and the spherically focused beam will be about 2.45 mm. The amplitude of the first sidelobes of the zeroth-order Bessel beam and the focused beam are about 8 dB and 17.6 dB lower than the amplitude of the mainlobe respectively.*

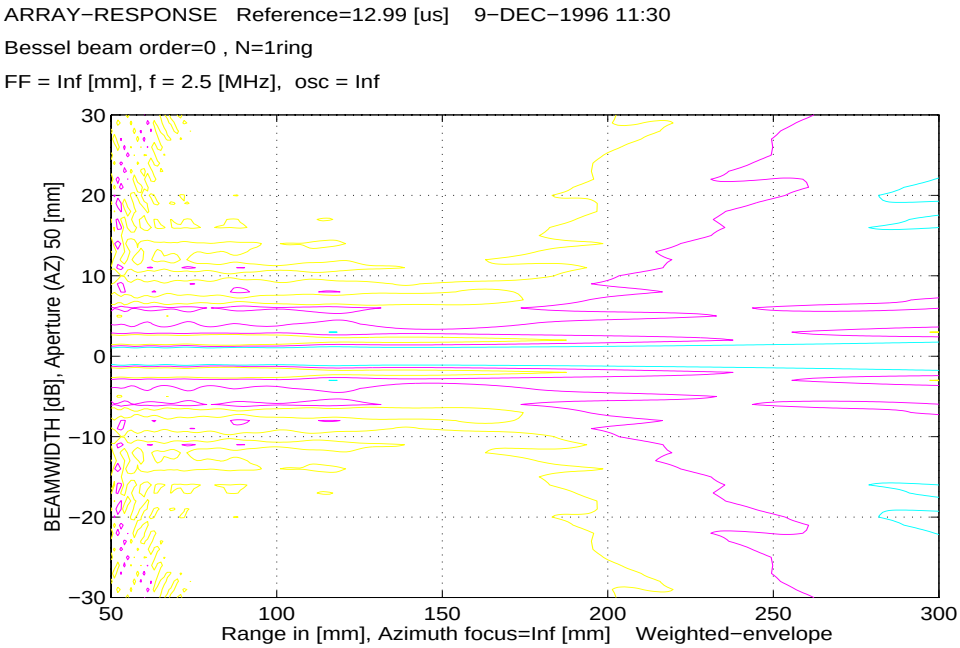

Figur 6.2: Normalized contour plot showing -6, -12, -18 dB contours for the Bessel beam (the parameters for this plot are the same as in figure 6.1). The depth of field is about 210.7 mm.

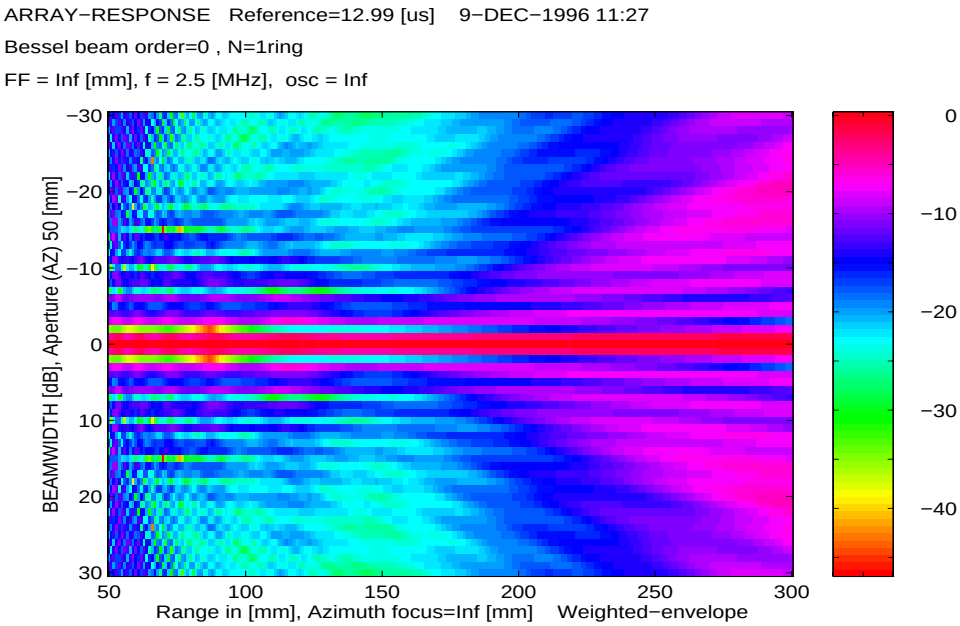

Figur 6.3: Image of figure 6.2 observed at 140 mm away from the transducer. The FWHM of the Bessel beam at the transducer surface is the same as FWHM obtained along the depth of field.

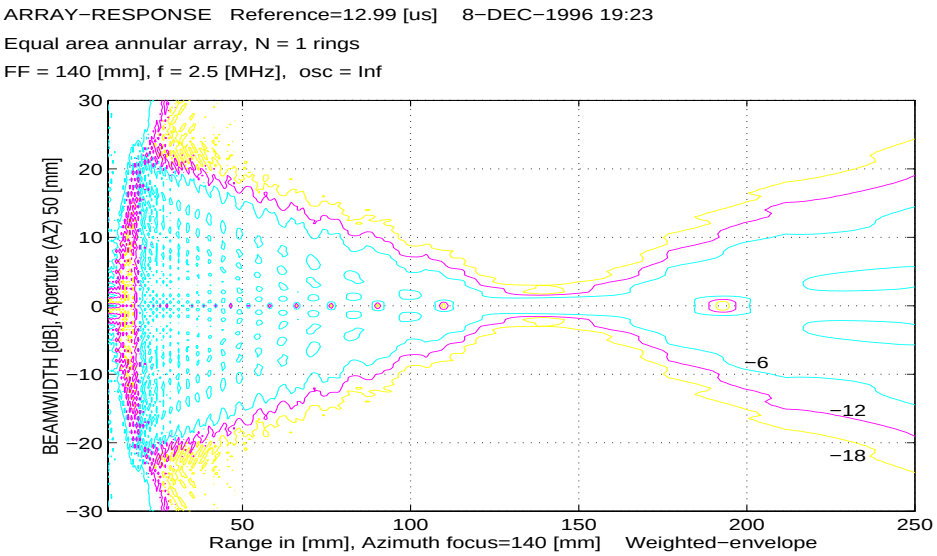

Figur 6.4: Normalized contour plot showing -6, -12, -18dB contours for a spherically focused circular transducer. The parameters for this plot are the same as that in figure 6.1. *The depth of field is about 34.7 mm. The FWHM of the beam at the transducer surface is about 25 mm.*

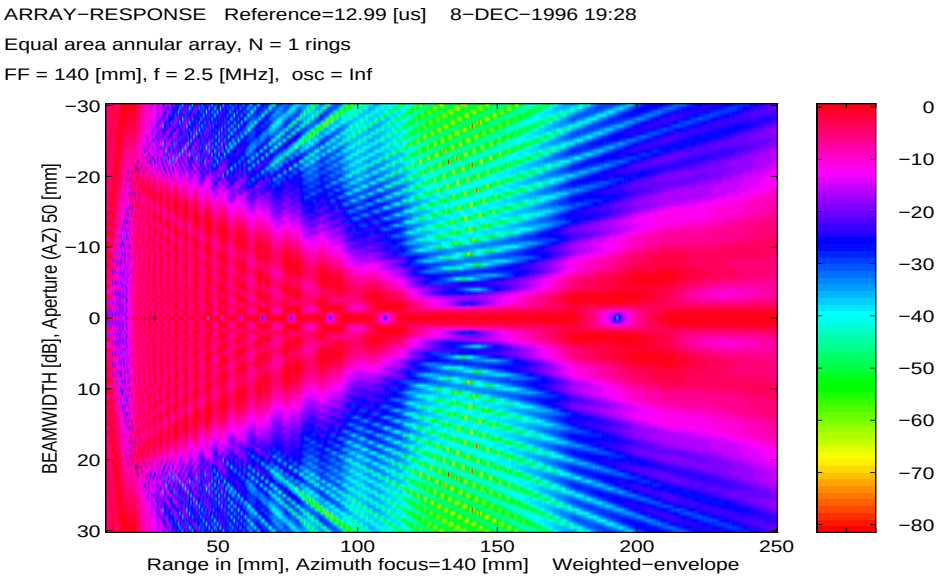

Figur 6.5: Image of figure 6.4. Focal length F is 140 mm.

The sidelobe levels, depth of fields and the lateral resolutions of the zeroth_order Bessel beam and the conventional focused beam obtained from figures 6.1 to 6.5 are summarized in table 6.1.

Beam type	Depth of field in [mm]	Lateral beamwidth in [mm]	Amplitude of first sidelobe in dB
Conv. focused beam	$L_f(3dB) = 7.12\lambda(F_N)^2 = 34.5mm$	$D_f(6dB) = 1.44\frac{\lambda F}{2a} = 2.53mm$	-17.6dB
Zeroth Order Bessel Beam	$Z_{max} = a\sqrt{\left(\frac{k}{\alpha}\right)^2 - 1} = 210.66mm$	$D_{f_{Bessel}}(6dB) = \frac{3.04}{\alpha} = 2.54mm$	-8dB

Tabell 6.1: *λ is the central wavelength, $k=2\pi/\lambda$ is the wavenumber, FN=F/2a is the F-number, a is the radius of the transducer, F is the focal length, α is the scaling factor of a Bessel beam. For our example, λ=0.616 mm, F=140 mm, and a=25 mm.*

As illustrated in figure 6.1, the lateral beamwidth of the zeroth-order Bessel beam is comparable with the lateral beamwidth (FWHM) of the spherically focused beam, i.e. about *2.53 mm* for both beams. But the FWHM of the focused beam in the surface of the transducer is about 50 mm, while the FWHM of the Bessel beam at the transducer surface is the same as FWHM obtained along the entire depth of field.

Conventional spherically focused beams suffer from a short depth of field (for this case obtained from Eq. 70 $L_f(3dB)$ is about *34.7 mm*) but have low sidelobes (the first sidelobes are *17.6 mm* lower in amplitude than the mainlobe) in their focal plane. In contrast to focused beams, zeroth-order Bessel beams have large depth of field (obtained from Eq. 92 Z_{max} is about *210.3 mm*), but higher sidelobe (the first sidelobes are *8 dB* lower in amplitude than the mainlobe). As discussed in chapter 5 these high sidelobes can be suppressed by different methods (summation_subtraction [23], [24], deconvolution [28], etc.), but these methods have some disadvantages such as: frame rate reduction, having to use two-dimensional arrays which tends to increased complexity, etc.

As we discussed in chapter 4, the lateral beamwidth and the depth of field of circular transducer are related to each other. For a given central wavelength λ and aperture size *D*, the depth of field and lateral beamwidth will increase by increasing the focal length *F*. One effective way to increase the depth of field of the focused transducer without sacrificing the lateral beamwidth and maintaining the low sidelobes is called ***dynamically focusing*** (transmission and reception) [17]. But dynamically focused transmission reduces the frame rate of the image

significantly. Previous work [32] has shown that for transducers with 50 mm in radius, the combination of the Bessel beam in transmission and dynamically focused reception will help to avoid the above mentioned problem. In the next chapter we will use a particular type of annular array transducers called equal-area annular transducers, and will look at their performance in approximating the Bessel beam for transmission and dynamically focused reception [34].

Chapter 7 A study of annular array transducer for approximation of Bessel beam

In previous chapters we have discussed the details of limited diffraction beams and spherically focused beams and their trade-offs among the beam parameters such as sidelobes, resolution, frame rate, central frequency, bandwidth, aperture, and depth of field. In [11] it was shown that imaging systems may take advantage of both limited diffraction beams and conventional beams. If limited diffraction beams are used in transmission and conventional beams in dynamically focused reception, the combination may produce high frame rate, large depth of field and low sidelobe images because the high sidelobes of limited diffraction beams are suppressed by the low sidelobes of the dynamically focused reception. It was also shown that the Bessel beam can be well approximated by a flat, finite circular aperture when annular rings are made at the location of the zeroes of the Bessel excitation function.

One way to approximately produce rotary symmetric limited diffraction beams, is to use an annular array transducer of the type that is in common use. In this chapter we will approximate Bessel beam with a 4-elements annular array transducer of low-frequency (3.5 MHz) where the division of the elements is equal-area with a fixed focus. Example of high_frequency can be found in [34].

7.1 Equal-area annular transducer

Annular transducer is made up of concentric rings(elements), that can be focused both in the plane as well as transverse to the plane, i.e. the focus is symmetric. Since annular transducer consists of rings, it can not be electronically steered and thus have to be mounted so that it can be mechanically steered or moved linearly, and dynamically focused by dynamically varying the delay on each ring with time to produce an image. One effective way to transmit with a Bessel beam and receive with conventional dynamically focused beam is equal-area division of the transducer rings in combination with fixed mechanical focus. The concept of equal-area division is based on the fact that each element has the same area, the division between the elements *n* and *n+1* is found at [34]:

$$r_n = R\sqrt{\frac{n}{N}} \qquad n \in [1, N] \tag{108}$$

where N is the number of elements and R is the radius of the transducer.

Figure 7.1 show the two-dimensional plot of a 4-elements annular array when the area of each ring is obtained from Eq. 108.

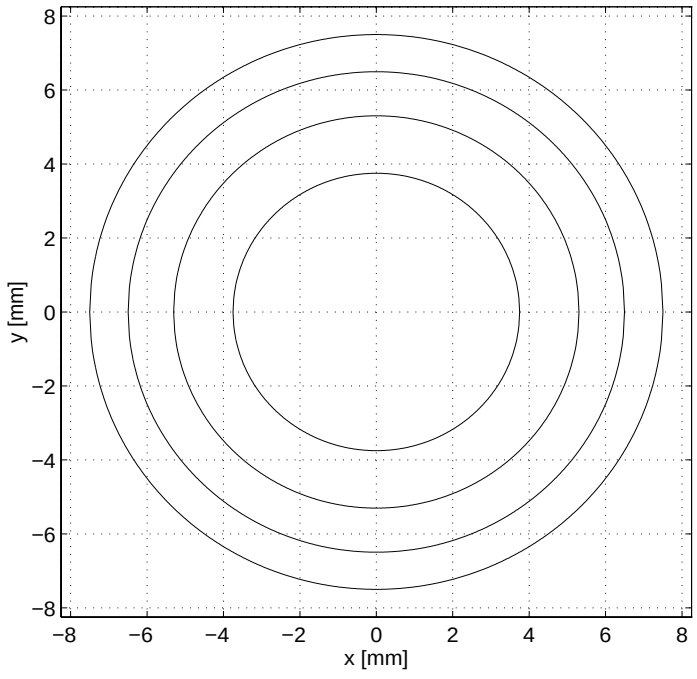

Figure 7.1: *A proposed transducer for producing both zeroth-order Bessel beams and focused beams. When each ring has the same area.*

One of the advantages of the equal-area division over other existing methods is equal defocusing of the elements as the range moves away from the prefocus (Fresnel condition). The electrical characteristics of the elements will also be the same.

7.2 Step-wise approximation of Bessel beam on equal-area annular transducer and choosing a correct scaling factor.

Because an annular array transducer has only a finite number of elements, the Bessel beam given by Eq. 82 must be approximated with the step-wise approximation along the radial distance. The equal-area assumption gives a relatively large radius for the inner ring.

In order to place the first zero points of the Bessel function in the inner ring of the transducer, the correct scaling factor should be found. This can be achieved by combining $\alpha r = 2.404$ that is the distance between the zeros of the Bessel function and Eq. 108. For *n=1* we will have:

$$\alpha = 2.404\frac{\sqrt{N}}{R} \tag{109}$$

For the 4-rings annular transducer with 15 mm diameter, the scaling factor α obtained from Eq. 109 is $641.30\ \ m-1$.

The amplitude of each element at the surface of the transducer can be achieved by using the average (mean value) or maximum amplitude (positive or negative) of the corresponding lobe of the zeroth-order Bessel function J_o.

Figure 7.2 presents the average amplitude of each element of the given lobe of the zeroth-order Bessel function. The values are calculated for element division at *3.5 MHz* equal-area annular transducer with 4 rings and a diameter of 15 mm. As illustrated in this figure the annular transducer is symmetric in both the scan plane (azimuth) as transverse to the scan plane (elevation). Also in figure 7.2 *(b)* a 3-dimensional plot of the beam (represented in figure 7.2 *(a)*) is given. As it can be seen, the inner ring with high amplitude is evident.

As shown in figure 7.4, the mean values give lower sidelobes than the maximum ones, therefore we will use the average amplitude.

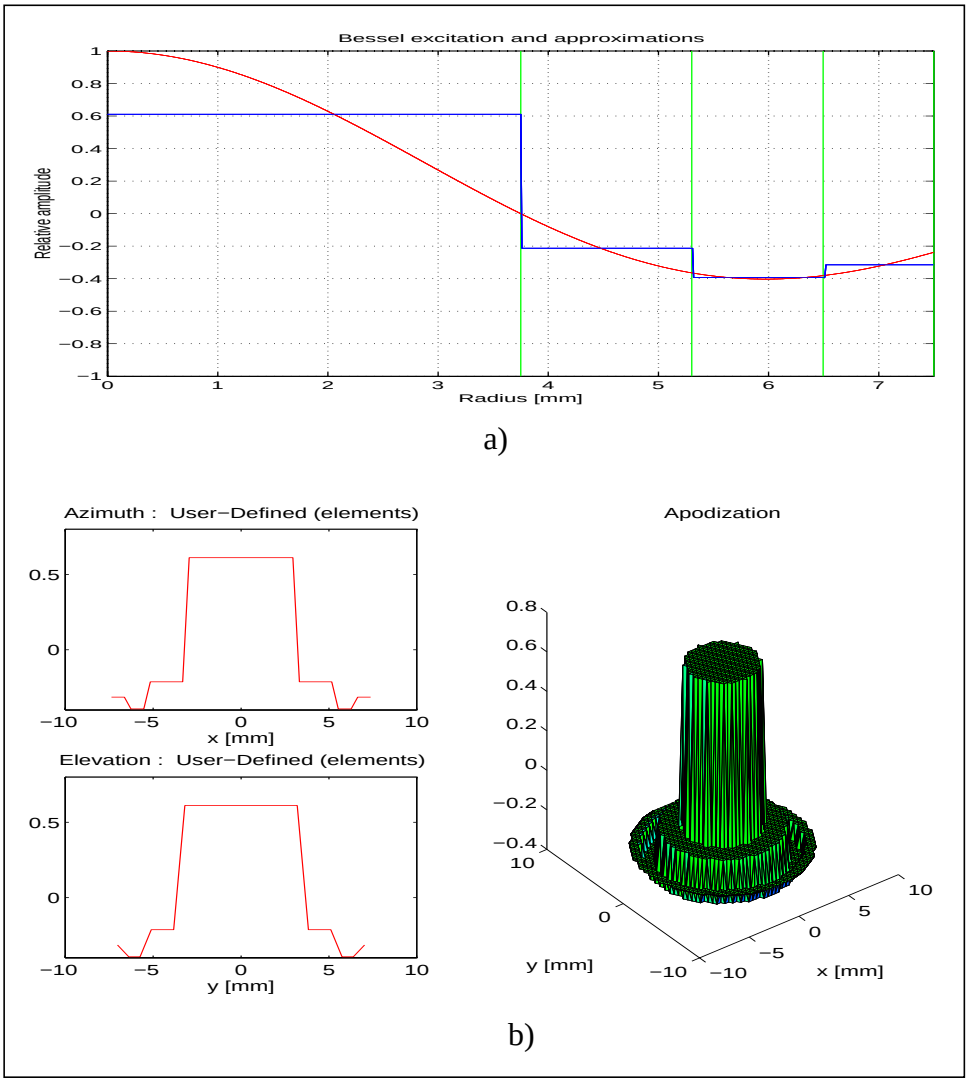

Figure 7.2: *a) Equal-area, exact Bessel and approximate excitation (piecewise constant curve). b) Four lobes Bessel function from transducer face.*

7.3 Simulation of Bessel and focused beam with the same annular array transducer

In this section we will verify the simulation results obtained from a transducer with four annular rings discussed in the previous section. The transducer diameter is 15 mm and operates with 3.5 MHz central frequency. The scaling parameter from Eq. 109 is $\alpha = 640.3\ m^{-1}$.

An ideally excited transducer follows a continuous curve. This is shown in figure 7.2 *(a)* which is the result of the exact aperture weigthing function Eq. 82. The calculated acoustic field for such transducer beam is given in figure 7.3. Note the existence of the extra peaks from the depth 175 mm and outwards as predicted by Eq. 93 for depth of field (167 mm).

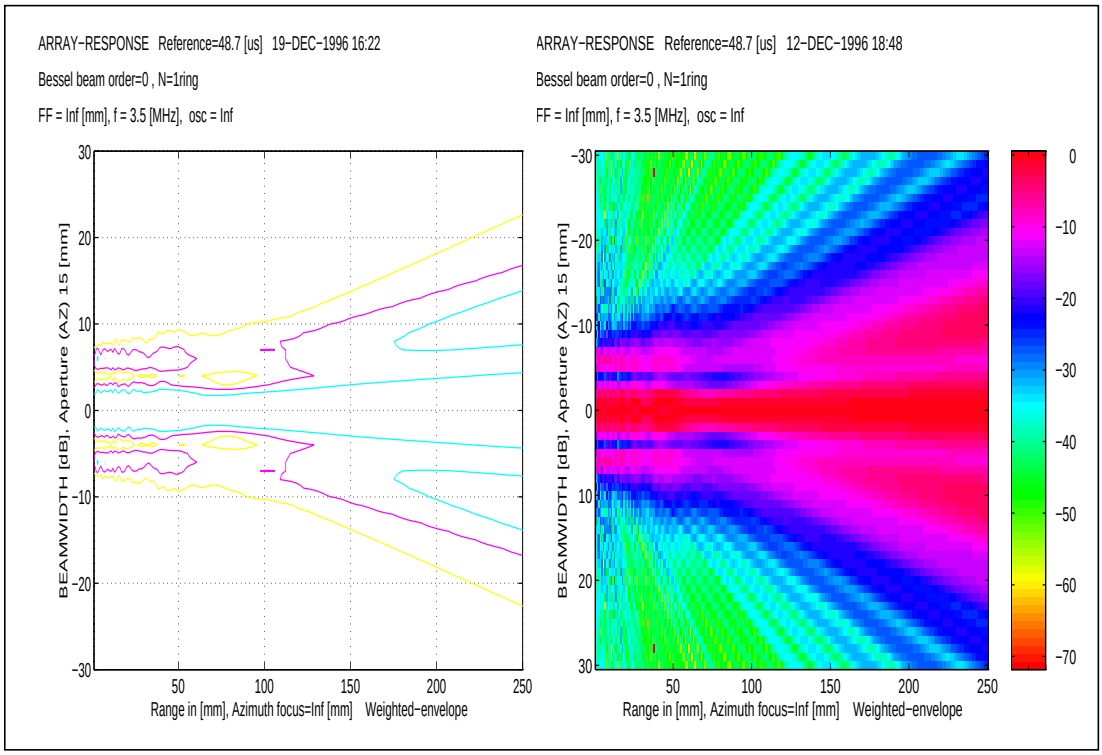

Figure 7.3: *The acoustic field from a four ring annular transducer with a 15 mm diameter. The excitation is the continuous curve given in figure 7.2. The scaling factor* α *is* $640.3 \ \ m-1$ *. The depth of field obtained from this figure is abut 175 mm.*

The beam profile of the acoustic field for a four ring transducer is plotted in figure 7.4 where the excitation is the step-wise approximation of the Bessel function.

The amplitude of each element at the surface of the transducer is proportional to the average amplitude (positive or negative) of the corresponding lobe of the zeroth-order Bessel function J_o (see figure 7.2 *a*). For comparison, the beam profile for the same transducer is also shown, but the amplitude of each element at the surface of the transducer is proportional to the maximum amplitude (positive or negative) of the corresponding lobe of the zeroth-order Bessel function. As illustrated in

this figure, the first sidelobes of the mean beam profile are lower in amplitude than the max-amplitude profile, therefore we will use the mean-amplitude approximation.

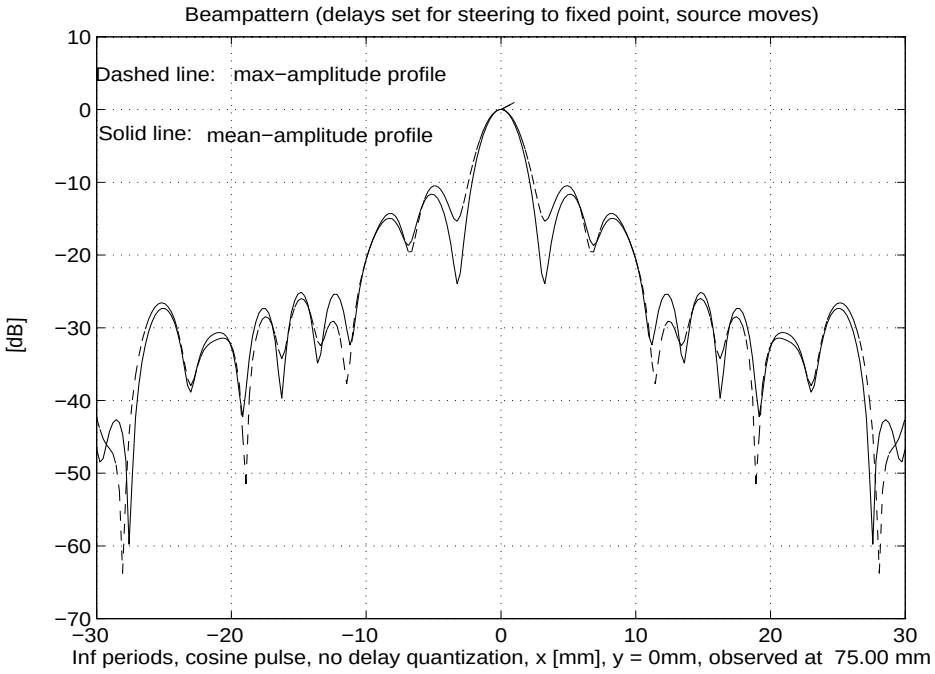

Figure 7.4: *Lateral beam profile for a four ring annular transducer. Dashed line shows the lateral beam profile for the four ring annular transducer where the amplitude of each element at the surface of the transducer is proportional to the maximum amplitude (positive or negative) of the corresponding lobe of the zeroth-order Bessel function. Solid line shows the beam profile where the amplitude of each element at the surface of the transducer is proportional to the average (mean) amplitude of the corresponding lobe of the zeroth-order Bessel function* J_o.

In figure 7.5, we have plotted the acoustic field for the equal-area approximated Bessel beam with the typical value for a fixed focus of *F=75 mm*. The delays for each element has been set to compensate for the mechanical curvature. The Fresnel parameter is *S=0.59* and the phase error for operation at infinity is 0.42π.

However, figure 7.3 shows the contour for a non-focused exact Bessel beam. The effect of using step-wise approximation can be clearly seen. One of these effects is the increased level of near-field artifacts and the other is a reduction of the depth of field. Majority of deterioration is due to the step-wise approximation to the Bessel function.

Figures 7.5 *(a)* and *(b)* show the contour plot and the image of the acoustic field for approximated Bessel beam respectively. For comparison, contour plot figure 7.5 *(c)* and image figure 7.5 *(d)* for the standard spherically focused transducer are also shown.

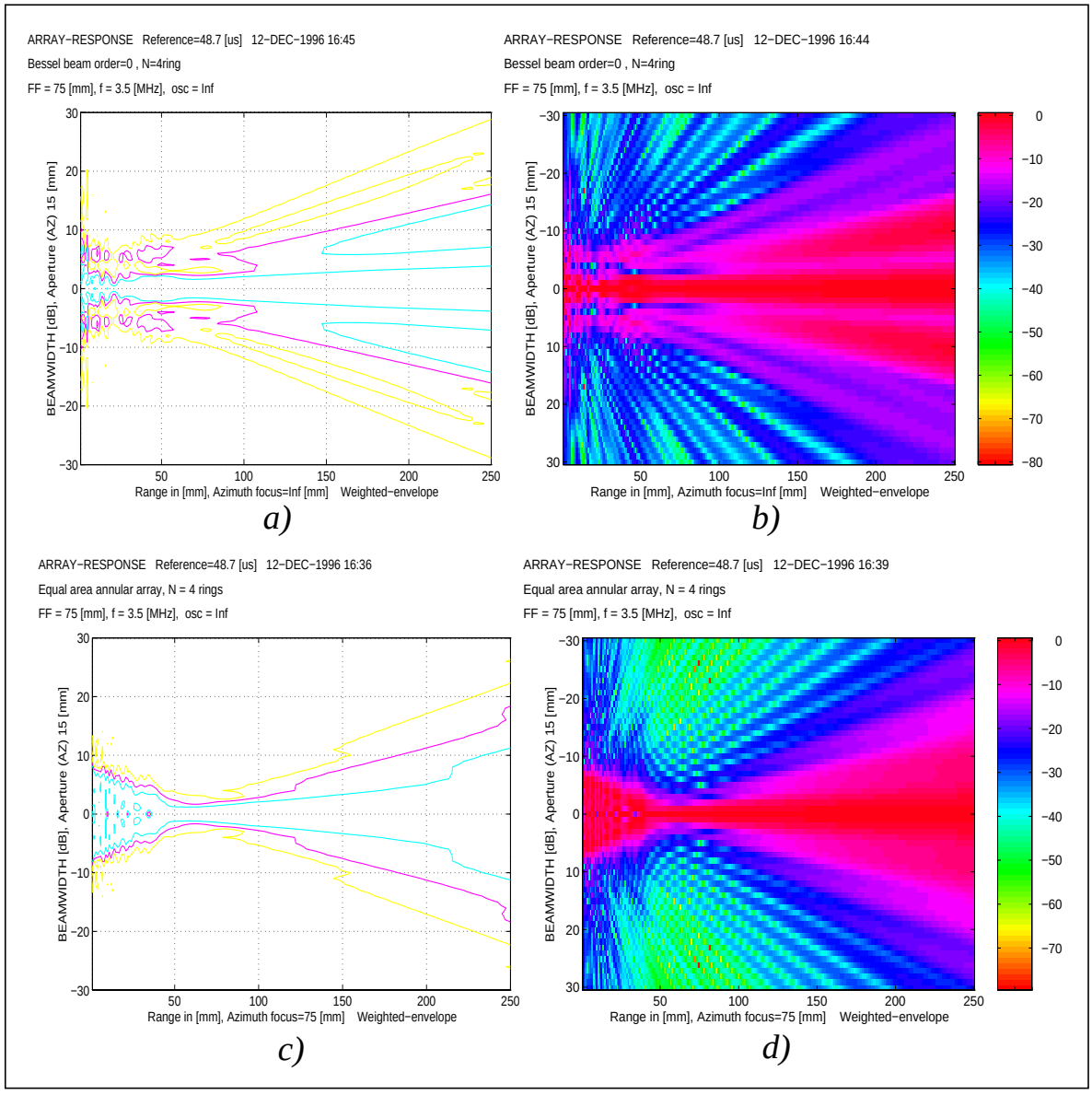

Figure 7.5: *a) Normalized contour plot showing -6, -12, and -18 dB for the equal-area approximated Bessel beam with a fixed focus. b) Image of the simulated field. c) Contour plot with -6, -12, and -18 dB contours for the spherically focused transducer with fixed focus. d) Image of the simulated field.*

In figure 7.6 *(a)* we have plotted lateral beam profiles (at depths *12.5, 25, 75, 125, 175 mm*) with a *20 dB* increment of the acoustic field for the approximated Bessel function. For comparison, lateral beam profiles for the standard spherically focused transducer at the same depths are also shown in figure 7.6 *(*b).

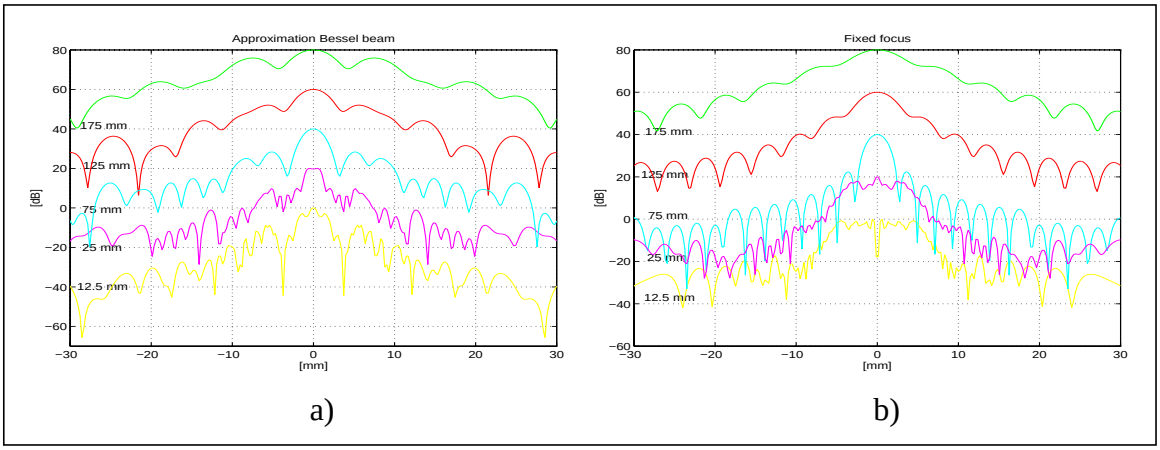

Figure 7.6: *a) One-way cw response at selected depths for a Bessel beam (cuts through* figure 7.5 (a)). b) *One-way cw response at selected depths for a beam with fixed focused at 75 mm (cuts through figure 7.5 (c)).*

In figure 7.7 we have plotted on_axis energy distribution for the Bessel beam and for the fixed focused beam. The parameters of the beams in this figure are the same as those in figure 7.5.

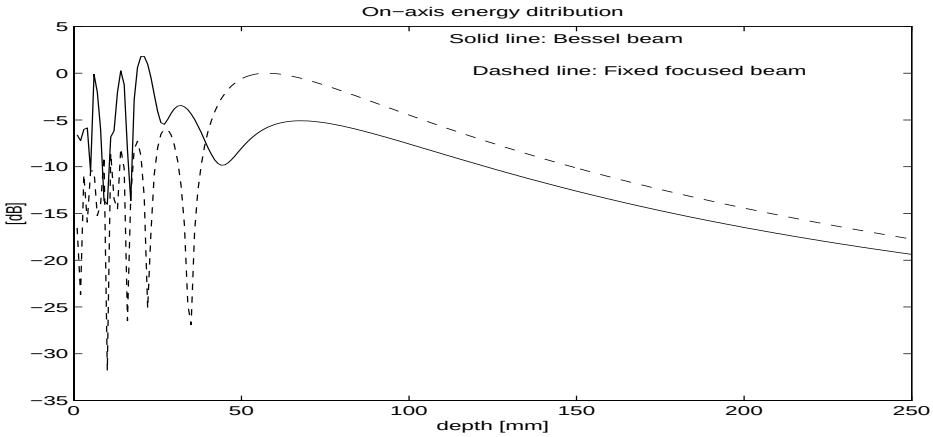

Figure 7.7: *On-axis intensities for approximate Bessel beam (Solid line) and for 75 mm fixed focused beam (Dashed line). As illustrated in this figure, the intensity distribution with depth is more uniform for the Bessel beam.*

As an example, the *-6 dB* lateral beamwidth at *75 mm* depth for the Bessel beam is about *5 mm* but for the conventional focused beam is *3.16 mm*. The depth of field for Bessel beam is about *150 mm*, but for focused circular transducer is about *78 mm*.

As illustrated in the above figures the nearfield of the approximated Bessel beam is sharper, and the beamwidth is more uniform along the depth of field. A sharper beam is seen at the spherically focused transducer focus, and it dose not have the increase in sidelobes at the end of the depth of field. This is related to the fixed focus. Bessel beam gives more uniform intensity distribution, see figure 7.7. In applications where peak intensity is limited, the uniform intensity distribution can be useful. As we discussed in chapters 4 and 5 there is a trade-off between depth of field and lateral beamwidth, but usually the Bessel beam will give better beams in the near- and farfield at the expense of a wider lateral beamwidth compared to spherically focused beams.

In fact, by using approximated Bessel beam with annular array to transmit the beam and dynamically focused beam to receive the beam one can produce a high frame rate, large depth of field and low sidelobe images because high sidelobe of the Bessel beams are suppressed by the low sidelobes of the dynamically focused reception. This is provided that the scaling factor, α, is calculated correctly to fit the first lobe of the Bessel function on the first element of the array.

Chapter 8 **Conclusion**

One of the families of limited diffraction solution to the isotropic-homogeneous scalar wave equation termed Bessel beam, represent waves that propagate to an infinite distance without spreading. In practice, however, these beams can only be approximated over a large depth of field by employing a finite size aperture and finite energy.

Although limited diffraction beams have a large depth of field, they have higher sidelobes as compared to *conventional focused beams* in their focal plane. High sidelobes may lower contrast in medical imaging and make it difficult to detect low scattering objects such as small cysts. High sidelobes also increase the effective sampling volume, which lowers the image resolution in tissue characterization[29]. To obtain pulse-echo images of low sidelobes and large depth of field one can use the *summation-subtraction* method which was derived theoretically and was verified with computer simulation for a finite aperture transducer. This method reduces sidelobes of the limited diffraction beams dramatically (the first two sidelobes are reduced about *7 dB* in amplitude), but it lowers the imaging frame rate to one third and is therefore motion sensitive.

Another method for reducing the sidelobes of limited diffraction beams, called bowtie limited diffraction beams, is also derived theoretically and verified with computer simulation for a finite aperture transducer. This method has several advantages as compared to the summation-subtraction method. It dos not reduce image frame rate or dynamic range of signals and is not motion sensitive. But the main disadvantage of this method is the need to use a two-dimensional transducer for both

transmission and reception and transducer is not symmetric. The large number of elements of a two-dimensional transducer in a small aperture may cause problems such as difficulty in wiring, electronic and mechanical crosstalk among the elements, high impedance of each element, and also a complex multiplexing among the elements[26].

One way to approximately produce rotary symmetric limited diffraction beams, is to use an annular array transducer of the type that is in common use where the division of the elements is equal-area with a fixed focus. A program doing this has been written.

By using approximated Bessel beam with an annular array to transmit the beam and dynamically focused beam to receive the beam one can produce a high frame rate, a large depth of field and low sidelobe levels because high sidelobes of the Bessel beams are suppressed by the low sidelobes of the dynamically focused reception. To achieve this, the value of scaling factor, α, most be correctly calculated in order to fit the first lobe of the Bessel function on the first element of the array. There is a trade-off between depth of field and lateral beamwidth, but usually the Bessel beam will give better beams in the near- and far-field at the expense of a wider lateral beamwidth compared to a spherically focused beam.

Further work

It is shown that the limited diffraction beam of zero order can be approximated by a annular transducer with equal-area division of elements and with a fixed focus.

One way to go forward from here is to discuss the X-waves [9] in connection to the present work and the methods which have been implemented here. The X-waves can replace the Bessel beams and the simulation can be implemented for the equal-area annular rings used in this work. X-waves can also be inplemented on linear arrays.

Appendix A Equipment and programs

Following is a concise description of the equipment and materials used in the current work.

A.1 Hardware Equipment

The necessary hardware was provided by the Department of Computer Science, University of Oslo. Programs were developed on Unix-based Sun Sparc stations (SunOs, Solaris) and Silicon graphics Indy (IRRIX) work stations in the X-windows graphical environment. The hard copy output consist of several Hewlet Packard laser printers.

A.2 Software Equipment

All the programs in this work were developed in **MATLAB** version 4. MATLAB (Matrix laboratory) is a trade mark of Math works Inc. and is matrix based interactive program for numeric computation and data visualization. The programs take advantage of another Matlab based function library called **Ultrasim**; a simulation program developed by Vingmed Sound (VMS), Horten, Norway, Department of Physiology and Biomedical Engineering (IFBT) and Department of Mathematical Sciences (IMF), Norwegian University of Science and Technology, Trondheim, and Department of Informatics (IFI), University of Oslo[35].

Source code of two of the programs used to calculate and simulate Bessel beams and Bowtie Bessel beams are provided in appendix A.3. The programs as described previously are based on Matlab and ultrasim function libraries.

A.3 Source code

```
%**************************************************************************
% Routine          : t3usim
% Description      : Configuring transducer-parameters   ANNULAR ARRAY
% Language         : Matlab 4.1
% Written by       : Vebjorn Berre, IBT
% Version no.      : 1.0 VEB 27.10.93 First Version
% Version no.      : 2.0 VEB 28.03.93
% Version no.      : 3.0 SH 16.04.93
%Version no.       : 3.1 FT 27.09.93 Created menu for selection of transducer type. Added User-
                      Defined Width
%                  : 3.2 FT 09.02.93 Parameter change depend on flagg(3)
%                  : 3.3 FT 23.02.94 Removed disp('EXIT = "x"')
%                  : 3.5 SH 03.06.96 centres as output
%                  : 3.4 SH   6.12.94 Changed call: t3usimtxt to t3usimtx
%                  : 3.6 HJG 29.01.96 Bessel-Beam is added to the menu & 4th- and
                                       10th- derivative bowtie Bessel beam
% Called by: usimcnf
% Calling      : t3usimtx

%**********************************************************************
2   function [transducer,elem_pts, centers]=t3usim(transducer,flagg,excitation,media)
3   global amp_ud
4   fid=1;
5   lambda=media(1,2)/excitation(1);
6   if length(flagg)>4
7    if flagg(5)==1
8      lambda_local=1;
9    elseif flagg(5)==2
10       lambda_local=media(1,2)/excitation(1)*1e3;
11    end
12   else
```

```
13      lambda_local=1;
14     end
15
16     tmp=size(transducer);
17     if tmp(2)<18
18      tmp=transducer;
19      transducer=zeros([1,18]);
20      transducer([1:1:length(tmp)])=tmp;
21     end
22
23     com1=0;
24     while com1~='x'
25      clc
26      t3usimtx;
27      disp('    CHANGE                                    = "number"')
28      com1 = input('-> Decision (<CR> = exit): ','s');
29      if isempty(com1) com1 = 'x'; end
30      if length(com1)==1 com1=['0',com1];end
31      if length(com1)>2
32        com1 = '00'
33     %************************ changing of parameters*****************************
34      if com1=='01'
35        temp=input('Transducer diameter D = ');
36        if ~isempty(temp) transducer(1)=temp*lambda_local*1e-3; end
37      elseif com1=='02'
38        temp=input('# elements                N  =  ');
39        if ~isempty(temp) transducer(2)=temp; end
40      elseif com1=='03'
41        if flagg(3)~=2
42          temp=input('# points on transducer surfaceP = ');
43        else
44          temp=input('# rays from transducer surfaceP = ');
45        end
46        if ~isempty(temp) transducer(3)=temp; end
47       elseif com1=='18'
48        temp = menu35_0('Choose Transducer Type', ...
49              'Equal Area','Equal Width','Circular','User-Defined Width', ...
```

```
50          'Exact Bessel(n) beam (1 element)', ...
51          'Bessel(n) equal-area transducer (N elements)',...
52          'Bessel(n) transducer (N elements)', ...
53          '4th derivatives bowtie Bessel beam', ...
54          '10th Derivatives bowtie Bessel beam ', ...
55          'Exact non-rotating Bessel(n) beam (1 element)');
56    %*****************************Bessel*****************************************
57    order = transducer(12);
58    scl_factor = transducer(13);
59    phi = transducer(14);
60  %************************nth-order Bessel beam (1 element)***********************
61    if (temp== 4 )                                  % nth-order Bessel beam (1 element)
62      disp(' ')
63       disp('Make sure that Apodization is User-Defined (points) !!!')
64              scl_factor=vinput(['Scaling  factor  [m](',num2str(0),'...',num2str(2*pi/lambda*2*1e-
    1),')'],0,2*pi/lambda*2*1e-1,scl_factor);
65       order=vinput('Order of Bessel function (>= 0)',0,1000,order);
66       transducer(2) = 1;
67       phi = 0;
68  %******************Equal-area nth-order Bessel beam (N elements)******************
69    elseif (temp== 5)%  Equal-area nth-order Bessel beam (N elements)
70       disp(' ')
71       disp('Make sure that Apodization is User-Defined (elements) !!!')
72       disp('Transducer aperture D, and # elements N must be choosen')
73       disp('before choice of transducer type ......')
74              scl_factor=vinput(['Scaling  factor  [m](',num2str(0),'...',num2str(2*pi/lambda*2*1e-
    1),')'],0,2*pi/lambda*2*1e-1,scl_factor);
75       disp(' ')
76       phi = 0;
77       [transducer(2)]=lulu(scl_factor,transducer(2),transducer(1),'y');
78  %****************th-order Bessel transducer(N elements)**************************
79     elseif (temp== 6)%  nth-order Bessel transducer(N elements)
80       disp(' ')
81       disp('Make sure that Apodization is User-Defined (elements) !!!')
82       disp('Transducer aperture D, and # elements N must be choosen')
83       disp('before choice of transducer type ......')
84              scl_factor=vinput(['Scaling  factor  [m](',num2str(0),'...',num2str(2*pi/lambda*2*1e-
    1),')'],0,2*pi/lambda*2*1e-1,scl_factor);
```

```
85          disp(' ')
86          phi = 0;
87       %     disp('WAIT CALCULATING amp_ud.....')
88          [transducer(2)]=lulu(scl_factor,transducer(2),transducer(1),'n');
89          %******************** 4th derivatives bowtie Bessel beam ***********************
90        elseif (temp==7)                                % 4th derivatives bowtie Bessel beam
91                    scl_factor=vinput(['Scaling  factor  [m](',num2str(0),'...',num2str(2*pi/lambda*2*1e-
      1),')'],0,2*pi/lambda*2*1e-1,scl_factor);
92          transducer(2) = 1;
93          phi = 0;
94       %************************10th Derivatives bowtie Bessel beam**********************
95          elseif (temp==8)%  10th Derivatives bowtie Bessel beam
96                    scl_factor=vinput(['Scaling  factor  [m](',num2str(0),'...',num2str(2*pi/lambda*2*1e-
      1),')'],0,2*pi/lambda*2*1e-1,scl_factor);
97          transducer(2) = 1;
98          phi = 0;
99       %*******************nth-order non-rotating Bessel beam (1 element)*****************
100         elseif (temp == 9)% nth-order non-rotating Bessel beam (1 element)
101           disp(' ')
102           disp('Make sure that Apodization is User-Defined (points) !!!')
103                   scl_factor=vinput(['Scaling  factor  [m](',num2str(0),'...',num2str(2*pi/lambda*2*1e-
      1),')'],0,2*pi/lambda*2*1e-1,scl_factor);
104           order=vinput('Order of Bessel function (>= 0)',0,1000,order);
105           phi=vinput('Rotation angle [deg] = ',-360,360,phi) %  Rotation angle
106           transducer(2) = 1;
107
108         end
109
110         if ~isempty(temp) transducer(18)=temp; end
111
112       elseif com1=='09'
113         temp=input('Fixed focus                         F = ');
114         if ~isempty(temp) transducer(9)=temp*lambda_local*1e-3; end
115
116       elseif com1=='10' & flagg(3)==2
117         temp=input('Rotation angle [deg]theta = ');
118         if ~isempty(temp) transducer(10)=temp*pi/180; end
119
```

```
120     elseif com1=='15' & flagg(3)==2
121       temp=input('Offset[mm]                                    dz = ');
122       if ~isempty(temp) transducer(15)=temp*1e-3; end
123     end
124     if exist('order'), transducer(12) = order; end % order of Bessel-beam
125     if exist('scl_factor'), transducer(13) = scl_factor; end
126     if exist('phi'), transducer(14) = phi; end % rotation angle of Bessel-beam
127   end      %while
128
129   if flagg(3)~=2
130     [elem_pts] = annular(transducer, excitation, media);
131      centers = []; % no separate calculation of element centers done so far!
132   end
133   %*****************Bessel Beam----------22.01.1996*********************************
134   if ( transducer(18)==4|transducer(18)==7|transducer(18)==8 | transducer(18)==9)
135     transducer(2) = 1;
136     if (transducer(18) == 4),
137       amp_ud=zeros(size(elem_pts(1:2,:)));
138     else
139       amp_ud=zeros(size(elem_pts(1:3,:)));
140     end
141     rho=sqrt(elem_pts(1,:).^2+elem_pts(2,:).^2); % m (rho is radial coordinate)
142     %****************nth-order Besselbeam (1 element)*******************************
143     if ( temp== 4)
144       jbes= (bessel(order,abs(rho)*scl_factor)); % Bessel Beam (nth-order)
145       amp_ud(1,:)=jbes;
146       amp_ud(2,:)=rho.*1000; % mm
147       %****************nth-order non-rotating Bessel beam (1 element)*****************
148     elseif (temp==9)
149       if (order == 0)
150         j0=(bessel(0,abs(rho)*scl_factor)); % Bessel Beam (nth-rotating)
151         amp_ud(1,:)=j0;
152       else
153         fi=atan2((elem_pts(1,:)),(elem_pts(2,:)));
154         jbes2=(bessel(order,abs(rho)*scl_factor)).*(cos(order*(fi-phi*pi/180)));
155         amp_ud(1,:)=jbes2;
156       end
```

```
157       amp_ud(2,:)=1000*elem_pts(1,:); % x
158       amp_ud(3,:)=1000*elem_pts(2,:);           % y
159       %**********4th derivatives Bowtie Bessel baem**********
160     elseif ( temp==7)
161       a=find(rho==0);
162       j0=(bessel(0,abs(rho)*scl_factor)); % Bessel Beam (nth-rotating)
163       j1=(bessel(1,abs(rho)*scl_factor));
164       alf=scl_factor;
165       y=elem_pts(2,:);
166       x1=-(24*alf.^2*y.^4)./rho.^6;
167       x1(a)=0;
168       x2=(alf.^2*y.^2.*(24+alf^2*y.^2))./rho.^4;
169       x2(a)=0;
170       x3=3*alf.^2./rho.^2;
171       x3(a)=0;
172       x4=(48*alf*y.^4)./rho.^7;
173       x4(a)=0;
174       x5=(8*alf*y.^2.*(6+alf.^2*y.^2))./rho.^5;
175       x5(a)=0;
176       x6=(6*alf*(1+alf.^2*y.^2))./rho.^3;
177       x6(a)=0;
178       j4=8/(3*alf^4)*((x1+x2-x3).*j0+(x4-x5+x6).*j1);
179       j4(a)=1;
180       amp_ud(1,:)=j4;
181       amp_ud(2,:)=1000*elem_pts(1,:);     % x
182       amp_ud(3,:)=1000*elem_pts(2,:);
183       %**********10th derivatives bowtie Bessel beam**********
184     elseif (temp==8)
185       a=find(rho==0);
186       j0=(bessel(0,abs(rho)*scl_factor)); % Bessel Beam (nth-rotating)
187       j1=(bessel(1,abs(rho)*scl_factor));
188       alf=scl_factor;
189       y=elem_pts(2,:);
190       xx1=-(92897280*alf.^2*y.^10./rho.^18);
191       xx1(a)=0;
192       xx2=1290240*alf.^2*y.^8.*(180+7*alf.^2*y.^2)./rho.^16;
193       xx2(a)=0;
```

```
194       xx3=201600*alf.^2*y.^6.*(1008+108*alf.^2*y.^2+alf.^4*y.^4)./rho.^14;
195       xx3(a)=0;
196       xx4=1200*alf.^2*y.^4.*(60480+15120*alf.^2*y.^2+360*alf.^4*y.^4+alf.^6*y.^6)./rho.^12;
197       xx4(a)=0;
198     xx5=alf.^2*y.^2.*(9072000+6048000*alf.^2*y.^2+302400*alf.^4*y.^4+1800*alf.^6*y.^6+alf.^
        8*y.^8)./rho.^10;
199       xx5(a)=0;
200       xx6=630*alf.^2*(288+1080*alf.^2*y.^2+120*alf.^4*y.^4+alf.^6*y.^6)./rho.^8;
201       xx6(a)=0;
202       xx7=945*alf.^4*(12+5*alf.^2*y.^2)./rho.^6;
203       xx7(a)=0;
204       xx8=185794560*alf*y.^10./rho.^19;
205       xx8(a)=0;
206       xx9=10321920*alf*y.^8.*(45+4*alf.^2*y.^2)./rho.^17;
207       xx9(a)=0;
208       xx10=1693440*alf*y.^6.*(240+60*alf.^2*y.^2+alf.^4*y.^4)./rho.^15;
209       xx10(a)=0;
210       xx11=9600*alf*y.^4.*(15120+9072*alf.^2*y.^2+405*alf.^4*y.^4+2*alf.^6*y.^6)./rho.^13;
211       xx11(a)=0;
212     xx12=50*alf*y.^2.*(362880+604800*alf.^2*y.^2+60480*alf.^4*y.^4+720*alf.^6*y.^6+alf.^8*
              y.^8)./rho.^11;
213       xx12(a)=0;
214         xx13=45*alf*(8064+80640*alf.^2*y.^2+20160*alf.^4*y.^4+448*alf.^6*y.^6+alf.^8*y.^8)./
              rho.^9;
215       xx13(a)=0;
216       xx14=630*alf.^3*(108+135*alf.^2*y.^2+5*alf.^4*y.^4)./rho.^7;
217       xx14(a)=0;
218       xx15=945*alf.^5./rho.^5;
219       xx15(a)=0;
220       j10=-256/((63*alf.^10))*((xx1+xx2-xx3+xx4-xx5+xx6-xx7).*j0+(xx8-xx9+xx10-xx11+xx12-
        xx13+xx14-xx15).*j1);
221       j10(a)=1;
222       amp_ud(1,:)=j10;
223       amp_ud(2,:)=1000*elem_pts(1,:); % x
224       amp_ud(3,:)=1000*elem_pts(2,:);
225     end
226   end
```

```
%*************************************************************************
% Routine       : lulu
% Description   : Bessel excitation and approximations
% Language      : Matlab 4.1
% Written by    : Hossein Jamshidi
% Version no.   : 1.0 HJG 11.9.96 First Version
%                       Calculating width of each annular
%                       element which is designed to be equal
%                       to a lobe of Zero order Bessel function.
%*************************************************************************
1   function Nn = lulu(alfa,Nn,d,EqualArea);
2   clear amp_ud
3   global amp_ud
4   temp=[];t=[];t1=[];amp_ud=[];amp=[];amp2=[];amp3=[];amp4=[];k=0;s=1;
5   radius = d/(2)*sqrt([1:Nn]/Nn);         % Equal area
6   %disp(' ')
7   %disp('Choose the Equal area or Bessel lobes ')
8   %disp('to replace the rings on the transducer ')
9   %EqualArea = input('Equal area [n/y] ? ','s');
10
11   if isempty(EqualArea)
12      EqualArea  = 'n';
13   end
14
15   maxAmplitude =  input('Maximum amplitude of respective Bessel lobes or mean [n/y] ? ','s');
16   if isempty(maxAmplitude)
17      maxAmplitude = 'n';
18   end
19
20   rho = 0:.00001:d/2;
21   j0 = bessel(0,abs(rho)*alfa);
22
23   %*****************************Find zeros of Bessel function **********************
24   ratio=(d/2)/length(j0);
25   i =1;
26   ratio=(d/2)/length(j0);
27      for ii=1:length(j0)-1
```

```
28          if sign(j0(ii+1)*j0(ii))<=0
29            zerose=((j0(ii)/((j0(ii)-j0(ii+1))))+ii)*ratio;
30            zerosBessel(i)=zerose;
31            i=i+1;
32           end
33          end
34      % ***************Add end element if no zero close to it************************
35      if (EqualArea == 'n' & (d/2-rho(max(zerosBessel*100000))>.001))
36        zerosBessel=[zerosBessel max(rho)];
37      end
38      %**********************Choose the Equal area or Bessel lobes************************
39      %***********************to replace the transducer rings*****************************
40      disp(' ')
41      disp('WAIT CALCULATING amp_ud.....')
42      if EqualArea == 'y'
43       zerosBessel = radius;
44       rho=0:.00001:max(zerosBessel);
45       else
46        rho=0:.00001:max(zerosBessel);
47        Nn = length(zerosBessel); % update number of elements
48      end
49      %***************Find maximum amplitude or minimum amplitude*********************
50      for j=1:length(zerosBessel)
51         temp=[];
52         temp2=0;
53        for x=k:.00001:zerosBessel(j)
54         if x<=zerosBessel(j)
55             temp=[temp j0(s)];
56          if maxAmplitude == 'y'
57             [temp2,I]=max(abs(temp)); % max. value
58             temp2=temp(I);
59             temp3 = temp2 * ones(1,length(temp));
60           else
61             temp2 = mean(temp);
62             temp3 =  temp2 * ones(1,length(temp));
63           end
64         end
```

```
65        if s<length(rho)
66           s=s+1;
67        end
68       end
69        k=x;
70        amp2=[amp2 temp2];
71        amp_ud=amp2;
72        amp=[amp temp3];
73        amp3=[amp3 temp];
74    end
75
76    %************************** Plotting of Bessel function*****************************
77    yyy=[-1 1];
78    zerosBessel=zerosBessel*1000;
79    for jj=1:length(zerosBessel)
80        plot([zerosBessel(jj) zerosBessel(jj)],yyy,'g')
81        axis([0 max(zerosBessel) -1 1])
82        hold on
83        plot(rho*1000,amp3(1,1:length(rho)),'r')   % Plot of Bessel function
84        plot(rho*1000,amp(1,1:length(rho)),'b')    % Plot of average amplitude of corresponding lobe
85                                                   % of Bessel function
86    end
87      hold off
88      xlabel('Radius [mm]')
89      ylabel('Relative amplitude')
90      title('Bessel excitation and approximations')
91      grid
92    amp4(1)=[ (zerosBessel(1)/2)*1000];
93    for jjj=2:length(zerosBessel)
94      amp4=[amp4 (zerosBessel(jjj)+zerosBessel(jjj-1))/2*1000];
95    end
96    amp_ud(2,:)=amp4*1e-3;
```

References

[1] *David Halliday, Robert Resnick, "Fundamental Of Physics", Copyright 1970, 1974, by John Wiley &Sons, Inc.*

[2] *Beranek, L.L. "Acoustics", ASA, 1993, "Unabridged republ. of 1954"*

[3] *Don H. Johnson and Dan E. Dudgeon "Array Signal Processing, Concepts and Techniques", 1993.*

[4] *Bjørn A.J. Angelsen, Hans Torp, Sverre Holm, Kjell Kristoffersen, T.A. Whittingham, "Which transducer array is best?" European Journal of Ultrasound 2 (1995) 151-164.*

[5] *Jan Ove Erstad "Design of sparse and non-equally spaced arrays for medical ultrasound" University of Oslo Department of informatics, November 14th 1994.*

[6] *Philip M. Morse and K. Uno Ingard, "Theoretical Acoustics". McGraw-Hill Book Company, New York, 1968.*

[7] *M. Fatemi and S. Shirani "Application of hexagonal arrays in generation and steering of limited diffraction beams" Biomedical Eng. Department, Amirkabir University, Tehran, Iran. Ultrasonics symposium 1994.*

[8] *Jian-Yu Lu, "A study of two-dimensional array transducer for limited diffraction beams" IEEE Transaction on ultrasonic, Ferroelectric, and Frequency control, vol. 41, no. 5, September 1994.*

[9] *Lu, J.-Y.; Greenleaf, J.F. Nondiffracting X Waves-Exact Solution to Free-Space Scalar Wave Equation and Their Finite Aperture Realization,. IEEE Trans. Ultrasound. Ferroelec. Freq. Contr. 39:19-31; 1992a.*

[10] *Durnin, J. Exact solution for nondiffracting beams. I. The scalar theory. J. Opt. Soc. Am. 4:651-654; 1987.*

References

[11] *Durnin, J,; Miceli, J. J., Jr.; Eberly, J. H. Diffraction-free beams. Phys. Rev. Lett. 58:1499-1501; 1987.*

[12] *Fatemi, M.; Arad, M. A. Ultrasonic nondiffracting beam image formation and restoration. IEEE 1991 Ultrason. Symp. Proc. 91CH3079-1. 2:1305-1308;1991.*

[13] *Born, Max, "Principles of optics" Oxford, Pergamon, c1980*

[14] *K. Kirk Shung, Michael B. Smith, Benjamin Tsui, "Principles of medical imaging", Copyright 1992 by Academic press, Inc.*

[15] *Fredric J. Harris, "On the use windows for harmonic analysis with the discrete Fourier transform" reprinted from Proc. IEEE, vol., 66, pp.51-83, Jan. 1978.*

[16] *Kino, G. S. Acoustic waves: Devices, imaging, and analog signal processing. Englewood Cliffs, NJ: Prentice-Hall, Inc.; 1987.*

[17] *Jian-Yu Lu, Hehong Zou and James F. Greenleaf, Biomedical Ultrasound Beam Forming, Ultrasound in Med. & Biol., Vol. 20 No.5 pp. 403-428, 1994.*

[18] *J. W. Goodman, "Introduction to Fourier Optics". New York: McGraw-Hill Book Company, 1968 chs.*

[19] *Biørn A.J Angelsen, "Waves, Signals and Signal Processing in Medical Ultrasonics", Department of Biomedical Engineering University of Trondheim Norway 1991.*

[20] *M. Moshfeghi, "Sidelobe suppression in annular array and axicon imaging systems". J. Acoust. Soc. Am. 83:2202-2209; 1988.*

[21] *G. N. Watson, "Theory Of Bessel Functions" Second edition, Cambridge at the University Press 1966.*

[22] *C. J. Tranter, "Bessel Functions with some physical applications" First printed 1968.*

[23] *Lu, J.-Y.; Greenleaf, J.F. "Sidelobe reduction for limited diffraction pulse-echo systems". IEEE Trans. Ultrason. Ferroelec. Freq. Contr. 40:735-746; 1993b.*

References

[24] *Lu, J.-Y.; Greenleaf, J.F. "A study of sidelobe reduction for limited diffraction beams". IEEE 1993 Ultrason. Symp. Proc. 93CH3301-9. 2:1077-1082; 1993c.*

[25] *Lu, J.-Y.; Greenleaf, J. F. "Steering of limited diffraction beams with a two-dimensional array transducer" Biodynamics Research Unit, Department of Physiology and Biophysics, IEEE 1992 Ultrason. Symp. Proc. 92CH3118-7, 1:603-607; 1992d.*

[26] *D. H. Turnbull and F. S. Foster, "Beam steering with pulsed 2-D transducer arrays" IEEE Trans. Ultrason., Ferroelec., Freq. Contr., vol.38, no. 4, pp. 320-333, July 1991.*

[27] *Bjørn A.J. Angelsen, Hans Torp, Sverre Holm, Kjell Kristofersen, T.A. Whittingham. "Which transducer array is best?". European Journal of Ultrasound 2 (1995) 151-164.*

[28] *Lu, J.-Y.; Greenleaf, J. F. "Sidelobe reduction for limited diffraction pulse-echo image by deconvolution". Ultrason. Imaging 14:203, 1992e (Abs.).*

[29] *Jian-yu Lu, "Bowtie Limited Diffraction Beams for Low-Sidelobe an Large Depth of Field Imaging". IEEE Transactions on Ultrasonic, Ferroelectrics, and Frequency Control, Vol. 42, No. 6. November 1995*

[30] *Lu, J.-Y.; Greenleaf, J. F. "Simulation of imaging contrast of nondiffracting beam transducer," J. Ultrasound Med., Vol., 10, no, 3(suppl.), p. s4, Mar. 1991(Abs.).*

[31] *Lu, J.-Y.; Greenleaf, J. F. "Experiment of imaging contrast of J_0 Bessel nondiffracting beam transducer" J. Ultrasound Med., Vol., 11, no, 3(suppl.), p. S43., Mar. 1992(Abs.).*

[32] *Jian-Yu Lu and James F. Greenleaf "Ultrasonic Nondiffracting Transducer for Medical Imaging" IEEE Transactions on Ultrasonic, Ferroelectrics, and Frequency Control, Vol. 37, No. 5. September 1990 .*

[33] *Lu, J.-Y.; Greenleaf, J. F. "Evaluation of a nondiffracting transducer for tissue characterization" in IEEE 1990 Ultrason. Symp.*

References

Proc. 90CH2938-9, vol. 2 pp. 795-798, 1990.

[34] *Sverre Holm and G. Hossein Jamshidi "Approximation of Bessel Beams with Annular arrays" Department of Informatics, University of Oslo, November 1996. IEEE International ultrasonics symposium 1996.*

[35] *Sverre Holm, F Teigen, L. Ødegaard, V. Berre, J. O. Erstad. "Ultrasim User's Manual ver. 2.0" Department of informatics, University of Oslo. August 16, 1996.*